Analysis of bioactive lipids from different infection models during bacterial and viral infections

I n a u g u r a l d i s s e r t a t i o n

zur

Erlangung des akademischen Grades eines

Doktors der Naturwissenschaften (Dr. rer. nat.)

der

Mathematisch-Naturwissenschaftlichen Fakultät

der

Universität Greifswald

vorgelegt von

Daniel Schultz

Greifswald, 29.01.2021

Dekan: Prof. Dr. Gerald Kerth

1. Gutachter : Prof. Dr. Michael Lalk

2. Gutachter: Prof. Dr. Dieter Steinhilber

3. Gutachter: Prof. Dr. Hartmut Kühn

Tag der Promotion: 17.05.2021

Gewidmet meiner Familie!

Table of contents

List of abbreviations

12-(3-adamantan-1-yl-ureido)-dodecanoic acid	AUDA
arachidonic acid	AA
bronchoalveolar lavage fluid	BALF
butylated hydroxytoluene	BHT
ceramide 1-phosphate	C1P
c-Jun N-terminal kinase	JNK
collagen induced arthritis	CIA
cyclic adenosine monophosphate	cAMP
cyclooxygenase	COX
cytochrome P450 enzyme	CYP
day post infection	dpi
docosahexaenoic acid	DHA
dynamic multiple reaction monitoring	MRM
eicosapentaenoic acid	EPA
electrospray ionization	ESI
epoxyeicosatrienoic acids	EETs
ethylenediaminetetraacetic acid	EDTA
G protein-coupled receptor	GPCR
gas chromatography	GC
group A *Streptococcus*	GAS
high performance liquid chromatography	HPLC
human bronchial epithelial cell line	16HBE
hydroperoxyeicosatetraenoic acid	HpETE
hydroxydocosahexaenoic acid	HDHA
hydroxyeicosapentaenoic acid	HEPE
hydroxyeicosatetraenoic acid	HETE
hydroxyoctadecadienoic acid	HODE
hydroxyoctadecatrienoic acid	HOTrE

hydroxyperoxyeicosatrienoic acid	HpHETE
influenza A Virus	IAV
interleukin	IL
leukotriene	LT
lipopolysaccharide	LPS
lipoxygenase	LOX
magnetic resonance mass spectrometry	MRMS
mass spectrometry	MS
matrix-assisted laser desorption/ionization	MALDI
non-steroidal anti-inflammatory drugs	NSAID
pathogen-associated molecular pattern	PAMP
pattern recognition receptor	PRR
peroxisome proliferator-activated receptor	PPAR
polyunsaturated fatty acid	PUFA
ribonucleic acid	RNA
septic arthritis	SA
specialized pro-resolving mediator	SPM
sphingosine 1-phosphate	S1P
Staphylococcus aureus	*S. aureus*
Streptococcus pneumoniae	*S. pneumoniae*
Streptococcus pyogenes	*S. pyogenes*
tandem mass spectrometry	MS/MS
thromboxane	TX
tumor necrosis factor receptor	TNFR

Zusammenfassung

Bioaktive Lipide beeinflussen zahlreiche Prozesse wie die Reproduktion, den Knochenumbau, die Schmerzwahrnehmung, das kardiovaskuläre System und das Immunsystem. Zu den immunmodulatorischen Lipidmediatoren gehören die Eicosanoide und Oxylipine, welche sowohl durch enzymatische als auch durch nicht enzymatische Oxidationen aus mehrfach ungesättigten Fettsäuren (PUFAs) gebildet werden. Unter diesen Sammelbegriffen werden verschiedene Gruppen wie beispielsweise Prostaglandine oder Leukotriene zusammengefasst. Sie haben Eigenschaften, die sowohl die Aktivierung inflammatorischer Reaktionen als auch die Unterstützung der Auflösung von Entzündungen beinhalten. Sie wirken dabei ähnlich wie Hormone lokal begrenzt und in geringer Konzentration. Außerdem existieren noch weitere bioaktive Lipide wie Verbindungen aus der Klasse der Sphingolipide. Die Synthese einiger dieser Verbindungen wie die der Prostaglandine kann medikamentös beeinflusst werden, während andere Gruppen aktuell therapeutisch nicht gezielt inhibiert werden können. Ihr Einfluss während der Inflammationsprozesse und bei chronischen Entzündungen ist durch Studien belegt, aber Forschungsdaten im Zusammenhang mit Infektionen sind nur begrenzt vorhanden. Infektionen des oberen Respirationstraktes, verursacht durch virale und bakterielle Pathogene, stellen weltweit eine große Herausforderung für die menschliche Gesundheit dar. Wichtige Pathogene sind Influenza A Viren (IAV) sowie bakterielle Erreger wie *Staphylococcus aureus* (*S. aureus*), *Streptococcus pneumoniae* (*S. pneumoniae*) und *Streptococcus pyogenes* (*S. pyogenes*). Neben Monoinfektionen mit einem der genannten Erreger kommt es häufig zu viralen-bakteriellen Ko-Infektionen, was den Krankheitsverlauf negativ beeinflussen kann. Die Erkennung der Pathogenen und deren Beseitigung ist die Hauptaufgabe des Immunsystems, welches wesentlich durch Lipidmediatoren beeinflusst wird. Die leichte Oxidierbarkeit, das Vorkommen von verschiedenen Regioisomeren und die geringe Abundanz der Eicosanoide und Oxylipine sind die Hauptgründe, weshalb ihre Analytik eine große Herausforderung darstellt.

Eines der Hauptziele dieser Dissertation war die Etablierung geeigneter Messmethoden für ausgewählte Lipidmediatoren und deren Detektion in unterschiedlichen Probenmaterialien aus Infektionsversuchen. Die Trennung und Messung der bioaktiven Lipide erfolgte durch Hochleistungs-flüssigkeitschromatographie (HPLC) gekoppelt an ein *Triple Quadrupol*-Massenspektrometer, was als Tandem-Massenspektrometrie (MS/MS) bezeichnet wird. Für 30 Lipidmediatoren wurden die einzelnen MS-Parameter anhand von chemischen Standards optimiert und dann mit einer *dynamic multiple reaction monitoring* (MRM)-Methode gemessen. Außerdem konnte die räumliche Verteilung bestimmter Sphingolipide im Gewebe durch *matrix-assisted laser desorption ionization mass spectrometry imaging* (MALDI-MS-Imaging) analysiert werden. Neben den Messungen war die Probenaufarbeitung ein essentieller Bestandteil der Methodenetablierung. Während für die Analytik von Lipidmediatoren und deren Messung mittels HPLC-MS/MS gut erprobte Aufarbeitungsprotokolle existieren, standen solche für das neuartige MALDI-MS-Imaging nur begrenzt zur Verfügung. Schließlich konnten für beide Messmethoden robuste und reproduzierbare Protokolle erstellt und bei der Analyse zahlreicher Proben aus Infektionsexperimenten genutzt werden, in denen die wirtseigenen Lipidmediatorveränderungen von infizierten Zellkulturen, Mäusen und Schweinen untersucht wurden. Je nach Fragestellung wurden Zellpellets, Lungen, Milzen, Lebern, Blutplasma, Pfoten mit Knochen oder bronchoalveoläre Lavagen aufgearbeitet und die Proben analysiert. Durch das MALDI-MS-Imaging wurde die Verteilung ausgewählter Sphingolipide in Lunge und Milz der Mäuse detektiert.

Die vorliegende Dissertation umfasst vier zusammenhängende Themenbereiche, in denen der Einfluss von Pathogenen auf wirtseigene Lipidmediatoren mit den oben genannten Methoden analysiert wurde. Die

genutzten Infektionsmodelle Epithelzelllinie (Artikel II), Maus (Artikel III und IV) und Schwein (Artikel I), als humannahes Modell, zeigten unterschiedliche Aspekte der Wirts-Pathogen-Interaktion auf. Für alle drei Wirte konnten Proben aus einer IAV-Infektion analysiert werden, welche zahlreiche Gemeinsamkeiten für bestimmte Oxylipine zeigte, die in der Literatur auch für humanen Infektionen beschrieben sind. Zudem war es möglich, Proben aus Zellkultur- und Maus-Experimenten, welche mit den Pathogenen *S. aureus*, *S. pneumoniae* und IAV mono-infiziert und ko-infiziert wurden, zu untersuchen. Besonders bei den bakteriellen Infektionen und Ko-Infektionen handelt es sich um Erstbeschreibungen der Lipidmediatorveränderungen. Die zusätzliche räumliche Detektion der Sphingolipide Sphingosin-1-phosphat und Ceramid-1-phosphat lieferte wichtige Informationen über deren Gewebeverteilung und Veränderung während einer Ko-Infektion, was ebenfalls erstmalig untersucht wurde.

In **Artikel I** werden die IAV-spezifischen Veränderungen von Oxylipinen im Schwein (Deutsche Landrasse), als Wirtsmodell, analysiert. Dazu wurden Proben infizierter Tiere zu verschiedenen Zeitpunkten nach der Infektion von Lunge, Milz, Blutplasma und bronchoalveolären Lavagen analysiert und mit Proben nicht-infizierter Tiere verglichen. Vor allem das Gewebe der Lunge und Milz zeigte eine Zunahme an Verbindungen, welche teilweise aus Infektionen von Menschen und Mäusen bekannt sind. Die Analyse unterschiedlicher Probenarten lieferte zudem einen Überblick über gut geeignetes Probenmaterial. Erstaunlicherweise zeigten sich viele Veränderungen in der Milz, welche selbst nicht infiziert war. Da sich die meisten Studien aufgrund der lokalen Wirkung der Lipidmediatoren auf Probentypen konzentrieren, die sich in unmittelbarer Nähe zur Infektion befinden, liefert diese Dissertation neue Einblicke und zeigt zudem eine Form der systemischen Wirtsantwort auf. Neben der Infektionen von Tieren mit einem komplexen Immunsystem bezieht sich **Artikel II** auf die Infektion von humanen Bronchialepithelzellen (16HBE) mit den Erregern *S. aureus*, *S. pneumoniae* und IAV, wobei sowohl Einzelinfektionen als auch bakteriell-virale Ko-Infektionen untersucht wurden. Da solche Zellen als initiale Barriere für Pathogene dienen und auch erste Angriffsfläche dieser sind, ist das Verständnis dieser Wirt-Pathogen-Interaktion von entscheidender Bedeutung. Die meisten Veränderungen zeigten sich bei einer Pneumokokken-Infektion. Zudem wurde deutlich, dass sich die untersuchten bakteriellen Infektionen von der viralen durch die verstärkte Synthese von 5-Hydroxyeicosatetraensäure (HETE) unterscheiden.

Für die weiteren Infektionen wurden Mäuse als Infektionsmodell genutzt. Neben den untersuchten Infektionen mit Bezug zum Respirationstrakt wurde außerdem die Auswirkung einer *S. pyogenes*-Infektion in verschiedenen Mausstämmen analysiert und in **Artikel III** beschrieben. Infektionsbedingte Veränderungen von Prostaglandinen in geschwollenen Pfoten, welche beim Knochenumbau beteiligt sind, konnten ebenso beobachtet werden wie erhöhte Mengen an Sepsis- und Arthritis-assoziierten Lipidmediatoren, wenn der Infektion eine Arthritis vorangegangen war. Zudem wurden deutlich erhöhte Mengen an 20-HETE bei einer solchen schweren Infektion gemessen. Die gesteigerte Biosynthese von 20-HETE wurde in **Artikel IV** auch bei Infektionen mit dem hochpathogenen *S. aureus* LUG2012 bestätigt, wobei die Mengen dieses Eicosanoids in allen untersuchten Probentypen erhöht waren. In diesem letzten Artikel der vorliegenden Dissertation werden bakterielle und virale Infektionen ähnlich dem Ansatz in Artikel II beschrieben. Vor allem IAV-spezifische Veränderungen von Lipidmediatoren zeigten sich, die so auch in den Lungen und Milzen der Schweinen beobachtet werden konnten. Die zusätzlichen MALDI-MS-Imaging-Messungen ließen eine Akkumulation von Ceramid-1-phosphat in Milz und Lunge sowie eine Anreicherung in der roten Pulpa der Milz erkennen, welche bisher unbeschrieben ist.

Insgesamt lieferten die Arbeiten zu dieser Dissertation umfangreiche Profile von Lipidmediatoren bei Infektionen dreier verschiedener Infektionsmodelle mit ausgewählten bakteriellen und viralen Pathogenen. Diese Daten können als Basis für weiterführende Projekte dienen, in denen der Einfluss einzelner bioaktiver Lipide auf den Infektionsverlauf genauer untersucht werden könnte.

Summary

Bioactive lipids or lipid mediators influence numerous processes like the reproduction, the bone turnover, the pain perception, the cardiovascular function and the immune system. Eicosanoids and oxylipins are parts of the immunomodulatory lipid mediators, which can be synthesized from polyunsaturated fatty acids (PUFAs) by enzymatic and non-enzymatic reactions. Typical members of eicosanoids are prostaglandins and leukotrienes. The properties of bioactive lipids include the activation of inflammatory reactions as well as the support of resolution. Like hormones, they act locally restricted and in low concentrations. Further bioactive lipids exist i.e. intermediates of the sphingolipid class. The biosynthesis of some of these compounds like the prostaglandins can be influenced by different drugs whereas for other groups of lipid selective inhibitors are still missing. Their impact on inflammatory processes and against chronic diseases has already been analyzed, while studies in context with infection are largely limited. Infection of the upper respiratory tract caused by viral and bacterial pathogens constitute a huge burden for the human healthcare. The main pathogens are the Influenza A virus (IAV), *Staphylococcus aureus* (*S. aureus*), *Streptococcus pneumoniae* (*S. pneumoniae*) and *Streptococcus pyogenes* (*S. pyogenes*). Besides mono-infection with one of these pathogens, frequently occurring bacto-viral co-infections exist, which negatively influence the etiopathology. The main task of the immune system is the detection and the elimination of pathogens, which can essentially be affected by lipid mediators. Their instability due to oxidizability, the existence of regioisomers and the low abundance of eicosanoids and other oxylipins are the main problems for their analytical measurement.

The mayor objective of this dissertation was the establishment of a suitable analytical method for selected lipid mediators and the detection of infection-related changes. The separation and detection was performed by using high-performance liquid chromatography (HPLC) coupled with triple quad mass spectrometry. This combination is called tandem mass spectrometry (MS/MS). The MS parameters were optimized for approximately 30 lipid mediators by use of chemical standards and the detection was achieved by dynamic multiple reaction monitoring (MRM). Furthermore, the spatial resolution of selected sphingolipids was analyzed in tissue samples using matrix-assisted laser desorption ionization mass spectrometry imaging (MALDI-MS-Imaging). Concerning the HPLC-MS/MS detection, an MS method was established and optimized with standard compounds. Another crucial part of the establishment was the extraction of bioactive lipids from the different sampling materials. Whereas well tested protocols exist for the extraction and detection of lipid mediators, such protocols for MALDI-MS-Imaging are still limited due to the novelty of this measurement. Ultimately, robust and reproducible protocols for both techniques that were used for the analysis of a broad array of samples from infection experiments were established for both techniques. The analyses of infected cell culture, mice and pigs revealed infection-related perturbations of host lipid mediator levels. Depending on the scientific issue, the sample types cell pellets, lungs, spleens, livers, blood plasmas, pawns including bones or bronchoalveolar lavages were analyzed. For MALDI-MS-Imaging, the spatial distribution of sphingolipids in lung and spleen was detected.

The present dissertation includes four coherent research scopes, in which the pathogen impact on host-derived lipid mediators was detected with the above mentioned analytical methods. The infection models epithelial cells (article II), mouse (article III and IV) and pig (article I) – the latter as the most human like model - showed different aspects of the host-pathogen interaction. The analysis of samples from IAV infection for all three hosts revealed a couple of similarities for some oxylipins that were also described in human infections. Additionally, cell culture and mouse samples from mono-infections as well as co-infections with the pathogens *S. aureus* and *S. pneumoniae* were measured. In particular for the bacterial mono- and co-infections, these are the first published results with aspects of infection related changes of

lipid mediators. The additional spatial resolution of the sphingolipid intermediates sphingosine 1-phosphate and ceramide 1-phosphate revealed important new insights into their tissue distribution and changes during co-infection.

Article I describes the IAV-specific oxylipin changes in the pig (german landrace) as infection model. Therefore, the sample types lung, spleen, blood plasma, and bronchoalveolar lavage from infected animals at different time points after infection were analyzed and compared with samples from uninfected pigs. Mainly in the lung and the spleen, increased amounts of certain lipid mediators were observed. These changes coincide well with already described alterations in humans and mice. Furthermore, the analysis of different sample material provided an overview about appropriate sample types. Surprisingly, many perturbations were detected in the spleen, which itself was uninfected. Based on the local reaction of lipid mediators, most studies concentrate on sample material with close contact to side of infection. Therefore, this dissertation reveals new insights into a form of systemic immune response. Besides the use of animals with a complex immune system for infection experiments, human bronchial epithelial cells (16HBE) were mono- and co-infected with the pathogens *S. aureus*, *S. pneumoniae* and IAV as described in **article II**. Such cells are the initial barrier for and first contact site with pathogens and thus the comprehension of this host-pathogen interaction is of essential importance. Most changes were detected during pneumococcal infection. Furthermore, the analyzed infections with bacterial pathogens differed from IAV infection by an increased synthesis of 5-hydroxyeicosatetraenoic acid (HETE). For further infections with the above mentioned pathogens, the mouse was used as an infection model. Besides infections affecting the respiratory tract, also the impact of an *S. pyogenes* infection in different mice strains was analyzed and described in **article III**. Infection-related changes in prostaglandins, which are involved in bone turnover in swollen pawns as well as enhanced amounts of sepsis- and arthritis-associated lipid mediators were detected, in case arthritis had been induced prior to infection. Furthermore, increased amounts of 20-HETE could be observed for such severe infections. An enhanced biosynthesis of 20-HETE was further confirmed in a high-pathogenic *S. aureus* LUG2012 infection in **article IV** for all examined sample types. In this last article of this dissertation, bacterial and viral infections in mice were analyzed similar to those described in **article II**. Mainly IAV-specific lipid mediator alterations were detected, which are in accordance with the findings of the infected pigs. The additional MALDI-MS-Imaging measurements revealed so far unknown accumulation of ceramide 1-phosphate in lung and spleen as well as enrichment in the red pulp of the spleen.

In summary, this dissertation provides substantial lipid mediator profiles for infections in three different model systems with selected bacterial and viral pathogens. The obtained data constitute a suitable basis for continuative research projects, in which the influence of single bioactive lipids on the course of infection could be examined in more detail.

Introduction

Bioactive lipids

Lipids are generally regarded as membrane components or as important metabolites for energy storage due to their biological functions. They are also able to serve as potent bioactive signaling molecules that are involved in a wide array of processes like reproduction [1], modulation of cardiovascular functions [2], bone remodeling [3], nociception [4], inflammation and related immune system regulation [5,6]. Bioactive lipids that are able to induce inflammation or activate resolution of the immune system are called lipid mediators or oxylipins. They are derived from different ω-3 and ω-6 polyunsaturated fatty acids (PUFAs), and these PUFAs can be released from cell membranes by phospholipases. The main enzymes responsible for the biosynthesis of these oxylipins are lipoxygenases (LOX), cyclooxygenases (COX) and cytochrome P450 enzymes (CYPs) as shown in Figure 1. Additionally, some of the oxylipins can be synthesized by transcellular biosynthesis [7], non-enzymatic reactions or during lipid peroxidation processes [8]. Eicosanoids are lipid mediators of arachidonic acid (AA), that is further modified into prostanoids via the COX pathway. The prostanoids include prostaglandins (PGs), leukotriens and thromboxanes (TXs). Sune K. Bergström, Bengt I. Samuelsson and John R. Vane were awarded with the Nobel Prize for physiology or medicine in 1982 for their research on prostaglandins and related biologically active substances.

Other oxylipins derived from linoleic acid, linolenic acid, docosahexaenoic acid (DHA) and eicosapentaenoic acid (EPA) are involved in the activation of immune system resolution. Some oxylipins derived from DHA and EPA can be summarized to the specialized pro-resolving mediators (SPMs) [9]. Lipid mediators fulfill their function through interaction with their receptors. Currently, there are nine receptors for PGs and TXs described plus additional splice variants, which belong mostly to the G protein-coupled receptors (GPCRs). An interaction between lipid mediator and receptor results in the induction of cell calcium mobilization as well as alterations in the level of second messenger cyclic adenosine monophosphate (cAMP) [10]. Furthermore, the PG D_2 receptor DP2 represents a chemokine receptor as described in the literature [11]. For the majority of oxylipins, the receptors are GPCR and peroxisome proliferator-activated receptors (PPAR) [12], tumor necrosis factor receptors (TNFR) [13], formyl peptide-like receptors [14] and different members of the transient receptor potential cation channel subfamily [15]. Of these receptors multiple receptor isoforms exist, e.g. PG E_2 can be expressed differently in various cell types, resulting in cell and tissue specific effects on certain lipid mediators [16]. By the use of non-steroidal anti-inflammatory drugs (NSAID) or statins, an intervention in the biosynthesis of bioactive lipids can therapeutically be achieved. NSAID like acetylsalicylic acid mainly target the COX pathway resulting in inhibited prostaglandin production [17]. Statins are also able to influence the production of lipoxins, a group of SPMs resulting from AA conversion by LOX [18].

In addition to the described bioactive lipids originated from PUFA conversion, also mediators from the sphingolipids, sphingosine 1-phosphate (S1P) and ceramide 1-phosphate (C1P) in particular, are involved in immune system related processes like cell migration, cell survival, cell growth and the biosynthesis of eicosanoids [19-21]. Most research on lipid mediators focuses on chronic diseases, including asthma and inflammatory bowel disease or pharmacology processes as reviewed in [22-25].

Lipid mediators in immune system regulation and infection processes

The immune system is a complex host defense system that enables the identification and clearance of foreign agents like pathogens or tumor cells. This system consists of the innate and adaptive immune system and includes different cell types and organs. Pattern recognition receptors (PRRs) are part of the innate immune system. They are expressed in a large variety of different cells and are able to identify pathogen-associated molecular patterns (PAMPs). These PAMPs are microbial or viral components like lipopolysaccharides (LPS), lipoteichoic acids, flagellins or double-stranded ribonucleic acids (RNAs) [26]. The activation of PRRs through PAMPs leads to the onset of inflammation, which is characterized by the following symptoms: pain, swelling, heat, loss of tissue function and redness [27].

Role of analyzed pro-inflammatory lipid mediators

The pro-inflammatory immune system modulation is mediated by the majority of prostanoids and other oxylipins derived from AA and linolenic acid conversion. The biosynthesis of prostaglandins from AA starts with constitutive active COX-1 or inducible COX-2 leading to the formation of PG G_2 and PG H_2, which are both converted to different PGs and TXs by their synthases. PG E_2 (Figure 1) has vasodilatory properties and increases the microvascular permeability [28]. Furthermore, PG E_2 is able to attract macrophages [29]. Different pathogens like *Streptococcus pneumoniae* (*S. pneumoniae*), *Streptococcus pyogenes* (*S. pyogenes*), *Pseudomonas aeruginosa*, *Escherichia coli* and different *Burkholderia*, *Salmonella* and *Mycobacteria* species can promote PG E_2 production of host immune cells [30-36]. Besides its role in immune system modulation, PG E_2 is needed for a balanced bone turnover and influences the differentiation of osteoclasts and osteoblasts along with PG D_2 [37]. The impact of *S. pyogenes* infection on these PGs in a septic arthritis mouse model is described in **article III**. The PG D_2 shows pro-inflammatory effects including airway hyper reactivity and infiltration of eosinophils and leucocytes [38,39]. The immune modulation role of the prostanoid PG $F_{2\alpha}$ is thus far unexplored. Elevated levels, however, have been measured in patients suffering from different forms of arthritis [40]. Since some prostanoids undergo a rapid degradation, only their degradation products are measureable. This is the case for TX A_2, which degrades to TX B_2 and is involved in platelet aggregation with further vasoconstrictor properties. A potential role of TX B_2 as pro-inflammatory mediator is described for the activation of renal vasoconstriction resulting in renal failure during LPS induced septic mouse experiments [41].

The precursor AA can be the substrate of three different LOX enzymes resulting in the biosynthesis of leukotrienes (LTs) and hydroxyeicosatetraenoic acids (HETEs). The three enzymes 5-LOX, 12-LOX and 15-LOX have been described in the literature to mediate their conversion as reviewed in [42]. 5-LOX together with the 5-LOX-activating protein FLAP [43] is responsible for the synthesis of LTs and 5-HETE. Both LTs and 5-HETE are potent chemoattractant compounds for a number of different immune cells [44,45]. The role of 5-HETE in bacterial infections of the human bronchial epithelial cell line (16HBE) is described in **article II**. In addition, also 20-HETE, produced by CYP omega hydroxylases, is associated with sepsis and arthritis. This metabolite is able to influence vasoconstriction and vasodilation by releasing NO [46,47] and thus inducing cardiac protection in sepsis and inhibiting the synthesis of prostanoids like PG E_2 [48,49]. Alterations in 20-HETE levels associated with *S. aureus* LUG2012 and *S. pyogenes* infections are discussed in article **II-IV**.

The bioactive lipids S1P and C1P are able to induce eicosanoid synthesis through the activation of cytosolic phospholipase A_2 [50] and COX-2 [51] respectively. The sphingolipid derivative C1P has further pro-inflammatory properties like mast cell degranulation [52] or activation of cell migration. The latter have been described for murine macrophages [53] and human monocytes [20]. High amounts of S1P are found in blood plasma and lymph, whereas the concentration is very low in the secondary lymphatic organs. This S1P gradient is important for lymphocyte traffic. Alterations in S1P and C1P levels are described in **article IV**.

Besides AA derived lipid mediators, the oxylipin 9-hydroxyoctadecadienoic acid (9-HODE) produced by linoleic acid conversion is known for its pro-inflammatory properties including intracellular calcium mobilization, cytokine secretion [54] and activation of c-Jun N-terminal kinase (JNK) through the G protein-coupled receptor G2A [55,56]. Perturbations in the 9-HODE levels have been described from ischemic stroke patients [57], for mouse peritonitis models [58] and mice infected with *Toxocara* species [59].

Role of analyzed anti-inflammatory lipid mediators

Besides the above mentioned pro-inflammatory properties, some prostaglandins, PG E_2 and PG D_2 in particular are also known for their dual role in immune system regulation, including anti-inflammatory activities. The PG E_2 can switch the production induction from pro-inflammatory leukotriene B_4 to the anti-inflammatory AA-derived lipid mediator lipoxin A_4. This lipid mediator switch leads to a diminished immune cell infiltration and resolution of inflammation [60]. Furthermore, binding to the PG E_2 receptor increases levels of cyclic adenosine monophosphate (cAMP) [61] that in turn increasing the production of anti-inflammatory cytokines like interleukin-10 or serving as a negative regulator for pro-inflammatory macrophages [62]. Different animal pleuritis and colitis models show attenuated inflammation through reduced immune cell infiltration accompanied by enhanced PG D_2 synthesis [63,64]. Furthermore, an intratracheal application of PG D_2, results in enhanced bacterial clearance in *Pseudomonas aeruginosa* infected murine lungs [65]. This immunomodulation seems to be caused by inhibition of the pro-inflammatory macrophage receptor TREM-1 and induced expression of transcription factor Nrf2 [66]. Other important AA-derived anti-inflammatory eicosanoids are 12- and 15-HETE that are both capable inhibiting the interleukin-6 secretion from macrophages [67]. Elevated amounts of both HETEs from lung and spleen samples of Influenza A virus (IAV)-infected mice and pigs are described in **article I and IV**. Moreover, the epithelial cell line 16HBE also showed alterations of these lipid mediators during bacterial infections with *S. aureus* and *S. pneumoniae* as discussed in **article II**. However, certain differences in the LOX activity of humans, mice and pigs exist [61,68]. Even though human and mouse 12-LOX showed a comparable enzymatic activity, murine 15-LOX - encoded by the *ALOX15* gene - converted AA mainly to 12-HETE via a transformation of 12-hydroperoxyeicosatetraenoic acid (HpETE) instead to 15-HETE. While mice and pigs have different 12-lipoxygenating ALOX15 isoforms, this has not been described for the corresponding human ALOX15. Additionally, the murine ALOX15b has an 8-lipoxygenating activity that leads to the production of 8-HETE, without a comparable enzyme described for humans as reviewed in [69].

Besides prostaglandins and HETEs, the epoxyeicosatrienoic acids (EETs) are an important group of eicosanoids with anti-inflammatory properties. This includes the PPAR activation [12], suppression of cell degradation by the nuclear factor IKBα [13], inhibition of leucocyte adhesion to the vascular wall [70] and prevention of PG E_2 production in vascular smooth muscle cells [71]. An impact of IAV infection on EET levels was investigated in **article I and IV**.

DHA- and EPA-derived lipid mediators like hydroxydocosahexaenoic acids (HDHAs) and hydroxyeicosapentaenoic acids (HEPEs) are precursors of potent anti-inflammatory mediators, i.e. protectins, maresins and resolvins [72]. An important function of these specialized pro-resolving mediators (SPM) is the inhibition of immune cell migration [72,73]. In particular, the SPM precursor 17-HDHA (Figure 1) is known for its role in IAV-infections in mice and humans [42,74,75] as well as bacto-viral coinfections in humans [76]. The data of **article IV** support these findings for mice and **article I** expands the data upon the host response on IAV-infection to the animal model pig. 17-HDHA is known to have a positive effect on host antibody production against IAV [75]. Besides the positive effect on host B cell activation, 17-HDHA is able to inhibit viral nucleoprotein mRNA expression in human lung epithelial cells [74]. Other HDHA, like 14-HDHA and 13-HDHA, also seem to be affected by an IAV-infection in mice and pigs (**article I and IV**) and infection of 16HBE cells with *S. pneumoniae* (**article II**). 18-HEPE, an additional SPM precursor, is able to prevent macrophage-mediated fibroblast activation [77] and seems to be beneficial for the treatment of atherosclerosis [78].

The linoleic acid-derived lipid mediator 13-HODE can be produced by 15-LOX [56] and functions as a PPARγ agonist. PPAR is a ligand-activated transcription factor, and it is known for its anti-inflammatory properties. These include downregulation of the COX-2 gene [79], inhibition of NF-KB [80], and reduced production of pro-inflammatory cytokines and interleukins through its effect on macrophages [81]. The ratio of 13-HODE/9-HODE is used to describe the pro- versus anti-inflammatory state of an infection. The advantage is that both bioactive lipids share the same precursor and have a high abundance in different sample types [42]. In the different sample types - blood plasma, spleen and lung - stable ratios were detected for control animals, while *S. pneumoniae* infected animals showed an increased ratio as described in **article IV**. These results indicate that the 13-HODE/9-HODE ratio may be a useful tool to study infections. Another 15-LOX product from the precursor linoleic acid is 13-hydroxyoctadecatrienoic acid (HOTrE). Like 13-HODE, it can prevent the activation of the pyrin domain containing 3 (NLRP3) complex of the NLR family [82]. This complex acts as a PRR for PAMP detection and is essential for resistance to pneumococcal infections [83]. Anti-inflammatory properties have also been described for S1P and C1P [84]. The immunosuppressive function of S1P becomes evident when considering the ability of its receptor modulator FTY720 to promote a macrophage subtype switch to anti-inflammatory M2 macrophages [85] and the interference of neuroinflammation [86]. C1P seems to prevent the biosynthesis of pro-inflammatory ceramides, and therefore being beneficial for the host during an infection with *S. aureus* that under normal circumstances can lead to lung edema and sepsis [87]. Moreover, C1P stimulates the biosynthesis of antimicrobial defensins against *S. aureus* [88] and concurrently hinders the LPS-induced production of TNFα and different pro-inflammatory interleukins [89].

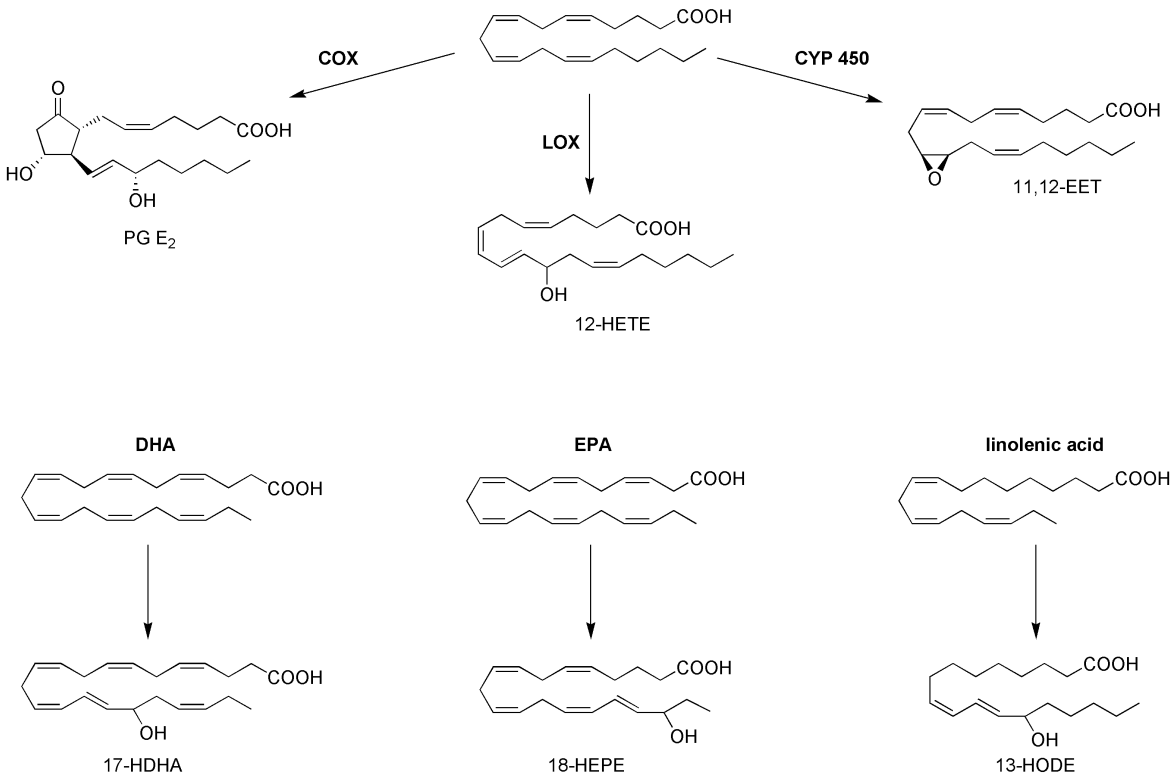

Figure 1: Selected lipid mediators with pro- and anti-inflammatory properties from different PUFAs that were analyzed by HPLC-MS/MS.

Analytical methods

The accurate analysis and quantification of lipid mediators in biological samples is afflicted with several major challenges. First of all, the oxylipin concentrations are extremely low (typically in the pmol/mL range) and the compounds are not stored in tissues, but rather formed on demand with limited stability. Different tissues express several patterns of lipid mediator synthesizing and degradating enzymes. Even the same precursor can be oxidized at different positions of its acyl chain by various enzymatic and non-enzymatic reactions. These oxidations respectively leading to different regio- and stereo-isomeric species, that each have different biological effects. Therefore, optimized sampling strategies including sample storage, lipid mediator extraction and internal standards combined with highly sensitive, accurate and specific measurements are needed [6,90-93]. Radiometric measurements and enzymatic immunoassays are used, but they have some limitations: the availability of corresponding antibodies, the lack of accurate absolute quantification and specificity due to cross reactivity combined with reduced possibility to detect multiple species within the same measurement [94,95]. Therefore, high performance liquid chromatography (HPLC) and gas chromatography (GC) based detection coupled to mass spectrometry (MS) was used for multiple oxylipin analyses. For GC-MS, the samples have to be volatile and thermal stable, which can be achieved by additional derivatization steps [96,97]. Hence, the main analytical interfaces for multiple lipid mediator analyses are HPLC-MS/MS systems. Other MS detection systems like time of flight or ion trap mass analyzer are not suitable for eicosanoid detection, as there is no discrimination of the different regio isomers.

HPLC-MS/MS analysis

The detection of multiple eicosanoids and other lipid mediators in this work was established in the lab by the application of dynamic multiple reaction monitoring (MRM) LC-MS/MS analysis using an Agilent® HPLC system (1200 series), coupled to an Agilent® 6460 Triple quadrupole mass spectrometer with electrospray ionization (ESI) source. The advantages of dynamic MRM measurements are an improved sensitivity and reduction of concurrent transitions due to time segmentation leading to excellent quantitative data. Unlike MRM scans, the triple quad MS exclusively monitors the transitions from compounds of interest in just a single time segment within the analyte elutes. This allows for fewer MRM transitions during each MS scan and enables longer dwell times as well as reduced overall cycle time. Hence, more data points per peak can be achieved, resulting in improved quantitative data. A requirement for dynamic MRM measurements is the knowledge about the transitions of each oxylipin of interest. That means that it can only be used for targeted analysis. For this dissertation, several lipid mediators of interest for infection and related inflammation processes were selected from the literature [5,42,58,74,82,98] and purchased as pure standards. The MS parameters including the source parameters of these substances were optimized as shown in **article I** and additionally in **article II**. Next to the oxylipin analysis, the limited stability of these analytes has to be considered during sampling and extraction. Moreover, long-term storage (more than a year) affects the blood plasma samples, in particular, it increases non-enzymatic formed oxylipins [99] as well as the degradation of lipid mediators in cell culture media [100]. Therefore, all samples were immediately placed on dry ice or snap frozen in liquid nitrogen and stored at -80 °C. The maximum duration from storage to extraction was three months and this time period was kept for all extracted samples until measurement. For the inhibition of auto- oxidation processes, different inhibitors were used in literature, including general antioxidants like butylated hydroxytoluene (BHT), divalent metal cation dependent enzyme inhibitors like ethylenediaminetetraacetic acid (EDTA), COX inhibitors like indomethacin and inhibitors of the soluble epoxide hydrolase like 12-(3-adamantan-1-yl-ureido)-dodecanoic acid (AUDA). The last of these mentioned compounds prevents the conversion of EETs to the less bioactive dihydroxyeicosatrienoic acids. The use of different inhibitors should be handled with great care, because their appearance in the sample in large amounts can negatively influence the measurement. BHT was used for all samples and additionally AUDA exclusively for murine liver analysis (**article III**), because liver and kidney show high activity of this enzyme [101]. Furthermore, pig blood plasma was collected using EDTA monovettes (**article I**). A cryoPREP® CP02 tissue disruption system was used for samples homogenization and mechanical pulverization, enabling a very fast pulverization of frozen samples including murine bone and cartilage. The lipid mediators were extracted with cold 50% methanol containing BHT and AUDA if needed. For the quantification internal deuterated standards were added, consisting of 12-HETE-d_8, 13-HODE-d_4, PG E_2-d_4, resolvin D1-d_5 and AA-d_{11}. Depending on the research hypothesis an alkaline hydrolysis step was done, carried out to obtain the total amounts of lipid mediators independent of their chemical modification. The disadvantage of this extraction step is the loss of prostanoids, LTs and SPMs. To compensate for this limitation, the samples were split in half, when enough material was available, and extracted both with and one without alkaline hydrolysis. This option was especially exploit for samples from infected pigs. A purification of the sample through solid phase extraction is very useful to eliminate contaminants like proteins, inorganic salts and non-lipid metabolites, can cause ion-suppression effects depending on their matrix. The detailed extraction procedure was adapted with modifications from Rothe et al. [102] and described in **article I** along with the HPLC-MS/MS methods.

MALDI-FTICR-MS-Imaging

MS-Imaging systems like the solariX MRMS (magnetic resonance mass spectrometry) generates information on the localization and distribution of metabolites or proteins within the tissue. In general, samples for metabolome analyses were obtained as extracted homogenates that were often ionized through electrospray ionization (ESI), which results in the loss of localization information of compounds in the tissue. For MS-Imaging, cryosections were analyzed and metabolites were ionized through matrix-assisted laser desorption/ionization (MALDI). This technique enables spatially resolved mass spectra of metabolites inside the sample and is therefore of interest when study host-pathogen interactions. A very important factor of this technique is the resolution size of the images, which is constantly improved and can reach a spot size several hundred nm. This, however, requires post-ionization steps [103]. The resolution of the mostly frequently used, commercial available instruments are only in a µm range [104,105] and a resolution size of 50 µm was used on the solariX MRMS. The insufficient resolution and the disruptive feature of the laser are great challenges in the study of host-pathogen interactions. The commercial solariX laser destroys antigen surfaces structures and RNA, which is why neither a staining with antibodies nor fluorescent *in situ* hybridization failed. The group of Manuel Liebeke recently showed that with a special atmospheric pressure MALDI-MS-Imaging, samples for fluorescent *in situ* hybridization could be used [106]. However, MALDI-MS-Imaging can be used to identify distribution patterns within the tissue histology even with its low spatial resolution. It also expands the information about bioactive lipids like S1P and C1P, which cannot be detected with the used HPLC-MS/MS measurement, through the MS scan data. For the practical application of MS imaging measurements, MALDI matrices suitable for low-molecular weight compounds in negative and positive ionization mode are needed as reviewed in [107]. The main tasks of the matrices are an efficient analyte ionization, including incorporation of the metabolites into the matrix [108], and a high absorption at the irradiation laser wavelength. The general advantage of MALDI matrices compared to other ionization techniques for MS analysis are their high sensitivity and the solely generation of single charged ions [107]. The analysis of S1P and C1P species with different matrices was tested and optimized. The non-toxic matrix 9-aminoacridine [109] was found to be appropriate with respect to handling and C1P and S1P signal intensity, and was hence used for the measurements. Furthermore, this matrix has been successfully used in the literature for the detection of bioactive lipids [110]. As for other analytical methods, the sample preparation is a critical step for MALDI-MS-Imaging. Fresh cryosections from snap-frozen material are superior to paraffin embedded sections regarding metabolite degradation processes and additional background signals derived from the embedding medium. Therefore, cryosections should be made without contact to embedding media, dried using freeze drying to sustain spatial-resolution, mounted with matrix and measured within one day. Some tissues like mice lungs are not robust to be sliced without the stabilizing embedding matrix. Supporting embedding matrix like carboxymethylcellulose can be used, if matrix signals are outside the analyzed mass-to-charge-ratio [111]. The complete sample preparation and MS-Imaging parameters are described in **article IV**.

Respiratory tract infections and corresponding lipid mediator analyses

Infections of the respiratory tract are the fourth most common reason for the cause of mortality worldwide [112]. Major pathogens causing such infections are IAV [113] and the Gram-positive bacteria *S. aureus*, *S. pneumoniae* [114] and *S. pyogenes* [115]. There is evidence that bacterial and viral co-infections accelerate the mortality rate as compared to infections with single agents [116]. The immune system plays a major role in the recognition and elimination of the pathogens and can be influenced by bioactive lipids, as described previously. This thesis elucidated lipid mediator profiles for the mentioned viral and bacterial infections in selected different infection models, i.e. 16HBE cells, C57Bl/6J, DBA/1 and B10.Q mice as well as German landrace pigs.

Epithelial cells like 16HBE are the initial protective barrier against viruses and bacteria and an important lung compartment with respect to initiate immune system regulation. It is well documented that IAV-mediated lung tissue damage increases the susceptibility of the human host to secondary bacterial infections [32,117]. The infection of 16HBE cells as an *in vitro* model reveals valuable insights into the oxylipin response. These insights, however, are restricted to a single cell type. During the events of microbial and viral infections, multiple cell types that all have different functions in the immune system and each express a specific pattern of bioactive lipids interact, guaranteeing a controlled induction and resolution of the immune response. Therefore, the analyses of lipid mediator profiles were extended to animal infection experiments using mice and pig as hosts. The immune system of both animal models has been part of extensive research in the past years [118,119]. With the short generation time and the simple husbandry mice became a well-established animal model with different genetic strains. A critical parameter for research focusing on infections with human-pathogenic virus and bacteria is the transfer of research results to human infections. Therefore, all infections within this thesis were done using human-adaptive strains of pathogens and the hosts were expanded to pigs. Pigs and their IAV can have an important role for human pandemic viruses due to gene reassortment and due to the fact that European pig livestock plays a role as IAV reservoir [120]. Compared to other infection models like the mouse, the pig is more closely related to humans in terms of anatomy, physiology and genetics. The organs of pigs and humans are similar in size and function [121,122]. Moreover, there are very close homologies between human and pig protein and genome sequences [123]. The immune system of the pig is also more closely related to the humans compared to the one of the mice in terms of immune cell populations and toll-like receptors [124,125]. These similarities suggest that the pig might be a more superior infection model than other organisms. Regarding this new approach, this thesis provides the first published dataset of lipid mediators detected under IAV infection in pigs.

Studies focusing on lipid mediator profiling during bacterial infection are unexplored, in particular for *S. pneumoniae*, and viral co-infections. The majority of studies on host eicosanoid profiles in infectious diseases is restricted to single infections with the pathogens *Escherichia coli* [126], *Borrelia burgdorferi* [127], *Pseudomonas aeruginosa* , and IAV [42,128] or is focused solely on PG E_2 [129-132] and its related receptors [132]. This thesis expands the knowledge of host-derived oxylipins of pigs during IAV (H1N1pdm09) infection for the sample types lung, spleen, blood plasma and bronchoalveolar lavage fluid (BALF). Furthermore, this work provides data on bacterial infection with human-adapted strains of *S. aureus* (strains LUG2012 and 113), *S. pneumoniae* (strains TIGR4 and 19F), IAV (H1N1pdm09) as well as bacterial-viral co-infections in C57Bl/6J mice and 16HBE cells using HPLC-MS/MS analysis. For mouse infections, the oxylipin profiles were detected in lung, spleen and blood plasma samples, while the intracellular lipid mediator concentration was detected for cell line infections. Additionally, the paws and liver lipid mediators upon *S. pyogenes* infected C57Bl/6J, F1 generation of DBA/1 and B10.Q mice were

analyzed. The measurements were extended with the spatial resolution of the sphingolipid C1P and S1P in mice organs using MALDI-MS-Imaging. Taken together, this thesis shows a broad influence of infections on lipid mediator profiles in all model systems and delivers interesting targets for further studies.

Perturbations in the lipid mediators profile of pigs caused by Influenza A H1H1 infection (article I)

Eight-week-old castrated German landrace piglets were infected intranasally with human-adapted IAV H1N1 (A/Bayern/74/2009) and necropsies were performed on days 4, 7, and 21 post infection (dpi) as described in **article I**. The infected animals were tested positive for intranasal virus load. Atelectasis was observed for the pigs during a mild infection. We analyzed the lipid mediators from the sample types blood plasma, spleen, lung and BALF of infected and control animals. The sample types were chosen to help monitor local (lung, BALF) and systemic (blood plasma, spleen) host dependent oxylipin perturbations resulting from an IAV infection. Other IAV infection studies in mice or human mainly focused on lung, BALF, nasal washes [42,74] or endotracheal aspirate [76], whereas data from sample types representative for a systemic immune response are missing.

Lipidomics revealed significant changes in IAV infected pigs compared to non-infected (control) animals for all types of sampling material. The most perturbations were observed for spleen and lung samples at four and seven dpi (Figure 1). For the spleen, elevated amounts of the oxylipin precursors AA, DHA and linoleic acid as well as eicosanoids like pro-inflammatory $PGF_{2\alpha}$, anti-inflammatory 12-and 15-HETE and 14,15-EET were found in the infected animals. Analyses of the lung revealed similarities to the changes detected in the spleen concerning enhanced amounts of 12-HETE, 15-HETE and 14,15-EET. Furthermore, 14- and 17-HDHA levels were increased during infection. For mice, 17-HDHA was shown to enhance specific influenza antibody production [75]. Furthermore, 17-HDHA was also able to promote B cell activation and differentiation [75]. Besides the positive effect on host B cell activation, 17-HDHA was able to inhibit viral nucleoprotein mRNA expression in human lung epithelial cells [74]. The same effect was reported for 12-and 15-HETE [74]. Indeed, our results showed that the infected pigs were able to overcome infection (no virus detection at seven dpi), while simultaneously most lipid mediator levels returned to the basal level. Both HETEs, derived from 12-and 15-LOX, have anti-inflammatory effects which may indicated resolution of inflammation even when intranasal virus load was still detectable. This hypothesis was supported by the detection of inhibitory CD8αα expressing T cells as early as four dpi in nose and BALF samples in these animals, which most likely prevents an excessive immune response [133]. Infection experiments in mice with the same IAV H1N1 strain confirmed the results of enhanced HETEs and HDHAs levels in the lung as displayed in **article IV**. Related to the lung, BALF analyses confirmed increased amounts of 17-HDHA during IAV infection as already observed in the lung.

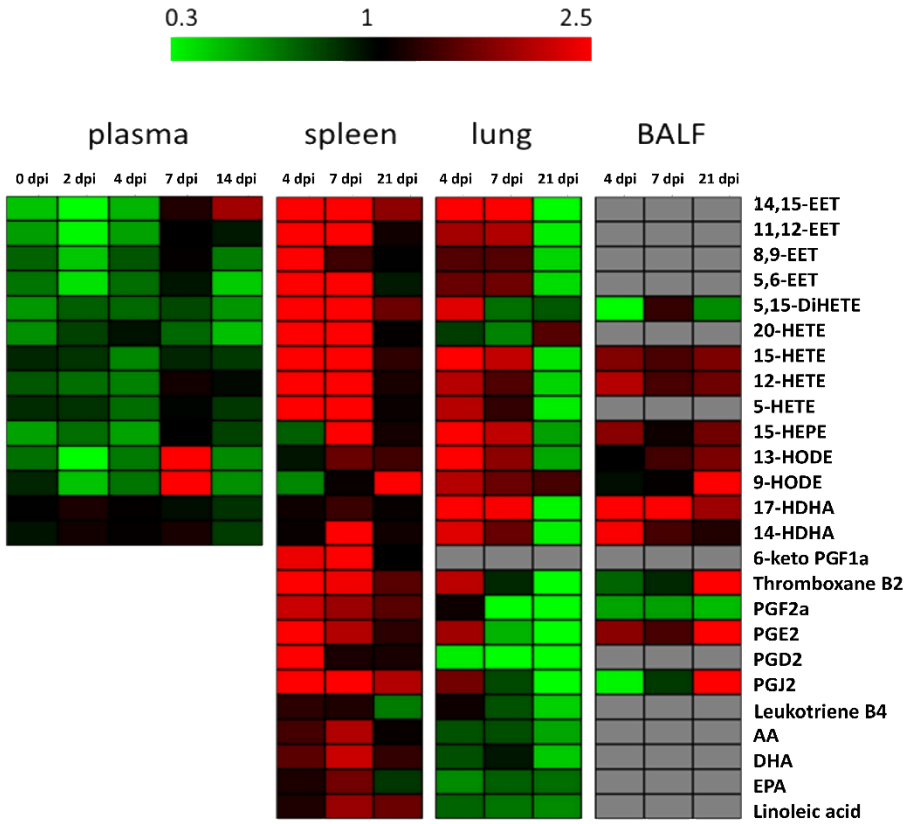

Figure 1: Heatmap displaying fold changes (infection/control) of all measured eicosanoid amounts of all sample types and time points. Decreased levels are shown in green, increased amounts in red and comparable amounts in black. Grey fields: below detection limit.

Studies on mice using mouse adapted high-pathogenic IAV strains [42,74] showed an impact on 12-HETE, 15-HETE and 17-HDHA levels in the lung similar to those in lungs of IAV infected pigs. The results were comparable despite different experimental setups i.e. choice of host, severity of infection and sampling time points. These results may indicate an IAV-specific eicosanoid pattern and the results from pig infection show affected splenic lipid mediators, which could be helpful regarding therapeutic treatment.

Lipid mediator screening of 16HBE cells during bacterial and viral infections (article II)

Epithelial cells like 16HBE are the initial protective barrier against viruses and bacteria and an important lung compartment to initiate immune system regulation. It is well documented that IAV-mediated lung tissue damage increases the susceptibility of the human host to secondary bacterial infections [32,117]. The analysis of the pathogen-mediated changes in the intracellular lipid mediator profile could help us to understand pathogen-specific host immune responses in viral and bacterial single as well as co-infections. In particular, oxylipin analysis of *S. pneumoniae* and viral co-infections, is unexplored. Therefore, 16HBE cells were used for mono-infections with *S. aureus* LUG2012, *S. pneumoniae* TIGR4 and IAV (A/Bayern/74/2009) as well as for corresponding co-infections.

The infections were conducted at a multiplicity of infection (MOI): 50 for *S. pneumoniae* and MOI of 10 for *S. aureus*, followed by 4 h of antibiotic treatment. Viral infections were performed at MOI 0.1 for 24 h. This amount of virus and the time point were determined in preliminary studies as an optimal infection with no significant cell death. Co-infection experiments were performed with a secondary bacterial infection after virus infection for 24 h. The strongest effects were observed for *S. aureus* in single and co-infection with IAV. The number of vital cells dropped down by approximately 50% and a multitude of altered intracellular lipid mediator levels could be observed. Eicosanoids from AA conversion (HETEs) showed perturbations for all tested infections compared to control and the DHA- and EPA-derived and analyzed lipids (HDHAs and 18-HEPE) were only affected by single infection with *S. pneumoniae* TIGR4.

The pro-inflammatory 5-HETE, in particular, was elevated in all bacterial infections, including co-infections (Figure 2). We detected a basal level of approximately 1.4 ng/sample (control), which was significantly increased in all single bacterial and bacterial and viral co-infections. The IAV single infection itself had no impact on 5-HETE production. This observation may indicate a prominent role of the pro-inflammatory metabolite 5-HETE in bacterial infections of the bronchial compartment. 5-HETE is known to enable transcellular migration and aggregation of neutrophils and to induce airway contraction [44,134]. This lipid mediator is generated from AA within the 5-LOX pathway [135]. The interplay of 5-LOX with the nuclear membrane-associated 5-LOX activating protein FLAP results in AA oxidation to 5-hydroxyperoxy-eicosatrienoic acid (5-HpHETE). Subsequently, 5-HpHETE is then converted by glutathione peroxidase to 5-HETE or to leukotrienes. Moreover, the different pro-inflammatory 5-LOX pathway intermediates are associated with diseases like diabetes [136], Alzheimer [137], and atherosclerosis [138].

The majority of changes in the lipid mediator profiles were detected upon *S. pneumoniae* infections. Enhanced amounts of 15-HETE, 13-HODE, 18-HEPE, 13-HDHA, and 14-HDHA were exclusively detected in pneumococcal infections (Figure 1). Both 15-HETE and 13-HODE are PPARγ agonists. This receptor is known for its anti-inflammatory properties and Solleti et al. [139] showed that the loss of epithelial PPARγ in the lung leads to increased inflammatory mediator production. This could explain why enhanced PPARγ activation is necessary for the resolution of inflammation. The observed changes during bacterial infections have not been reported before and this study helps to understand the host response on epithelial cell type level. For future studies, infection experiments that are closer to *in vivo* conditions of tissues like air–liquid interface cell culture should be taken into account for verification of our findings.

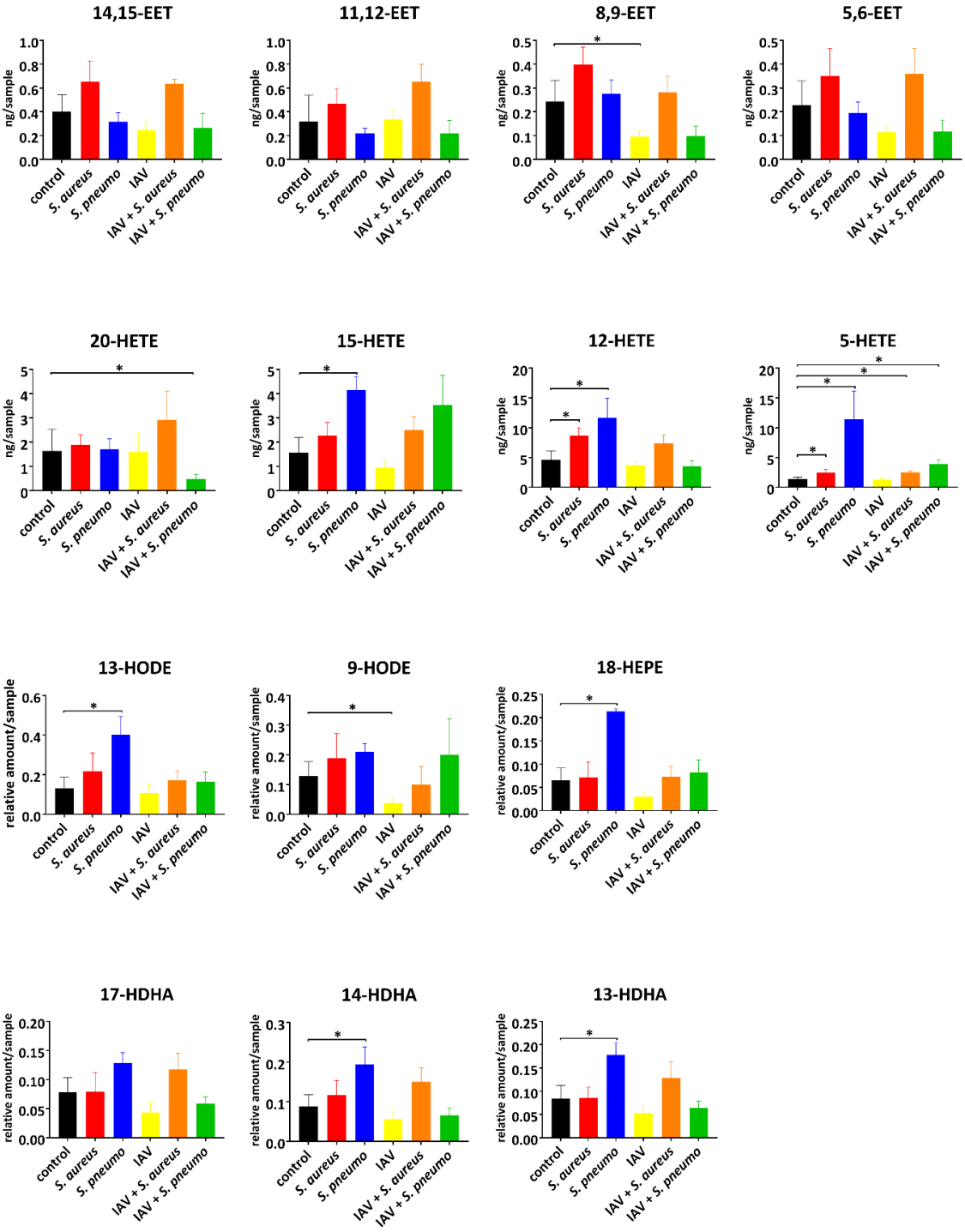

Figure 2: Intracellular lipid mediator amounts in response to indicated bacterial and viral infections: *S. aureus* LUG2012 (red), *S. pneumoniae* TIGR4 (blue), IAV rH1N1 (yellow), uninfected control (black) and the co-infections IAV/*S. aureus* (orange), as well as IAV/*S. pneumoniae* (green). The bars denote mean values ± standard deviations. For statistical analysis, the Mann–Whitney U-test was used for $n = 15$ (controls) and $n = 4$ (infections). The p-values were compared to a significance level α of 0.05 corrected for multiple comparisons using Bonferroni correction for 9 clusters of oxylipins and 5 comparisons resulting from infection conditions. Asterisks indicate significant changes.

Oxylipin analysis of mice during septic arthritis (article III)

S. pyogenes (Group A *Streptococcus*, GAS) is a gram-positive pathogen causing a wide variety of usually non-severe disorders like impetigo and pharyngitis [115]. However, GAS infection can also turn into a severe disease courses like streptococcal toxic shock syndrome, necrotizing fasciitis, and septic arthritis (SA). In order to investigate both, autoimmunity as a facilitator of aggravated sepsis and pre-existing inflammatory joint disease as risk factors for septic arthritis, we here turned to the mouse model of collagen induced arthritis (CIA). CIA shares important homologies with rheumatoid arthritis like synovial hyperplasia and articular immune cell infiltration [140-142]. Triggering CIA prior to GAS infection, therefore, allowed for the analysis of the immune response, bone metabolism and the contribution of the synovial lining of the joint and the stromal cells to the disease process of septic arthritis.

The infection of GAS strain AP1 combined with CIA was induced in genetically susceptible DBA/1 × B10.Q (F1) mice by primary and secondary immunization with bovine collagen type II. Thereafter, the development of CIA was monitored until the start of the remission phase, 11 weeks post immunization, when mice were infected by GAS (Figure 3A). By the time of the infection, the swelling of paws induced by CIA had subsided, hence allowing subsequent detection of SA signs. Lipidomic analyses of the paws demonstrated correlations of the anti-inflammatory lipid mediators 13-HODE, 13-HDHA, and 13-HOTrE with the respective sepsis scores (Figure 3D). As with the cytokines, CIA itself did not cause an increase in eicosanoid levels. Moreover, eicosanoid levels in paws correlated positively with systemic interleukin-6 (IL-6) concentrations, suggesting interdependencies between immunologically relevant mediators during aggravated sepsis. Analysis of the lipid profiles in the liver also confirmed an increase in 13-HODE, 13-HDHA and 13-HOTrE together with pro-inflammatory 20-HETE in mice that were subjected to CIA and GAS infection when compared to controls (Figure 3E). The oxylipin 13-HOTrE was also found to be enhanced in serum samples of patients with psoriatic arthritis [143]. Both 15-lipoxygenase metabolites 13-HODE and 13-HOTrE are able to inhibit the NLRP3 inflammasome complex [82]. Increased levels of 13-HODE were also discovered in patients suffering from sepsis [144]. The lipid mediator 20-HETE is known to be involved in both sepsis and arthritis. This metabolite is capable of influencing vasoconstriction and vasodilation by the release of nitric oxide [46,47], the inducement of cardiac protection in sepsis [48] and the inhibition of prostanoid synthesis like PG E_2 [49]. It seems that high levels of 20-HETE in the liver from CIA+GAS animals (fold change > 7) were a result of the combined disorders. Furthermore, the analysis of paws from C57BL/6 mice infected with GAS led to the finding of increased amounts of PG E_2 and PG D_2, which are both involved in a balanced bone turnover [37].

In summary, the results demonstrated that a pre-existing inflammatory joint disease promotes the incidence and severity of SA and increased sepsis scores that are also coupled with elevated cytokines and eicosanoid levels.

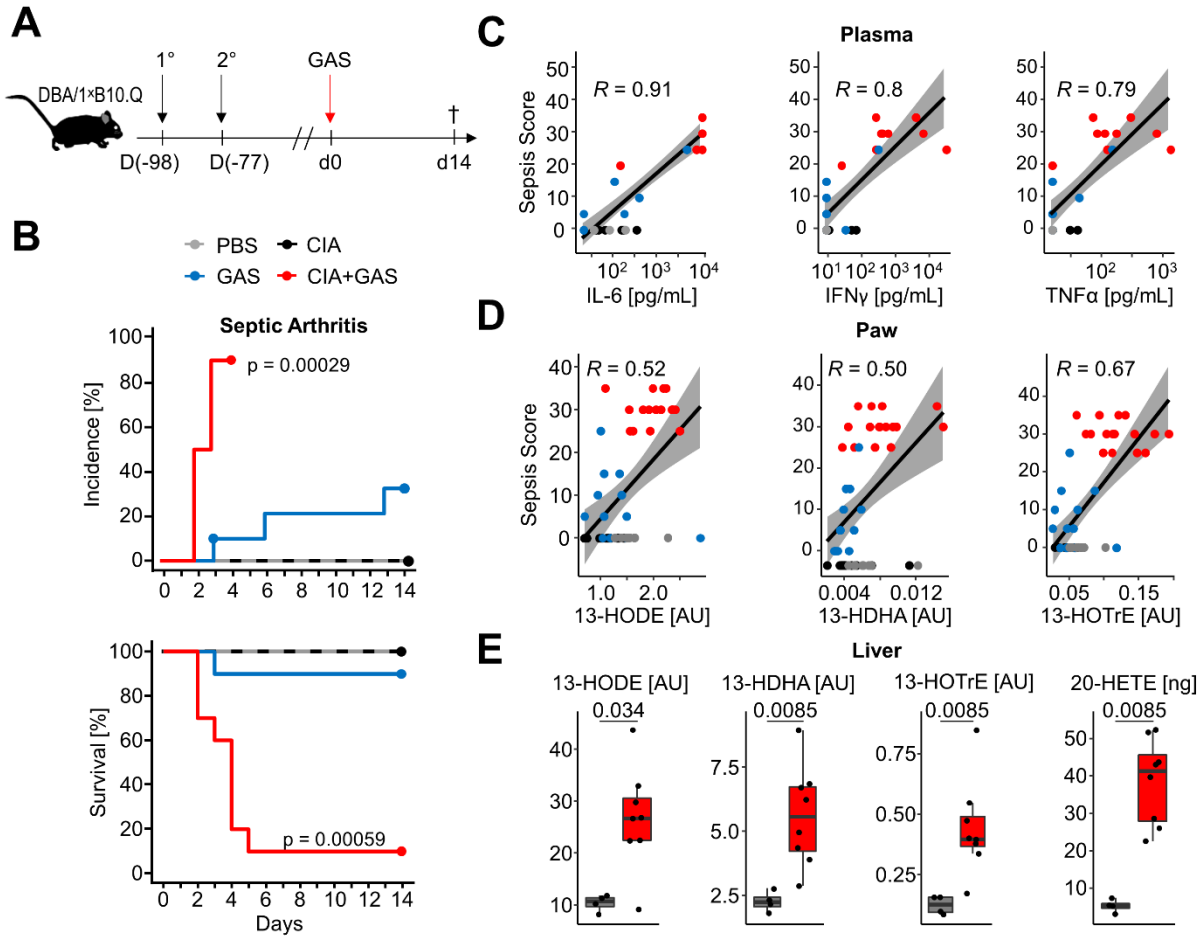

Figure 3 Preceding collagen-induced arthritis (CIA) aggravates sepsis and septic arthritis. (**A**) Scheme for experimental procedure. 6-8 week old DBA/1 ˣ B10.Q mice of the F1 generation were immunized with bovine collagen type II in complete Freund's adjuvant (1°) and were boosted 3 weeks later (2°). CIA developed and was monitored for 11 weeks prior to infection with 2 ˣ 106 colony-forming units of Group A *Streptococcus* (GAS). (**B**) Kaplan-Meier estimator curves of septic arthritis incidence (top) and survival (bottom) illustrate that preceding CIA (n = 10) exacerbates disease severity which is accompanied by a significant increase of septic arthritis occurrence when compared to mice without a previous CIA (n = 10). ***p < 0.001, log-rank test. (**C, D**) Bivariate linear correlation of sepsis scores with plasma levels of pro-inflammatory cytokines in plasma (C) and amounts of eicosanoids in paws (**D**). Mice with combined CIA and GAS infection show the highest sepsis scores which moderately to strongly correlate with Interleukin (IL-)6, Interferon (IFN)γ, Tumor Necrosis Factor (TNF)α, 13-HODE, 13-HDHA and 13-HOTrE. Gray areas depict the 0.95 confidence interval of the regression line. R: Pearson product-moment correlation coefficient. (**E**) Boxplots showing the increased eicosanoid levels in liver from mouse with CIA and GAS infection (red boxes, n = 8) compared to PBS controls (gray boxes, n = 4). *p < 0.05, **p < 0.01, Mann-Whitney U test.

Lipid mediator analysis of mice during bacterial and viral infections (article IV in preparation)

C57BL/6 mice were chosen for infection experiments similar to 16HBE cells. Therefore, mice were infected with *S. pneumoniae* 19F, *S. aureus* strains LUG2012 (high pathogenic) and 113 (low pathogenic) or IAV H1N1 (A/Bayern/74/2009). In addition, a pneumococcal-IAV co-infections was performed. Concordant to pig infections described in **article I**, the sample types blood plasma, lung and spleen were screened for lipid mediator perturbations. Moreover, the spatial resolution of S1P and C1P was detected in tissue samples using MALDI-MS-Imaging. The existence of bacterial pathogens was confirmed by immunofluorescent staining. The proteome analysis of the lungs demonstrated changes of certain proteins involved in lipid mediator analysis.

Oxylipin analysis of the lungs revealed increased amounts of lipid mediators mainly derived from LOX conversion during an IAV infection (5 dpi) namely pro-inflammatory 5- and 20-HETE as well as anti-inflammatory 12- and 15-HETE, as shown in Figure 4. Furthermore, we measured enhanced levels of anti-inflammatory 13-HDHA, 14-HDHA and 17-HDHA in association with IAV infection. Additional proteome analysis revealed increased amounts of two proteins involved in oxylipin biosynthesis namely cytosolic phospholipase A_2 and the 5-LOX activating protein FLAP. The observed increase of 17-HDHA confirmed former IAV related mouse infection studies [42,74] as well as the results of the pig infection as described in **article I**. Furthermore, the analysis of the infected mice lungs showed that in addition to 17-HDHA, also other oxidation products from DHA conversion namely 13- and 14-HDHA were affected by IAV infection. Under co-infection conditions, the HDHAs and HETEs were not found to be elevated. For 17-HDHA this phenomenon has also been described for IAV infected children with a bacterial co-infection [145]. Although the underlying reason remains still elusive, this could be a sign for dampened inflammation.

Moreover, the amount of the pro-inflammatory 20-HETE was enhanced (5 ng/100 mg) upon infection with the high-pathogenic strain *S. aureus* LUG2012. Besides, *S. aureus* LUG2012 infection led to increased levels of the EPA metabolite 18-HEPE. In general, infections with *S. pneumoniae* and *S. aureus* 113 had only little influence on the analyzed lipid mediators. The co-infection led to decreased amounts of 20-HETE and 12-HETE as well as an increased 18-HEPE level compared to the control and to corresponding mono-infections. The level of 15-HETE upon co-infection was reduced compared to controls, and 5-HETE was negatively affected by the co-infection compared to IAV infected animals. A further decrease in the amount of oxylipins upon co-infection compared to IAV mono-infection was measured for 14- and 17-HDHA. Analyses of plasma and spleen samples from infected mice revealed perturbations for *S. aureus* LUG2012 in particular. For both sample types the increase of 20-HETE during severe staphylococcal infection was observed and also detected in the lung. Besides the local immune response, a systemic reaction of the lipid mediator response was visible. This oxylipin was also affected in mice infected with GAS in combination with CIA as described in **article III**. On the single oxylipin level, the pneumococcal infection was quite unobtrusive. Whereas the pneumococcal infection was unremarkable on the single oxylipin level, an increase in the 13-HODE/9-HODE ratio was exclusively detected for this infection in all sample types. This observation suggests an anti-inflammatory state and might help to evaluate this specific infection.

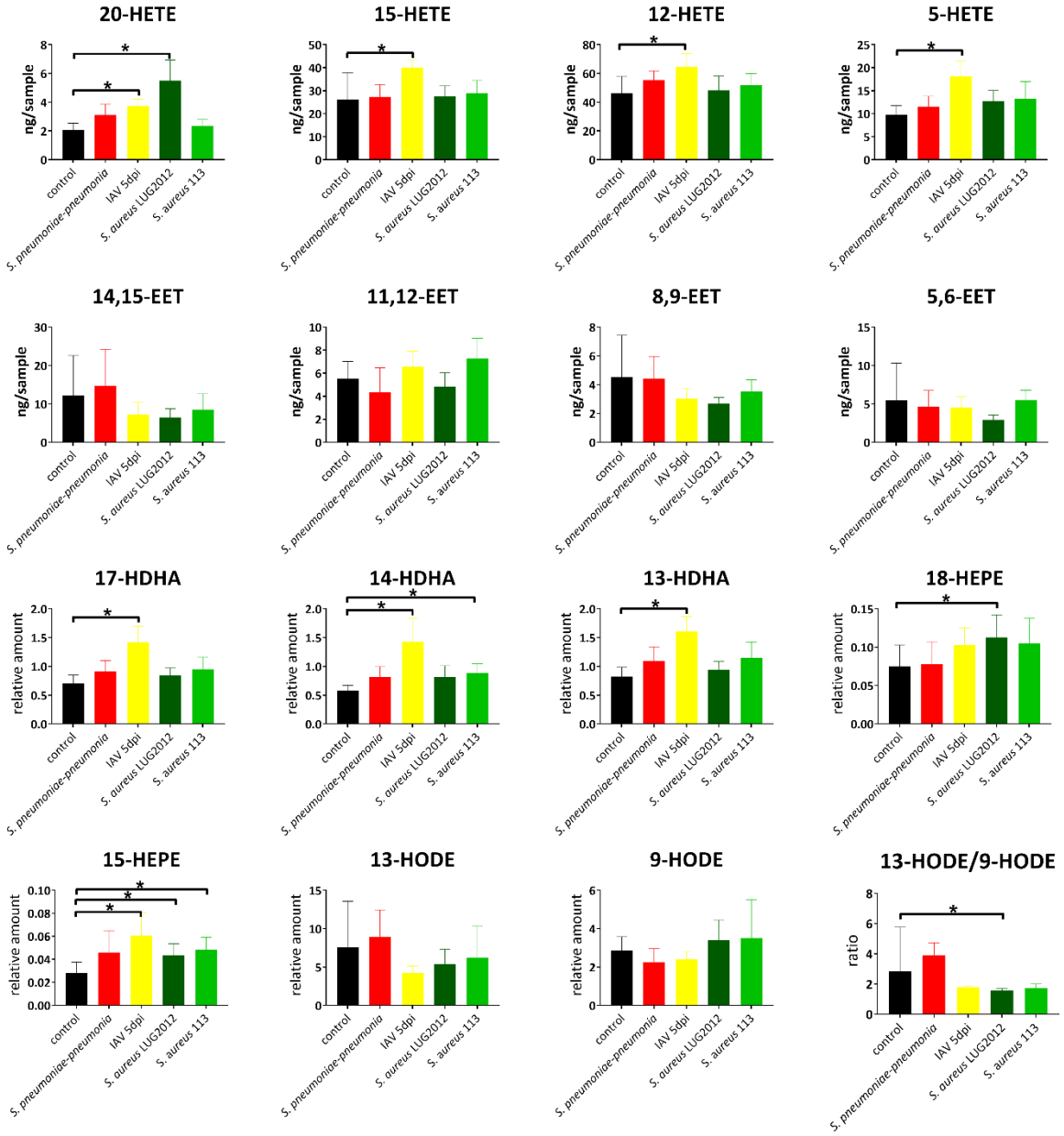

Figure 4: Lung oxylipin amounts in response to bacterial and virus mono-infections: control (black), *S. pneumoniae* induced pneumonia (red), IAV (yellow), *S. aureus* strain LUG2012 (dark green) and strain 133 (light green). The bars denote mean values ± standard deviations. For statistical analysis, Kruskal-Wallis test with Dunn´s multiple comparison test for n =13 replicates (control) and n = 8-10 replicates (infections). The p-values were compared to a significance level α of 0.05 and significant changes were marked using asterisk. For analysis, the samples were normalized to 100 mg.

In addition to the HPLC-MS/MS analysis of lipid mediators, the spatial resolution of bioactive lipids within the lungs and spleen was detected through MALDI-MS-Imaging. For statistical evaluation, ROC analysis was performed, which led to the finding that the amounts of C1P and S1P in particular were affected by infections. For lung and for spleen, increased levels of different C1Ps were detected during co-infection with *S. pneumoniae* 19F and IAV. For C1P, several derivatives with different acyl chain lengths exist. On

the one hand, C1P has pro-inflammatory properties including activation of cell migration, which is described for murine macrophages [53] and human monocytes [20]. On the other hand, C1P seems to prevent the biosynthesis of pro-inflammatory ceramides during respiratory infections [87]. Three different derivatives (C18:0, C24:1 and C26:1) showed a decrease under IAV infection and an increase under co-infection conditions compared to control and corresponding mono-infections in the spleen (Figure 5). Moreover, an alignment of MS-Imaging with histology scans from hematoxylin and eosin (HE) staining revealed that the distribution of the long chain C1P (d18:1/26:1(17*Z*)) was higher in the red pulp than in the white pulp. Furthermore, the coinfection had an impact on the red pulp leading to increased amounts of long chain C1P. A splenic pulp-specific distribution is known for S1P [146], but had not been described for C1P so far. For lung tissues, an increase of the C1P (d18:1/18:0) and C1P (d18:1/24:1(15*Z*)) amounts compared to control and mono-infections was measured in co-infected lungs. The observed accumulation of C1Ps during co-infection in lung and spleen may suggest a local and systemic host immune reaction. The pneumococcal infection alone caused a decrease in C1P (d18:1/18:0) and thus differed from spleen samples in its effect.

Furthermore, a decrease in S1P concentration upon *S. pneumoniae* infection was observed for the lung but not for the spleen. An additional difference to the spleen findings was the impact of IAV leading to increased S1P levels in the lung. Whereas splenic levels decreased, an increased amount in the lung was detected. Indeed, the enzyme sphingosine kinase SphK, which is responsible for S1P biosynthesis, was shown to be upregulated by the IAV to promote virus propagation [147]. The accumulation of S1P in the lung was not measured upon co-infection. This could be due to the pneumococcal influence or due to reduced IAV infection time. The latter was necessary to reduce the infection burden.

The amounts of S1P in lung and spleen samples were decreased under co-infection conditions. S1P is mainly known for its pro-inflammatory properties including the activation of eicosanoid synthesis through activation of COX-2 [51]. S1P is not distributed equally among organ and body fluids. High amounts of S1P are found in blood plasma and lymph, whereas the concentration in the secondary lymphatic organs is very low. This S1P gradient is important for lymphocyte traffic [148]. The decrease during IAV and corresponding co-infection may be beneficial for facilitating immune cell migration into the spleen which seems to be independent of pneumococcal infection.

A key finding of this study was, that apart from eicosanoids and oxylipins derived from DHA, EPA or linolenic acid also other bioactive lipids like S1P and C1P also seem to play an important role in host immune response and showed infection-specific alterations. The alterations were particularly observed during co-infection conditions, where perturbations in the classic lipid mediators were detected less. The role of C1P and S1P during infection processes is rarely understood but should be more analyzed in more detail in future lipidomic studies.

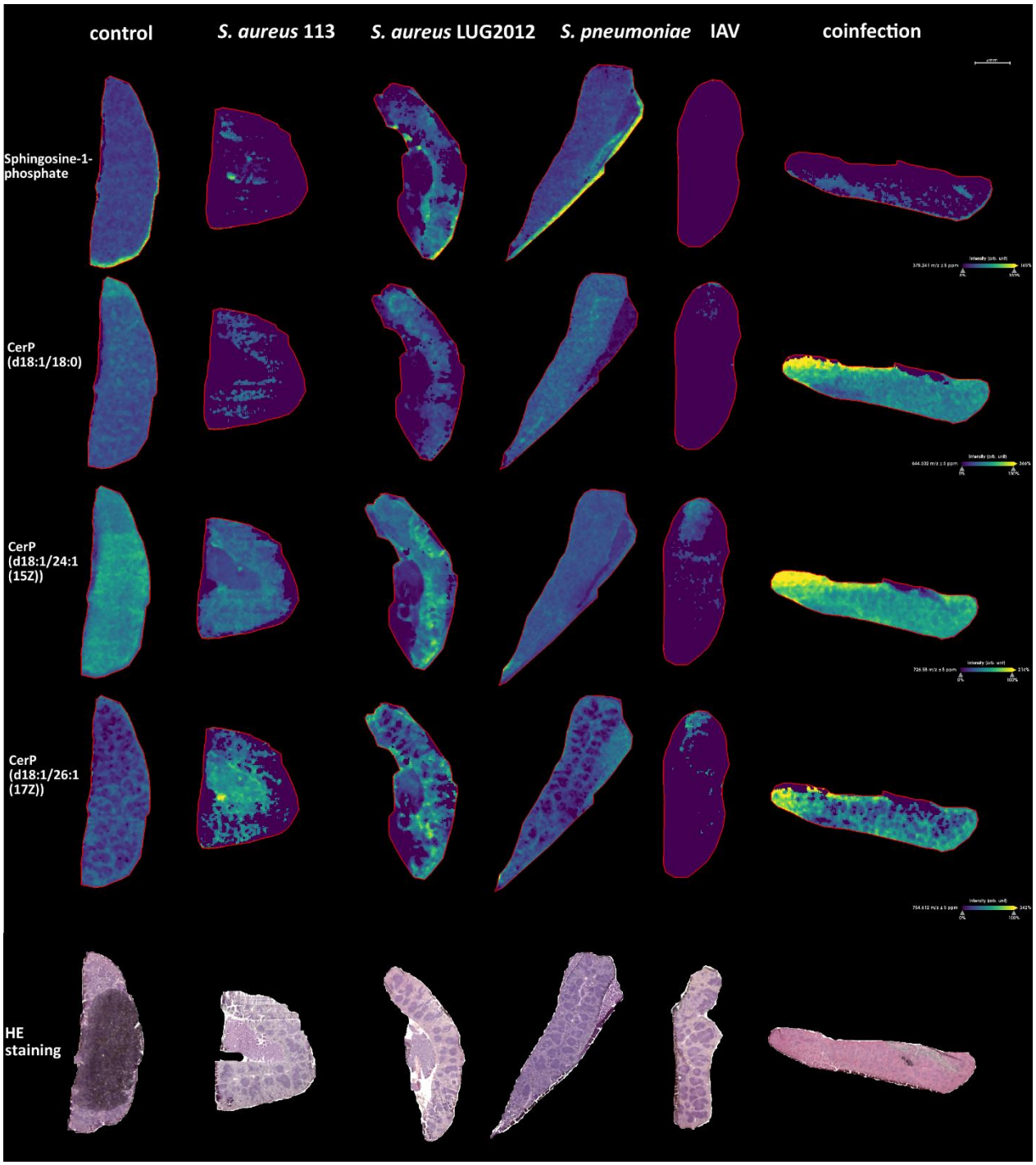

Figure 5: MALDI-MS-Imaging and HE staining of spleen samples. Representative images from three replicates per condition are shown. The measurements include samples from infection with *S. aureus* strains 113 and LUG2012, *S. pneumoniae* (colonization), IAV (5 dpi) and co-infection. The compound-related heatmaps illustrate high intensities in yellow and low abundances in purple normalized to total ion count.

Concluding remarks

The results of bioactive lipid analysis consolidated in this dissertation clearly demonstrated the involvement of lipid mediators in the host response towards infections with bacterial and viral pathogens, i.e. *S. aureus*, *S. pneumoniae*, *S. pyogenes* and IAV. Novel results in particular for bacterial infections were described for up to three different infection models that were mouse, pig and cell culture. A transfer to other hosts and pathogens should be possible. The introduction of the pig as an approximation to human (**article I**), showed oxylipin changes, of which most, were also reproduced in mouse infections (**article IV**). An increase of 17-HDHA is described for other IAV infection studies, as its supporting role on IAV-antibody production is described. The measurements performed in this dissertation expand the knowledge of the DHA oxidation products affected by IAV infection through the detection of enhanced levels of 13- and 14-HDHA. One main difference between pig and mouse infections was the detection of increased HDHA amounts in lung and spleen of the pig, whereas only the lungs were affected in murine samples. This difference should be analyzed in further studies, including the manipulation of their biosynthesis. Selective inhibitors are necessary to understand the impact on single lipid mediators. For many bioactive lipids, inhibiting drugs approved for clinical use in humans are still limited. An IAV infection of 16HBE cells (**article II**) led to minor changes compared to bacterial infections, which could be the result of the chosen cell line or provoked by the missing immune system. Due to the fact that lipid mediators are involved in immune system regulation, infection models with a complex immune system, like that of mice or pigs, seem to be superior models to study host bioactive lipid responses.

The increase of 20-HETE, described in **article III and IV**, in association with severe infections in different sample materials should be the target of further studies to elucidate the role of this eicosanoids during inflammation. Through the analysis of the different sample types of lung, spleen, liver, blood plasma, paws and bronchoalveolar lavage, there is evidence that perturbations of lipid mediators under certain circumstances are not restricted to the site of infection. Moreover, infections contemporaneous affected the amounts of oxylipins with pro- and anti-inflammatory properties. Kinetic data was received from pig infections. Experiments on the development over time should be the focus of further studies.

In general, diminished effects were observed for eicosanoid and oxylipin analysis in co-infections. The MALDI-MS-Imaging revealed an accumulation of S1P as well as C1P derivatives C1P (d18:1/18:0) and C1P (d18:1/24:1(15*Z*)) in murine lung and spleen. The knowledge of the biological function of these sphingolipids is very limited but the data suggest concentrating on these compounds for further co-infection experiments. Independent from the detected bioactive lipids, the resolution of commercially available MALDI-MS-Imaging systems must be revised for a resolution that enables single pathogen detection. Additionally, the use of soft ionization techniques instead of destructive laser beams would allow for FISH or immunofluorescent staining after the MS-Imaging measurement. This would facilitate pathogen imaging and be advantageous for the study of host-pathogen interactions.

metabolites

MDPI

Article

Eicosanoid Profile of Influenza A Virus Infected Pigs

Daniel Schultz [1], Karen Methling [1], KoInfekt Study Group [2], Michael Rothe [3] and Michael Lalk [1,*]

1 Institute of Biochemistry, University of Greifswald, 17487 Greifswald, Germany
2 Friedrich-Loeffler-Institute, Suedufer 10, 17493 Greifswald, Germany
3 Lipidomix, 13125 Berlin, Germany
* Correspondence: lalk@uni-greifswald.de; Tel.: +49-3834-420-4867

Received: 28 May 2019; Accepted: 28 June 2019; Published: 3 July 2019

Abstract: Respiratory tract infections caused by the Influenza A virus (IAV) are a worldwide problem for human and animal health. Within this study, we analyzed the impact of IAV infection on the immune-related lipidome (eicosanoids) of the pig as new infection model. For this purpose, we performed HPLC-MS/MS using dynamic multiple reaction monitoring and analyzed lung, spleen, blood plasma and bronchoalveolar lavages. IAV infection leads to collective changes in the levels of the analyzed hydroxyeicosatrienoic acids (HETEs), hydroxydocosahexaenoic acids (HDHAs) and epoxyeicosatrienoic acids (EETs), and moreover, unique eicosanoid changes in several sample types, even under mild infection conditions. In accordance with different mouse infection studies, we observed infection-related patterns for 12-HETE, 15-HETE and 17-HDHA, which seem to be common for IAV infection. Using a long-term approach of 21 days we established an experimental setup that can be used also for bacterial-viral coinfection experiments.

Keywords: eicosanoids; lipid mediator; Influenza A virus; infection; pig

1. Introduction

In 2016, lower respiratory tract infections caused more than two millions deaths worldwide [1], with the influenza A virus (IAV) being one of the main etiologic agents. Co-infections of IAV and different bacterial pathogens like *Streptococcus pneumoniae* [2,3] are associated with even higher mortality rates. Humans and pigs are natural hosts of IAV, which was demonstrated during the IAV pandemic in 2009 [4]. Furthermore, the pig can be a mixing vessel [5] for different IAV strains. Compared to other infection model animals like mice, the pig is more related to humans regarding anatomy, physiology and genetics. The organs of pigs and humans are similar in terms of size and function [6,7]. Moreover, there are very close homologies between human and pig protein and genome sequences [8]. The immune system of the pig is more related to the human compared to the mice in terms of immune cell populations [9] and Toll-like receptors [10]. These facts suggest that the pig might be a superior infection model.

Many viruses are able to influence the host metabolic pathways like glycolysis, pentose phosphate pathway, glutaminolysis or fatty acid synthesis to obtain energy for their replication [11]. The IAV is known to be able to change the amount of glycolytic metabolites and nucleotides in cultured animal cells [12]. So far, little is known about the effect on metabolites that are related to the immune system in the context of IAV infection.

Eicosanoids are mainly involved in the activation and resolution of inflammatory reactions [13–17], as well as hypertension [18] and pain [19]. One of the most important precursors is arachidonic acid (AA), which can be converted to prostaglandins (PG) and thromboxanes by the cyclooxygenase pathway (COX). Many of these lipid mediators show pro-inflammatory effects [20]. Hydroxyeicosatrienoic acids (HETEs) produced from AA by lipoxygenases (LOX) are known to be anti-inflammatory, like

12-and 15-HETE, or have pro-inflammatory properties, like 5-HETE [21]. The conversion of AA by cytochrome P450-like enzymes produce epoxyeicosatrienoic acids (EETs) with anti-inflammatory activities [22]. Besides AA, docosahexaenoic acid (DHA), eicosapentaenoic acid (EPA) and linoleic acid are essential precursors for the synthesis of lipid mediators. DHA- and EPA-derived metabolites like hydroxydocosahexaenoic acids (HDHAs) and hydroxyeicosapentaenoic acids (HEPEs) are as well anti-inflammatory eicosanoids and precursors of potent anti-inflammatory mediators namely protectins, maresins or resolvins [15]. Moreover, metabolites derived from linoleic acid like hydroxyoctadecadienoic acids (HODEs) are able to activate G protein coupled receptors [23].

The aim of this study was to analyze the eicosanoid profile of IAV-infected pigs, in order to gain a better understanding of the host immune response. We also investigated which kind of sample material is promising for the analysis of the host immune response to respiratory tract infections on the lipid mediator level. Therefore, samples from the local infection site (lung tissue and bronchoalveolar lavage fluid [BALF]) and samples related to the systemic immune response (blood plasma and spleen tissue) were obtained from the animals and analyzed by HPLC-MS/MS.

2. Results

2.1. Virus Infection

All animals were tested negative for IAV prior to infection experiment. In contrast, infected animals were tested positive for intranasal virus load (partially tested positive for 2 days post infection [dpi] and all tested positive for 4 dpi, data shown in supplemental material). Furthermore, atelectasis could be observed for the pigs during necropsies, with the exception of three animals at 21 dpi. However, the infected pigs didn't show clinical symptoms during the trial. Virus detection was negative from 7 dpi for all pigs.

2.2. Spleen

The spleen tissue showed the most significant changes in the eicosanoid profile during IAV infection compared to all other analyzed sample types (Figure 1). Elevated levels of eicosanoid precursors (AA, DHA and linoleic acid) were detected in the spleen samples of infected animals in particular at 4 and 7 dpi (Figure 2). The observed changes in the eicosanoid precursor levels were exclusively detected in this tissue sample material but not for the lung tissue (Figure 1). Amounts of lipid mediators resulting from AA conversion like pro-inflammatory $PGF_{2\alpha}$, anti-inflammatory 12-and 15-HETE as well as the anti-inflammatory 14,15-EET were found to be increased in the infected animals, in general at 4 and 7 dpi. For the other analyzed EETs, there were also enhanced amounts detected during infection but the differences to controls were not significant. Enhanced amounts of PGF_{2a} were previously reported for patients with chronic inflammatory arthritic diseases [24]. 12-and 15-HETE are able to inhibit the interleukin-6 secretion from macrophages induced by tumor necrosis factor α [25]. EETs are known to have anti-inflammatory effects like the activation of the peroxisome proliferator-activated receptor α (8,9- and 11,12-EET [26]) and suppression of cell degradation by nuclear factor IKBα (14,15-EET [27]).

For PGF_{2a}, a significant response could only be seen at 4 dpi and for 12-HETE only at 7 dpi (Figure 2). At 21 dpi the detected eicosanoid amounts returned to basal levels. Furthermore, the amount of 9-HODE was increased at 21 dpi (Figure 2).

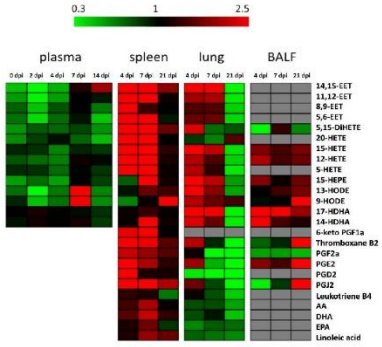

Figure 1. Heatmap displaying fold changes (infection/control) of all measured eicosanoid amounts of all sample types and time points. Decreased levels are shown in green, increased amounts in red and comparable amounts in black. Grey fields: below detection limit.

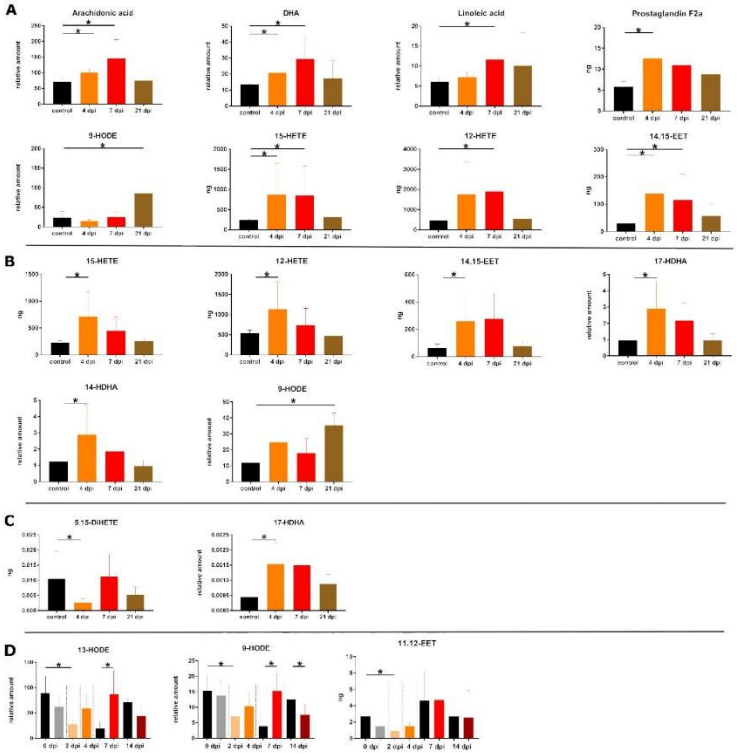

Figure 2. Overview of significant changed amounts of eicosanoids during infection in the spleen (**A**) and the lung (**B**) per g sample; the BALF per 5 mL (**C**) and blood plasma per mL (**D**). Asterisks indicate significant changes (p-value ≤ 0.05) using Mann-Whitney U test for control (n = 3 for tissue and BALF, and n at least 6 for plasma) and infection (n = 5 for tissue and BALF, and n at least 6 for plasma). The following color pattern was used: control (black), 4 dpi (orange), 7 dpi (red) and 21 dpi (brown) for **A**–**C**. For plasma (**D**) control samples for all days were illustrated in black and plasma samples from infected animals were shown for 0 dpi (grey), 2 dpi (light orange), 4 dpi (orange), 7 dpi (red) and 14 dpi (dark red).

2.3. Lung

Various changes in the lipid mediator profile could also be observed for the lung tissue representing local infection sample material (Figure 1). Like for the spleen, elevated amounts of anti-inflammatory 12-and 15-HETE, as well as 14,15-EET could be measured at 4 dpi.

In addition to the AA-derived lipid mediators, the amounts of 14-and 17-HDHA were enhanced at 4 dpi, which are products of DHA conversion (Figure 2). Perturbations in these HDHAs levels were also found in mice lungs infected with different mouse adapted influenza strains [21,28,29]. For mice, 17-HDHA was shown to enhance specific influenza antibody production [30]. Furthermore, 17-HDHA was able to promote B cell activation and differentiation [30]. With exception of 9-HODE, the analyzed eicosanoids were found in equal amounts to control at 21 dpi (Figure 2). The increased amounts of 9-HODE at 21 dpi were detected like for the spleen. Pro-inflammatory effects of 9-HODE were shown for the calcium mobilization and activation of kinase JNK through the G protein-coupled receptor G2A [23].

2.4. BALF

This sample type includes epithelial cells from the lower respiratory tract and immune cells, which is hypothesized to be useful for the analysis of respiratory tract infections. In accordance with the lung analysis, IAV infection led to enhanced amounts of 17-HDHA at 4 and 7 dpi. Moreover, a decrease of 5,15-DiHETE could be observed at 4 dpi for the infected pigs (Figure 2). The lipoxin precursor 5,15-DiHETE is a chemotactic fatty acid for eosinophils [31], which is produced in enhanced amounts from leucocytes after lipopolysaccharide activation [32]. Elevated levels of 5,15-DiHETE are known for patients suffering from chronic inflammation diseases like asthma [33] or rheumatoid arthritis [34]. At 21 dpi, no significant perturbations in the lipid mediator profile of the infected pigs were detected.

2.5. Blood Plasma

During early-state IAV infection at 2 dpi, changes in the amount of 11,12-EET were measured. For the following time points (4, 7 and 14 dpi) no significant differences between infection and control animals could be detected. Both, linoleic acid-derived lipids 9-and 13-HODE showed a drop at 2 dpi and increased levels at 7 dpi. In contrast to the pro-inflammatory 9-HODE, the lipid mediator 13-HODE has anti-inflammatory properties as peroxisome proliferator-activated receptor γ agonist [35]. Severe IAV infection in mice showed that the increasing ratio of 13:9-HODE could be useful as a potential biomarker for IAV infection but not for mild infections [29], which is in accordance with our findings.

3. Discussion

3.1. Eicosanoid Pattern of IAV-Infected Pigs Compared to Other Animal Infection Models

Most IAV infection studies focusing on eicosanoid analysis used C57BL/6 mice as animal models and analyzed the host lung [28,29]. In the study of Tam et al. [29], also the lipid mediator profile of the mice BALF and human nasal washes were analyzed. The group of Tam used two different IAV strains, the low-pathogenic H3N2 strain X31 and the high-pathogenic H1N1 strain PR8. Both strains are mouse-adapted and led to body weight loss in lethal and sublethal doses between 15% weight loss (X31, sublethal dose) and 25% weight loss (PR8, both doses) of the host [29]. The group of Morita used the high virulent PR8 strain and achieved a host body weight loss of 20% compared to other clinical scores. Furthermore, they used a H1N1 strain (A/California/04/2009) and an avian H5N1 strain (A/Vietnam/1203/04) [28]. Both research groups analyzed the mice lungs at different time points. Tam et al. used for both strains intervals of 2 days starting at 3 dpi until 19 dpi. However, Morita et al. used shorter time intervals starting 6 h after infection and in addition 12 h, 1 dpi and 2 dpi for the PR8 strain infection and for the two other strains 1 dpi and 2 dpi. In our infection experiments, we used 4, 7 and 21 dpi (plus 2 and 14 dpi for plasma) as sampling time points and could not observe body weight loss in the infected pigs. Furthermore, our mild infection led to atelectasis in the lung tissue.

Concerning these different experimental setups, it seems quite difficult to compare the obtained results. Surprisingly, many of the eicosanoid perturbations in the IAV-infected mice are in accordance with these of the infected pigs. For example, in mice infections, changes in the levels of 12-HETE, 15-HETE and 17-HDHA could be observed. We also observed elevated amounts of 12-and 15-HETE (lung, spleen and BALF) and 17-HDHA (lung and BALF) at 4 dpi. Both HETEs, derived from 12-and 15-LOX, have anti-inflammatory effects which may indicate resolution of inflammation even when intranasal virus load is still detectable. This hypothesis is supported by the detection of inhibitory CD8αα expressing T cells as early as 4 dpi in nose and BALF samples in these animals most likely to prevent excessive immune response [36]. Morita et al. showed a very dynamic process of different HETEs and HDHAs under high virulent IAV infection conditions using early sampling time points. Whereas, Tam et al. observed increased amounts of 12-HETE for the X31 strain compared to the PR8 strain at 11 dpi and concluded that some effects may be strain specific for IAV infection. Our experimental setup is more comparable to the work of Tam et al. than to Morita et al. concerning the clinical scoring of the host [28,29]. However, these findings point out that the sampling time point is crucial for the analysis of lipid mediator perturbations. Since we are also interested in bacterial-viral co-infections, we decided to use longer time intervals between the sampling time points that could be necessary for further bacterial and co-infection experiments.

The supposed resolution of inflammation could further be supported by the finding that also the levels of anti-inflammatory 14,15-EET (lung and spleen); 8,9-EET (spleen); 11,12-EET (spleen) and 14-HDHA (lung) were enhanced at 4 dpi. 17-HDHA is known to have a positive effect on host antibody production against IAV [30]. Besides the positive effect on host B cell activation, 17-HDHA is able to inhibit viral nucleoprotein mRNA expression in human lung epithelial cells [28]. The same effect was reported for 12-and 15-HETE [28]. Indeed, our results showed that the infected pigs were able to overcome infection (no virus detection at 7 dpi) and simultaneously most lipid mediator levels returned to basal level. The elevated levels of 9-HODE at 21 dpi detected in lung and spleen were unexpected, and cannot be explained by the experimental settings.

Our measuring method furthermore included Resolvin D5 and Protectin DX [10(S),17(S)-dihydroxy-4Z,7Z,11E,13Z,15E,19Z-docosahexaenoic acid], whose MRM parameters are described in Table S1 in the Supplemental Materials. Both eicosanoids could not be detected in the pig sample material, which is in accordance with Tam et al. for mice and human samples [29]. However, the group of Morita et al. proposed Protectin D1 [10(R),17(S)-dihydroxy-4Z,7Z,11E,13E,15E,19Z-docosahexaenoic acid] to be an important biomarker able to inhibit virus replication, but the commercially available Protectin DX was used as standard compound for analysis and their treatment experiments as previously noted [37].

In general, IAV infection in pigs showed comparable results for eicosanoid analysis to mice infections models with advantages concerning availability of the sample material and similarities to humans in the immunological and physiological parameters. This could be also very helpful for extended research when eicosanoid analysis would be linked to genomic or proteomic research. How bacterial infections and bacterial-viral coinfections will change the lipid mediator response in pigs is unclear, and will be a challenging task for further studies.

3.2. *Sample Material of Choice To Unravel Changes in the Eicosanoid Profile*

Within this study, sample types from local infection (lung tissue and BALF) and systemic immune response (spleen and blood plasma) were analyzed. Changes in the lipid mediator profile could be observed for all analyzed materials. The most changes were detected for lung and spleen. These sample types showed effects for several HETEs, EET and HODEs. Moreover, the spleen showed unique changes in eicosanoid precursor levels, whereas HDHAs perturbations were noticed for lung and BALF, suggesting lung and spleen as an ideal sample material.

Blood plasma and BALF showed only a few significant changes under mild IAV infection conditions. The advantage of plasma is that it can be sampled from the same animal over different time points in required amounts without the need to sacrifice the pig in contrast to the mice infection

model. This can be very useful for time dependent analysis in context of activating and resolving effects of eicosanoids. However, the measured eicosanoid plasma levels showed high variabilities. Maybe an enlargement in sample size would be helpful for further experiments. Moreover, using the pig as infection model it is possible to reduce the animal number to obtain enough sample material over the duration of the experiment compared to the mice model. Regarding the high individual response of the pig dealing with IAV infection (standard deviations in Figure 2) it seems useful taking plasma samples of the same animals for the understanding of the individual eicosanoid profile development. We did principal component analysis of plasma eicosanoid levels (data not shown), which showed no clustering for specific animals over time or gender even though sex dependent PG synthesis is known [38]. To handle this, we used 8-week-old castrated piglets and mixed the infection sampling group of a minimum of two male and two female animals.

Regarding further infection studies using respiratory bacterial pathogens and co-infections the authors recommend using lung, spleen and blood plasma as sample material. BALF could be a meaningful addition, if extracellular pathogens play a role for the infection model.

4. Materials and Methods

4.1. Chemicals and Standards

All eicosanoid standard compounds including the deuterated internal standards 12-HETE-d8, 13-HODE-d4, PG E2-d4, Resolvin D1-d5 and AA-d11 were purchased from Cayman chemicals. Solid phase extraction cartridges Bond Elut Certify II (200 mg, 3 mL) were obtained from Agilent®. Acetonitrile (99.97%, HPLC-MS grade) was purchased from Th. Geyer®, methanol from Roth® and acetic acid (glacial, HPLC grade) from VWR®. Butylated hydroxytoluene (≥99.0%) and all other chemicals including hexane, ethyl acetate and sodium hydroxide were obtained from Sigma-Aldrich®.

4.2. Cells and Virus

Influenza A Virus A/Bayern/74/2009 (H1N1pdm09) was propagated on Madin-Darby canine kidney cells (MDCK II) in MEM containing 0.2% bovine serum albumin, 1 unit/mL penicillin, 1 µg/mL streptomycin and 2 µg/mL N-tosyl-L-phenylalanine chloromethyl ketone (TPCK)-treated trypsin (Sigma-Aldrich). For TCID50 assay, serial tenfold dilutions in infection medium were prepared and added to MDCK II cells on 96-well tissue culture plates. After incubation for three days at 37 °C and 5% CO_2, each well was monitored for cytopathic effect. Viral titers were calculated according to Spearman-Kärber [39]. Intranasal virus load determination was done using swaps from the nostril and placed in media for incubation as previous reported [40]. The viral titers ($TCID_{50}$) were calculated as described above.

4.3. Pig Infection

All animal experiments were approved by the ethics committee of the State Office for Agriculture, Food Safety and Fishery in Mecklenburg-Western Pomerania (LALFF M-V) with the reference number 7221.3-1-035/17. All procedures were carried out in accordance with the relevant guidelines and animal welfare regulations. Animals had free access to water and standard diet.

Eighteen German landrace pigs at four weeks of age were obtained from a commercial high health status herd and separated randomly in three different sheds at the Friedrich-Loeffler-Institut on the island of Riems (Germany) as described previously [40]. Acute influenza virus infection was excluded by matrix gene quantitative RealTime-PCR (AgPath.ID™ One-Step RT-PCR Kit, Applied Biosystems) on nasal swabs (DRYSWAB™, mwe, UK) prior to experimental infection (modified from [41]). Prior to inoculation, blood samples were taken from all animals. Pigs were subsequently infected intranasally by mucosal atomization device (MAD) (Prosys International Ltd, London, UK) with 2 mL H1N1pdm09 on day 0. The control group of three animals received PBS only via the same route. Serum samples were taken on the same days from the same six animals randomly chosen on day 0. Further, necropsy was

performed on five animals each on days 4, 7, and 21. Necropsy of control animals was performed on day 30 after first mock-infection.

From centrifuged EDTA blood, plasma was obtained and directly frozen on dry ice. During necropsy, whole lung, including trachea, was removed to carry out bronchoalveolar lavages (BAL). Briefly, main bronchus of cranial lung lobe was cut with scissors, tube was inserted and 200 mL of sterile PBS supplemented with EDTA was injected with a syringe through the tube into the vessels of the lung lobe, which was then kneaded softly. BALF was removed by syringe. Lung tissue from two different parts of the cranial lung lobe (*pars caudalis* and *pars cranialis*) was excised. The whole spleen was also removed and all different sample types were placed on dry ice immediately after processing.

4.4. Eicosanoid Extraction

Completely frozen tissue samples were pulverized using a CP02 automated cryoPREP® (Covaris). The frozen tissue was cut in pieces of approximately 200 mg, transferred in a Covaris tissue tube (extra thick) and cooled down by dipping in liquid nitrogen for 60 s. Then the sample was pulverized with an impact level of four and after cooling, pulverization was repeated once as described above. 50 mg of powder were immediately extracted with 500 µL ice cold methanol containing 0.1% BHT and 500 µL ice cold water. An alkaline hydrolysis step was performed using 300 µL sodium hydroxide (10 mol/L) for 30 min at 60 °C. Immediately after the hydrolysis the pH was adjusted to a value of 6 using acetic acid (10 mol/L). For EDTA plasma samples, an aliquot of 500 µL was used and extracted as described for the tissue material. For BALF extraction, 5 mL BALF was extracted with 5 ml methanol containing 0.1% butylated hydroxytoluene. No alkaline hydrolysis was done for BALF samples. For the analysis, 100 µL of deuterated internal standard mixture (each compound 100 ng/mL in acetonitrile) was added to each sample. Further steps including solid phase extraction were done as previously described [42]. SPE cartridges were conditioned with 3 mL methanol and then with 3 mL sodium acetate buffer (0.1 mol/L sodium acetate, containing 5% methanol [*v*/*v*] at pH value of 6). The samples were loaded and washed with 3 mL 50% methanol. Eicosanoids were eluted using 2 mL of hexane/ethyl acetate (75/25, *v*/*v* containing 1% acetic acid (10 mol/L). Additionally, 50 mg of tissue samples was extracted according to the procedure described above but without hydrolysis with sodium hydroxide for PG measurement.

4.5. Eicosanoid Measurement

Extracts were dried under nitrogen flow (TurboVap® from Biotage®) and reconstituted in 70 µL 80% acetonitrile or 70 µL 25% acetonitrile (for PG analysis). Dynamic multiple reaction monitoring LC-MS/MS analysis was performed using an Agilent® HPLC system (1200 series), coupled to an Agilent® 6460 Triple quadrupole mass spectrometer with electrospray ionization source in negative mode. The injection volume was 10 µL. The separation was done with a Gemini® NX-C18 column (3 µm, 100 × 2 mm) and equivalent pre column. The mobile phase consisted of A: water with 0.05% acetic acid and B: acetonitrile according to [43] with reduced amount of acetic acid and a flow rate of 0.4 mL/min. For eicosanoid measurement optimized source parameters were: gas temperature 310 °C, gas flow 13 L/min; nebulizer pressure 40 psi; sheath gas temperature 400 °C, sheat gas flow 12 L/min; capillary voltage 3500 V, nozzle voltage 1600 V and delta EMV 400 V. The gradient elution started with 25% B, this was increased within 10 min to 30% B and to 70% B until 15 min. Then, B increased to 100% until 20 min and held for 5 min. After this, the system recovered to starting conditions with a total runtime of 31 min. For precursor analysis of spleen and lung samples, a gradient with a 14 min runtime was chosen starting with 60% B up to 100% B within 5 min. This was held for 3 min and then the system returned to starting conditions. Standard compounds were used for the identification of all detected lipid mediators (retention time, precursor and product ions) and for the optimization of fragmentation parameters (see Table S1 and S2). Calibration curves with MS-certified standards for absolute quantification (range between 0.5 ng/mL and 50 ng/ml for HETEs and EETs; for prostaglandins between 0.25 ng/mL to 50 ng/mL and 5 ng/mL to 1000 ng/mL for precursors, curve

type quadratic, weighting 1/x) and deuterated internal standard were used. Eicosanoids classes without appropriate MS-certified standards (HEPE, HODE; HDHA) were normalized to the response of the internal standard and stated as "relative amount" in the plots. Agilent Mass Hunter Qualitative Analysis software and Agilent Mass Hunter Quantitative Analysis software (both version B.07.00) were used for MS data analysis.

4.6. Statistics and Data Visualization

Statistical analysis and data visualization for the samples of control (n = 3 pigs) and infected animals (n = 5 per time point) was done using GraphPad Prism v. 7.05. For plasma analysis, group size was enlarged (n = 6 for control and n = 6–8 for infection). Heatmaps were created by MeV v.4.9.0. Tissue material was normalized to the powder weight. Normal distribution of data was tested with Shapiro-Wilk normality test. For significance, Mann-Whitney U-test was performed with a p value < 0.05.

Supplementary Materials: The following are available online at http://www.mdpi.com/2218-1989/9/7/130/s1, Raw data including virus load (excel file); Table S1: MRM parameters for analyzed eicosanoids with qualifier and quantifier ion. And Table S2: MRM parameters for analyzed precursors with qualifier and quantifier ion.

Author Contributions: The following are members of the KoInfekt Study Group: Ulrike Blohm, Claudia Karte, Bernd Köllner, Alexander Schäfer, Charlotte Schröder, Theresa Schwaiger, Julia Sehl, Reiner Ulrich (all Friedrich-Loeffler-Institute, Germany). Conceptualization, D.S., K.M., M.L. and K.S.G.; methodology, D.S., K.M. and M.R.; software, D.S., K.M. and M.R.; validation, D.S., K.M. and M.R.; formal analysis, D.S.; investigation, D.S.; resources, M.L.; data curation, D.S.; writing—original draft preparation, D.S.; writing—review and editing, D.S.; visualization, D.S.; supervision, K.M., M.R. and M.L.; project administration, M.L.; funding acquisition, M.L.

Funding: This research was funded by Federal Excellence Initiative of Mecklenburg Western Pomerania and European Social Fund (ESF) Grant KoInfekt (ESF_14-BM-A55-00xx_16). Moreover, this research was funded by the Deutsche Forschungsgemeinschaft (DFG) within the GRK 1870.

Acknowledgments: We thank the Friedrich-Loeffler Institute (isle of Riems) with all involved animal caretakers for the provided animal samples. Furthermore we thank Anne Leonard for critical reading and Martina Wurster for lab support.

Conflicts of Interest: The authors declare no conflict of interest.

References

1. Collaborators, G.B.D.L.R.I. Estimates of the global, regional, and national morbidity, mortality, and aetiologies of lower respiratory infections in 195 countries, 1990-2016: A systematic analysis for the global burden of disease study 2016. *Lancet Infect. Dis.* **2018**, *18*, 1191–1210.
2. McCullers, J.A. The co-pathogenesis of influenza viruses with bacteria in the lung. *Nat. Rev. Microbiol.* **2014**, *12*, 252–262. [CrossRef] [PubMed]
3. Brundage, J.F.; Shanks, G.D. Deaths from bacterial pneumonia during 1918-19 influenza pandemic. *Emerg. Infect. Dis.* **2008**, *14*, 1193–1199. [CrossRef] [PubMed]
4. Rice, T.W.; Rubinson, L.; Uyeki, T.M.; Vaughn, F.L.; John, B.B.; Miller, R.R., 3rd; Higgs, E.; Randolph, A.G.; Smoot, B.E.; Thompson, B.T.; et al. Critical illness from 2009 pandemic influenza a virus and bacterial coinfection in the united states. *Crit. Care Med.* **2012**, *40*, 1487–1498. [CrossRef] [PubMed]
5. Scholtissek, C.; Burger, H.; Kistner, O.; Shortridge, K.F. The nucleoprotein as a possible major factor in determining host specificity of influenza h3n2 viruses. *Virology* **1985**, *147*, 287–294. [CrossRef]
6. Mohiuddin, M.M.; Reichart, B.; Byrne, G.W.; McGregor, C.G.A. Current status of pig heart xenotransplantation. *Int. J. Surg.* **2015**, *23*, 234–239. [CrossRef]
7. Niemann, H.; Petersen, B. The production of multi-transgenic pigs: Update and perspectives for xenotransplantation. *Transgenic Res.* **2016**, *25*, 361–374. [CrossRef]
8. Meurens, F.; Summerfield, A.; Nauwynck, H.; Saif, L.; Gerdts, V. The pig: A model for human infectious diseases. *Trends Microbiol.* **2012**, *20*, 50–57. [CrossRef]
9. Summerfield, A. Special issue on porcine immunology: An introduction from the guest editor. *Dev. Comp. Immunol.* **2009**, *33*, 265–266. [CrossRef]
10. Summerfield, A.; McCullough, K.C. The porcine dendritic cell family. *Dev. Comp. Immunol.* **2009**, *33*, 299–309. [CrossRef]

11. Sanchez, E.L.; Lagunoff, M. Viral activation of cellular metabolism. *Virology* **2015**, *479*, 609–618. [CrossRef] [PubMed]
12. Ritter, J.B.; Wahl, A.S.; Freund, S.; Genzel, Y.; Reichl, U. Metabolic effects of influenza virus infection in cultured animal cells: Intra- and extracellular metabolite profiling. *BMC Syst. Biol.* **2010**, *4*. [CrossRef] [PubMed]
13. Masoodi, M.; Eiden, M.; Koulman, A.; Spaner, D.; Volmer, D.A. Comprehensive lipidomics analysis of bioactive lipids in complex regulatory networks. *Anal. Chem.* **2010**, *82*, 8176–8185. [CrossRef] [PubMed]
14. Arita, M. Mediator lipidomics in acute inflammation and resolution. *J. Biochem.* **2012**, *152*, 313–319. [CrossRef] [PubMed]
15. Serhan, C.N. Pro-resolving lipid mediators are leads for resolution physiology. *Nature* **2014**, *510*, 92–101. [CrossRef] [PubMed]
16. Dennis, E.A.; Norris, P.C. Eicosanoid storm in infection and inflammation. *Nat. Rev. Immunol.* **2015**, *15*, 511–523. [CrossRef]
17. Sugimoto, M.A.; Sousa, L.P.; Pinho, V.; Perretti, M.; Teixeira, M.M. Resolution of inflammation: What controls its onset? *Front. Immunol.* **2016**, *7*. [CrossRef]
18. Fan, F.; Muroya, Y.; Roman, R.J. Cytochrome p450 eicosanoids in hypertension and renal disease. *Curr. Opin. Nephrol. Hypertens.* **2015**, *24*, 37–46. [CrossRef]
19. Wagner, K.; Vito, S.; Inceoglu, B.; Hammock, B.D. The role of long chain fatty acids and their epoxide metabolites in nociceptive signaling. *Prostaglandins Other Lipid Mediat.* **2014**, *113*, 2–12. [CrossRef]
20. Holtzman, M.J. Arachidonic acid metabolism in airway epithelial cells. *Annu. Rev. Physiol.* **1992**, *54*, 303–329. [CrossRef]
21. Tam, V.C. Lipidomic profiling of bioactive lipids by mass spectrometry during microbial infections. *Semin. Immunol.* **2013**, *25*, 240–248. [CrossRef] [PubMed]
22. Spector, A.A.; Fang, X.; Snyder, G.D.; Weintraub, N.L. Epoxyeicosatrienoic acids (eets): Metabolism and biochemical function. *Prog. Lipid Res.* **2004**, *43*, 55–90. [CrossRef]
23. Obinata, H.; Izumi, T. G2a as a receptor for oxidized free fatty acids. *Prostaglandins Other Lipid Mediat.* **2009**, *89*, 66–72. [CrossRef] [PubMed]
24. Ricciotti, E.; FitzGerald, G.A. Prostaglandins and inflammation. *Arterioscler. Thromb. Vasc. Biol.* **2011**, *31*, 986–1000. [CrossRef] [PubMed]
25. Kronke, G.; Katzenbeisser, J.; Uderhardt, S.; Zaiss, M.M.; Scholtysek, C.; Schabbauer, G.; Zarbock, A.; Koenders, M.I.; Axmann, R.; Zwerina, J.; et al. 12/15-lipoxygenase counteracts inflammation and tissue damage in arthritis. *J. Immunol.* **2009**, *183*, 3383–3389. [CrossRef] [PubMed]
26. Wray, J.A.; Sugden, M.C.; Zeldin, D.C.; Greenwood, G.K.; Samsuddin, S.; Miller-Degraff, L.; Bradbury, J.A.; Holness, M.J.; Warner, T.D.; Bishop-Bailey, D. The epoxygenases cyp2j2 activates the nuclear receptor ppar alpha in vitro and in vivo. *Plos ONE* **2009**, *4*. [CrossRef] [PubMed]
27. Morin, C.; Sirois, M.; Echave, V.; Gomes, M.M.; Rousseau, E. Eet displays anti-inflammatory effects in tnf-alpha stimulated human bronchi: Putative role of cpi-17. *Am. J. Respir. Cell Mol. Biol.* **2008**, *38*, 192–201. [CrossRef] [PubMed]
28. Morita, M.; Kuba, K.; Ichikawa, A.; Nakayama, M.; Katahira, J.; Iwamoto, R.; Watanebe, T.; Sakabe, S.; Daidoji, T.; Nakamura, S.; et al. The lipid mediator protectin d1 inhibits influenza virus replication and improves severe influenza. *Cell* **2013**, *153*, 112–125. [CrossRef] [PubMed]
29. Tam, V.C.; Quehenberger, O.; Oshansky, C.M.; Suen, R.; Armando, A.M.; Treuting, P.M.; Thomas, P.G.; Dennis, E.A.; Aderem, A. Lipidomic profiling of influenza infection identifies mediators that induce and resolve inflammation. *Cell* **2013**, *154*, 213–227. [CrossRef] [PubMed]
30. Ramon, S.; Baker, S.F.; Sahler, J.M.; Kim, N.; Feldsott, E.A.; Serhan, C.N.; Martinez-Sobrido, L.; Topham, D.J.; Phipps, R.P. The specialized proresolving mediator 17-hdha enhances the antibody-mediated immune response against influenza virus: A new class of adjuvant? *J. Immunol.* **2014**, *193*, 6031–6040. [CrossRef]
31. Morita, E.; Schroder, J.M.; Christophers, E. Identification of a novel and highly potent eosinophil chemotactic lipid in human eosinophils treated with arachidonic-acid. *J. Immunol.* **1990**, *144*, 1893–1900. [PubMed]
32. Tejera, N.; Boeglin, W.E.; Suzuki, T.; Schneider, C. Cox-2-dependent and -independent biosynthesis of dihydroxy-arachidonic acids in activated human leukocytes. *J. Lipid Res.* **2012**, *53*, 87–94. [CrossRef] [PubMed]

33. Chavis, C.; Chanez, P.; Vachier, I.; Bousquet, J.; Michel, F.B.; Godard, P. 5-15-dihete and lipoxins generated by neutrophils from endogenous arachidonic-acid as asthma biomarkers. *Biochem. Biophys. Res. Commun.* **1995**, *207*, 273–279. [CrossRef] [PubMed]
34. Thomas, E.; Leroux, J.L.; Blotman, F.; Chavis, C. Conversion of endogenous arachidonic-acid to 5,15-dihete and lipoxins by polymorphonuclear cells from patients with rheumatoid-arthritis. *Inflamm. Res.* **1995**, *44*, 121–124. [CrossRef] [PubMed]
35. Altmann, R.; Hausmann, M.; Spottl, T.; Gruber, M.; Bull, A.W.; Menzel, K.; Vogl, D.; Herfarth, H.; Scholmerich, J.; Falk, W.; et al. 13-oxo-ode is an endogenous ligand for ppargamma in human colonic epithelial cells. *Biochem. Pharmacol.* **2007**, *74*, 612–622. [CrossRef] [PubMed]
36. Schwaiger, T.; Sehl, J.; Karte, C.; Schäfer, A.; Hühr, J.; Mettenleiter, T.C.; Schröder, C.; Ulrich, R.; Köllner, B.; Blohm, U. Minor clinic, major immunology–experimental h1n1pdm09 infection in pigs mimics human seasonal influenza infections. **2019**. Unpublished manuscript.
37. Balas, L.; Guichardant, M.; Durand, T.; Lagarde, M. Confusion between protectin d1 (pd1) and its isomer protectin dx (pdx). An overview on the dihydroxy-docosatrienes described to date. *Biochimie* **2014**, *99*, 1–7. [CrossRef] [PubMed]
38. Pace, S.; Rossi, A.; Krauth, V.; Dehm, F.; Troisi, F.; Bilancia, R.; Weinigel, C.; Rummler, S.; Werz, O.; Sautebin, L. Sex differences in prostaglandin biosynthesis in neutrophils during acute inflammation. *Sci. Rep.* **2017**, *7*, 3759. [CrossRef] [PubMed]
39. Mahy, B.W.J.; Kangro, H.O. *Virology methods manual*; Academic Press: London, UK, 1996.
40. Traxler, S.; Bischoff, A.C.; Sass, R.; Trefz, P.; Gierschner, P.; Brock, B.; Schwaiger, T.; Karte, C.; Blohm, U.; Schroder, C.; et al. Voc breath profile in spontaneously breathing awake swine during influenza a infection. *Sci. Rep.* **2018**, *8*, 14857. [CrossRef] [PubMed]
41. Spackman, E.; Senne, D.A.; Myers, T.J.; Bulaga, L.L.; Garber, L.P.; Perdue, M.L.; Lohman, K.; Daum, L.T.; Suarez, D.L. Development of a real-time reverse transcriptase pcr assay for type a influenza virus and the avian h5 and h7 hemagglutinin subtypes. *J. Clin. Microbiol.* **2002**, *40*, 3256–3260. [CrossRef] [PubMed]
42. Rivera, J.; Ward, N.; Hodgson, J.; Puddey, I.B.; Falck, J.R.; Croft, K.D. Measurement of 20-hydroxyeicosatetraenoic acid in human urine by gas chromatography-mass spectrometry. *Clin. Chem.* **2004**, *50*, 224–226. [CrossRef] [PubMed]
43. Gomolka, B.; Siegert, E.; Blossey, K.; Schunck, W.H.; Rothe, M.; Weylandt, K.H. Analysis of omega-3 and omega-6 fatty acid-derived lipid metabolite formation in human and mouse blood samples. *Prostaglandins Other Lipid Mediat.* **2011**, *94*, 81–87. [CrossRef] [PubMed]

Article I

Eicosanoid Profile of Influenza A Virus Infected Pigs

Daniel Schultz, Karen Methling, KoInfekt Study Group, Michael Rothe, and Michael Lalk

Metabolites

2019 Jul; 9(7): 130

Published: July 3, 2019

For supplementary information see DOI: 10.3390/metabo9070130

Author Contributions: Conceptualization, **D.S.**, K.M., M.L. and K.S.G.; methodology, **D.S.**,K.M. and M.R.; software, **D.S.**, K.M. and M.R.; validation, **D.S.**, K.M. and M.R.; formal analysis, **D.S.**; investigation, **D.S.**; resources, M.L.; data curation, **D.S.**; writing—original draft preparation, **D.S.**; writing—review and editing, **D.S.**; visualization, **D.S.**; supervision, K.M., M.R. and M.L.; project administration, M.L.; funding acquisition, M.L. The following are members of the KoInfekt Study Group: Ulrike Blohm, Claudia Karte, Bernd Köllner, Alexander Schäfer, Charlotte Schröder, Theresa Schwaiger, Julia Sehl, Reiner Ulrich (all Friedrich-Loeffler-Institute, Germany).

_____ _____

Daniel Schultz **Michael Lalk**

metabolites

MDPI

Article

16HBE Cell Lipid Mediator Responses to Mono and Co-Infections with Respiratory Pathogens

Daniel Schultz [1], Surabhi Surabhi [2], Nicolas Stelling [2], Michael Rothe [3], KoInfekt Study Group [†], Karen Methling [1], Sven Hammerschmidt [2], Nikolai Siemens [2,*] and Michael Lalk [1,*]

1 Institute of Biochemistry, University of Greifswald, 17487 Greifswald, Germany; daniel.schultz@uni-greifswald.de (D.S.); methling@uni-greifswald.de (K.M.)
2 Department of Molecular Genetics and Infection Biology, University of Greifswald, 17487 Greifswald, Germany; surabhi.surabhi@uni-greifswald.de (S.S.); nicolas.stelling@uni-greifswald.de (N.S.); sven.hammerschmidt@uni-greifswald.de (S.H.)
3 Lipidomix, 13125 Berlin, Germany; michael.rothe@lipidomix.de
* Correspondence: nikolai.siemens@uni-greifswald.de (N.S.); lalk@uni-greifswald.de (M.L.); Tel.: +49-3834-420-5711 (N.S.); +49-3834-420-4867 (M.L.)
† The members of the KoInfekt Study Group are listed in Appendix A.

Received: 26 January 2020; Accepted: 13 March 2020; Published: 18 March 2020

check for updates

Abstract: Respiratory tract infections are a global health problem. The main causative agents of these infections are influenza A virus (IAV), *Staphylococcus aureus* (*S. aureus*), and *Streptococcus pneumoniae* (*S. pneumoniae*). Major research focuses on genetics and immune responses in these infections. Eicosanoids and other oxylipins are host-derived lipid mediators that play an important role in the activation and resolution of inflammation. In this study, we assess, for the first time, the different intracellular profiles of these bioactive lipid mediators during *S. aureus* LUG2012, *S. pneumoniae* TIGR4, IAV, and corresponding viral and bacterial co-infections of 16HBE cells. We observed a multitude of altered lipid mediators. Changes in the amount of 5-hydroxyeicosatetraenoic acid (5-HETE) were prominent for all bacterial infections. The infection with *S. pneumoniae* showed the strongest impact on bioactive lipid production and led to alterations in the amount of PPARγ ligands and precursors of pro-resolving lipid mediators.

Keywords: eicosanoids; lipid mediators; oxylipins; respiratory tract infection; co-infection; *S. aureus*; *S. pneumoniae*; influenza A virus

1. Introduction

Infections of the respiratory tract are the fourth most common reason for the cause of mortality worldwide [1]. Major pathogens causing such infections are influenza A virus (IAV) [2], *Staphyloccocus aureus* (*S. aureus*), including methicillin-resistant strains of the USA300 lineage, and *Streptococcus pneumoniae* (*S. pneumoniae*) [3]. There is evidence that bacterial and viral co-infections even accelerate the mortality rate as compared to infections by single agents [4]. The immune system plays a major role in the recognition and elimination of the pathogens, which can be influenced by bioactive lipids. Such bioactive lipid mediators are eicosanoids. They play a role in, e.g., induction and resolution of inflammation [5–7]. These oxidized unsaturated fatty acids are synthesized from arachidonic acid (AA), docosahexaenoic acid (DHA), eicosapentaenoic acid (EPA), and linoleic acid (LA) [8]. The main enzymes responsible for the biosynthesis of these oxylipins are lipoxygenases (LOX), cyclooxygenases (COX), and cytochrome P450 enzymes (CYP). AA conversion by LOX results in the production of hydroxyeicosatetraenoic acids (HETEs) or hydroxydocosahexaenoic acids (HDHAs) with DHA as substrate. CYP are responsible for the production of epoxyeicosatrienoic acids (EETs)

and hydroxyeicosapentaenoic acids (HEPEs). The main products of COX are prostaglandins. For a review, see [8–11]. Several immuno-supportive properties are described for eicosanoids and other lipid mediators. These includes vasomodulation [12], chemoattraction [13], and G protein-dependent secretion of interleukin (IL)-6 and IL-8 [14]. Anti-inflammatory eicosanoids (e.g., 12-HETE, 15-HETE), mainly block immune cell infiltration [15], inhibit secretion of interleukins [16] or activate the peroxisome proliferator-activated receptor (PPAR) on immune cells [17]. Most research on eicosanoids is focused on chronic diseases, including asthma or inflammatory bowel diseases [18,19]. However, the majority of research on host eicosanoid profiles in infectious diseases is restricted to single infections with the pathogens *Escherichia coli* [20], *Borrelia burgdorferi* [21], *Pseudomonas aeruginosa* [22], and IAV [5,23,24] or focused solely on prostaglandin E_2 [25–28] and its related receptors [28].

To our knowledge, lipid mediator profiling in bacterial, in particular *S. pneumoniae* and viral co-infections, is unexplored (Table 1). Here, we used human bronchial epithelial cell line 16HBE [29–31] for single and co-infections with IAV, *S. aureus*, and *S. pneumoniae*. Epithelial cells are the initial protective barrier against viruses and bacteria and an important lung compartment to initiate immune system regulation. It is well documented that IAV-mediated lung tissue damage increases the susceptibility of the human host to secondary bacterial infections [32,33]. The analysis of the pathogen-mediated changes in the intracellular lipid mediator profile could help to understand pathogen-specific host immune responses in viral and bacterial single as well as co-infections.

Table 1. Overview of measured lipid mediators with precursor and involved major enzymes. Enzyme abbreviations: lipoxygenase (LOX), cytochrome P450 (CYP), and cyclooxygenase (COX).

Precursor	Key Enzymes	Measured Lipid Mediators
arachidonic acid	5-LOX, 12-LOX, 15-LOX CYP ω-hydroxylase CYP epoxygenases	5-HETE; 12-HETE; 15-HETE 20-HETE 5,6-EET; 8,9-EET; 11,12-EET; 14,15-EET
linoleic acid	15-LOX	9-HODE, 13-HODE
docosahexaenoic acid	12-LOX; 15-LOX	13-HDHA, 14-HDHA, 17-HDHA
eicosapentaenoic acid	COX-2; CYP enzymes	18-HEPE

2. Results

2.1. Viability of 16HBE Post Infections

Most infections led to a minor, insignificant drop in cell viability (Figure S1). These included IAV rH1N1 and *S. pneumoniae* TIGR4 single and respective co-infection. However, the strongest effects were observed for *S. aureus* LUG2012 in single and co-infection with IAV rH1N1. The amount of vital cells dropped down by approximately 50% (Figure S1).

2.2. Intracellular Lipid Mediator Profile in Response to Bacterial and Viral Single and Co-Infections

For all indicated infection conditions, we were able to detect 14 eicosanoids and oxylipins (Figure 1 and Table 1) out of 21 lipid mediators via our MRM method (Table S1). In general, a mixed profile of AA, DHA, EPA, and LA derived lipid mediators was observed.

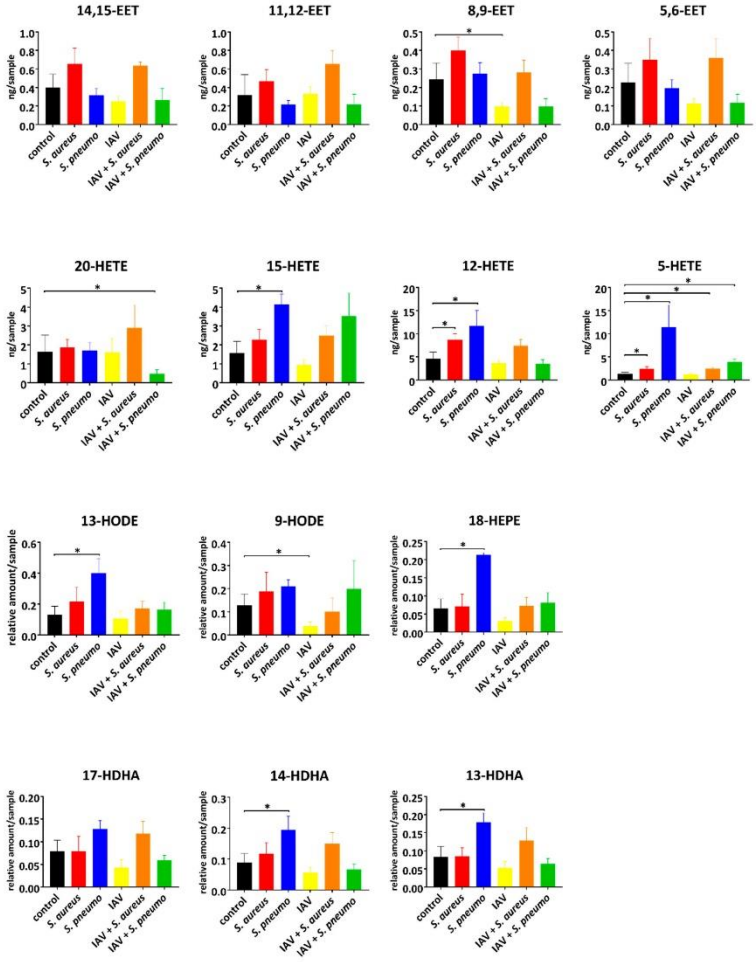

Figure 1. Intracellular lipid mediator amounts in response to indicated bacterial and viral infections: *S. aureus* LUG2012 (red), *S. pneumoniae* TIGR4 (blue), IAV rH1N1 (yellow), uninfected control (black) and the co-infections IAV/*S. aureus* (orange), as well as IAV/*S. pneumoniae* (green). The bars denote mean values ± standard deviations. For statistical analysis, the Mann–Whitney U-test was used for $n = 15$ (controls) and $n = 4$ (infections). The p-values were compared to a significance level α of 0.05 corrected for multiple comparisons using Bonferroni correction for 9 clusters of oxylipins and 5 comparisons resulting from infection conditions. Asterisks indicate significant changes.

Eicosanoids from AA conversion (HETEs) showed changes for all tested infections, whereas DHA- and EPA-derived and analyzed lipids (HDHAs and 18-HEPE) were only affected by single infection with *S. pneumoniae* TIGR4. In particular, the pro-inflammatory 5-HETE was elevated in all bacterial infections, including co-infections (Figure 1). We detected a basal level of approximately 1.4 ng/sample (control), which was significantly increased in all single bacterial and bacterial and viral co-infections. The IAV single infection itself had no impact on 5-HETE production (Figure S2). In addition, increased levels of 12-HETE were detected in both staphylococcal and pneumococcal mono infections.

The majority of changes in the lipid mediator profiles were detected in *S. pneumoniae* infections. Enhanced amounts of 15-HETE, 13-HODE, 18-HEPE, 13-HDHA, and 14-HDHA were exclusively detected in pneumococcal infections (Figure 1 and Figure S2). Both anti-inflammatory lipids 13-HODE and 18-HEPE showed high levels (fold change >3) under infection conditions compared to control. In IAV single infections, only suppressive effects on the amounts of 8,9-EET and 9-HODE were observed. The production of 9-HODE can be derived by enzymatic and autoxidation processes [34]. Moreover, decreased levels of 20-HETE were detected in pneumococcal and IAV co-infections (Figure 1).

3. Discussion

Lipid mediator profiling of infected 16HBE cells revealed that 5-HETE might play a major role at initial steps of bacterial infections of the respiratory tract. 5-HETE levels were significantly increased in 16HBE cells infected with *S. aureus* LUG2012, *S. pneumoniae* TIGR4, and during the corresponding co-infections with bacteria and IAV rH1N1, respectively. This observation may indicate a prominent role of the pro-inflammatory metabolite 5-HETE in bacterial infections of the bronchial compartment. 5-HETE is known to enable transcellular migration and aggregation of neutrophils and to induce airway contraction [35,36]. This lipid mediator is generated from AA within the 5-lipoxygenase (LO) pathway, encoded by the *ALOX5* gene [37]. The interplay of 5-LO with the nuclear membrane-associated 5-LO activating protein FLAP results in AA oxidation to 5-hydroxyperoxyeicosatrienoic acid (5-HpHETE). Subsequently, 5-HpHETE is than converted by glutathione peroxidase to 5-HETE or to leukotrienes. Moreover, the different pro-inflammatory 5-LO eicosanoids are associated with diseases like diabetes [38], Alzheimer [39], and atherosclerosis [40]. For example, leukotriene A_4 can be converted to the pro-inflammatory leukotriene B_4. Clementsen et al. observed enhanced amounts of leukotriene B_4 by antibody based detection in the supernatants of human bronchoalveolar cells treated with inactivated *S. aureus*. However, this was not seen in IAV-infected cells [41]. This indicates that, besides the pathogenic bacteria itself, toxins or bacterial surface structures may also lead to alterations in eicosanoid production. Indeed, lipopolysaccharide of Gram-negative bacteria is able to induce increased production of prostaglandins in endothelial cells [42]. Furthermore, no changes in the 5-HETE production in response to IAV rH1N1 single infection were observed. This is in line with other studies showing that IAV infections of mice [5,23], as well as pigs [24], do not show changes for this lipid mediator, suggesting a lack of 5-LO activation by IAV. In the pig IAV infection study [24], whole organs and BAL-fluid did not discriminate between different cellular compartments, which can be obtained by single-cell experiments. However, a study by Tam and colleagues showed increased levels of 5-HETE in nasopharyngeal washes of human high responders during the 2009-2011 influenza seasons [5]. Whether such responses are linked to a certain human organ, cellular compartment or host genetics remains to be elucidated. In contrast to other IAV infection studies [5,23] using high pathogenic IAV strains, we used the rH1N1 (A/Bavaria/74/2009), which is non-high pathogenic and more appropriate for co-infections. This could be a possible reason for the missing 5-LO activation by IAV. However, the interplay between IAV and secondary bacterial infection is complex. Thus it remains unclear how viral virulence and co-infection affect 5-HETE production in the whole human lung, even if there are some suggestions that higher virulent IAV strains increase rates of viral pneumonia and secondary bacterial infections together with associated mortality [4,43,44].

Furthermore, we show that *S. pneumoniae* TIGR4 infections have the strongest impact on the oxylipin profile. Induced 15-HETE and 13-HODE levels were exclusively seen in these infections. Both 15-HETE and 13-HODE are PPARγ agonists. PPARγ is a ligand-activated transcription factor, and it is known for its anti-inflammatory properties. These include downregulation of the cyclooxygenase-2 gene [45], inhibition of NF-κB [46], or reduced production of pro-inflammatory cytokines and interleukins through its action on macrophages [47]. The group of Solleti et al. [48] showed that the loss of epithelial PPARγ in the lung leads to increased inflammatory mediator production. This could explain why enhanced PPARγ activation is necessary for the resolution of inflammation.

Furthermore, we observed decreased amounts of 20-HETE in co-infections with *S. pneumoniae*. A relationship between changes in levels of 20-HETE and immune suppression in the context of immunosuppressant medication is described [49]. Nevertheless, the role of this lipid mediator in the context of inflammation is rarely explored.

In line with this, elevated amounts of other anti-inflammatory lipid mediators (12-HETE or 18-HEPE) were also detected in pneumococcal infected 16HBE cells. The simultaneous increase of both oxylipins with pro-inflammatory (5-HETE) and anti-inflammatory properties (15-HETE and 13-HDHA) was also documented in IAV-mediated respiratory tract infections of mice [23]. However, our study shows, for the first time, such a mixed profile in *S. pneumoniae* infections. For further studies, infection experiments that are closer to in vivo conditions of tissues like air–liquid interface cell culture should be taken into account for verification of our findings.

4. Materials and Methods

4.1. Chemicals

Lipid mediators and the deuterated standards 12-HETE-d8 and 13-HODE-d4 were purchased from Cayman chemicals. 12-HETE-d8 and 13-HODE-d4 were dissolved in acetonitrile (both 100 ng/ml as internal standard) on ice and aliquots were stored at −80 °C until usage. Acetonitrile (MS grade) was purchased from Th. Geyer®, methanol from Roth®, and acetic acid (HPLC grade) from VWR®. Solid-phase extraction cartridges Bond Elut Certify II (3 mL, 200 mg) were obtained from Agilent®. BHT and other chemicals, including hexane, ethyl acetate, and sodium hydroxide were purchased from Sigma-Aldrich.

4.2. Cell Culture

16HBE14o- (16HBE) cells were a gift from Dieter Gruenert (Mt Zion, Cancer Center, San Francisco, CA, USA). The cells were cultured in MEM medium (Gibco) supplemented with 10% (*v*/*v*) fetal bovine serum (FBS; Life Technologies), 2 mM L-glutamine (Invitrogen), 10 mM HEPES (GE Healthcare) and 1% (*v*/*v*) Minimal Essential Amino Acids (GE Healthcare) in fibronectin-coated flasks (Corning) at 37 °C and 5% CO_2 atmosphere.

4.3. Bacterial and Virus Strains

Streptococcus pneumoniae serotype 4 strain TIGR4 was grown on Columbia blood agar plates (Oxoid) and cultivated to mid-log phase (A_{600} 0.35–0.4) in Todd–Hewitt broth (Roth) containing 0.5% (*w*/*v*) yeast extract (Roth) at 37 °C and 5 % CO_2. *Staphylococcus aureus* strain LUG2012 (USA300 lineage) [50] was cultured overnight at 37 °C in casein hydrolysate and yeast extract (CCY) medium with agitation [51]. Influenza virus A/Bavaria/74/2009 (rH1N1) was propagated and cultivated, as described by Eisfeld and colleagues [52].

4.4. Cell Culture Infections Experiments

16HBE cells were seeded in T175 culture flasks and grown to approximately 80% confluence. For calculation of the multiplicity of infection (MOI), cell counts of the control flask were determined. The flasks were either left untreated or were infected with rH1N1 at MOI 0.1 for 24 h. This amount of virus and the time point were determined as an optimal infection with no significant cell death. After 24 h, bacterial infections of uninfected and rH1N1 infected cells were performed. TIGR4 infections were conducted at MOI 50 for 2 h, followed by 4 h of antibiotic treatment (200 µg/mL gentamycin (Sigma Aldrich, St. Louis, MS, USA), 100 U/mL penicillin G (HighClone™)). LUG2012 infections were conducted at MOI 10 for 2 h followed by 4 h of antibiotic treatment (550 µg/mL gentamycin, 280 U/mL penicillin G, 280 µg/mL streptomycin, 5 U/mL lysostaphin (Sigma Aldrich)). Uninfected or rH1N1 infected cells served as controls. Controls received the same antibiotic treatment. After antibiotic treatment, cells were detached using a scraper and counted. The cell number was

used for the normalization of oxylipin amounts (10 million cells per sample) for both absolute and relative quantified lipid mediators. The cells were harvested by centrifugation at 4 °C and the cell pellets were suspended in 500 µL ice-cold methanol supplemented with 0.1% BHT and 500 µL ice-cold water (HPLC–MS grade) and stored at −80 °C.

4.5. Oxylipin Extraction

The frozen cell pellets were thawed on ice and immediately transferred in a 2-mL tube containing FastPrep™ lysing matrix D and 100 µL internal standard was added. The cells were lysed for 45 s with 6 m/s using a FastPrep™. The supernatant was transferred into a new glass tube on ice. The lysing matrix was washed with 250 µL ice-cold water and 250 µL ice-cold methanol containing 0.1% BHT, then a second lysing cycle was performed and both supernatants were combined. Afterwards, an alkaline hydrolysis step and solid-phase extraction was performed as previously described [24].

4.6. HPLC-MS/MS Measurement

After drying under nitrogen flow (TurboVap®, Biotage®), the extract was reconstituted in 70 µL 80% ACN and measured (10 µL injection volume) with an Agilent® HPLC system (1200 series), coupled to an Agilent® 6460 Triple quadrupole mass spectrometer with electrospray ionization source in negative mode. The mobile phase was water with 0.05% acetic acid (A) and ACN (B). The gradient, column, and MS parameters are referred to in [24]. Using dynamic multiple reaction monitoring (MRM) measurements, the identification was done by standard compounds (MRM transitions, retention times, and optimized parameters can be found in Table S1).

4.7. Quantification and Statistics

Absolute quantification for HETEs and EETs was done using calibration curves (concentration range between 0.1 and 50 ng/sample; curve type quadratic, weighting 1/x) with MS-certified standards and 12-HETE-d8 as an internal standard. HEPE, HDHAs, and HODEs were normalized to the internal standard response (HEPE and HDHAs to 12-HETE-d8; HODEs to 13-HODE-d4) and stated as "relative amounts" in the plots. For absolute and relative quantified amounts of lipid mediators, the data were normalized to 10 million cells per sample. Data analysis was performed with Agilent Mass Hunter Qualitative and Quantitative Analysis software (version B.07.00 for both). Infection experiments were done with four biological replicates and 15 biological replicates for control (non-infection) experiments. Statistics were done using the Mann–Whitney U-test with Graph Pad Prism (version 7.05). The *p*-values were adjusted for multiple comparisons (control vs. three different mono-infections and two different co-infections) and the number of oxylipins using Bonferroni's correction. The strength of the relationship between the measured lipid mediators was tested by correlation analysis after Spearman ($\rho > 0.75$) and resulted in the integration of all EETs and all HDHAs into two clusters under the inclusion of their biosynthesis. The clustering reduced the number of oxylipins used to calculate the factor of Bonferroni correction. The *p*-values obtained after correction were compared to a significance level α of 0.05. Both *p*-values and results from the correlation analysis can be found in Supplementary Materials (Tables S2 and S3).

5. Conclusions

In summary, the presented study demonstrates alterations in the oxylipin profile of 16HBE cells in response to different viral and bacterial mono and co-infections. The pro-inflammatory arachidonic acid metabolite 5-HETE was shown to have a prominent role for all analyzed conditions involving bacteria, which warrants further experimental studies to identify up-stream and down-stream mechanisms driving lipid mediator production.

Supplementary Materials: The following are available online at http://www.mdpi.com/2218-1989/10/3/113/s1, raw data. Figure S1: Survival rate of 16HBE cells under indicated infection conditions; 16HBE cells were infected as described in the Materials and Methods section; 6 h post bacterial infections, the vital cells were detached and counted; cell counts were normalized to the uninfected controls and are displayed as percentage of the uninfected control. Figure S2: Heatmap displaying fold changes (infection/control) of measured lipid mediators; decreased levels are shown in green and increased amounts in red. Table S1: Optimized MRM parameters for analyzed lipid mediators with qualifier[1] and quantifier[2] ion; grey lipid mediators were not detected. Table S2: Calculated *p*-values from Mann–Whitney test. Table S3: Spearman´s range correlation.

Author Contributions: Conceptualization, D.S., S.S., N.S. (Nicolas Stelling), and N.S. (Nikolai Siemens); methodology, D.S., S.S., N.S. (Nicolas Stelling), K.M., and M.R.; software, D.S. and K.M.; validation, D.S. and K.M.; formal analysis, D.S.; investigation, D.S.; resources, M.L., N.S. (Nikolai Siemens), and S.H.; data curation, D.S.; writing—original draft preparation, D.S.; writing—review and editing, K.M., M.L., M.R., and N.S. (Nikolai Siemens); visualization, D.S.; supervision, K.M. and M.L.; project administration, M.L. and N.S. (Nikolai Siemens); funding acquisition, M.L., S.H. and KoInfekt Study Group. All authors have read and agreed to the published version of the manuscript.

Funding: This research was funded by the Mecklenburg-Pomerania Excellence Initiative (Germany) and European Social Fund (ESF) Grant KoInfekt (ESF_14-BM-A55-00xx_16). Moreover, this research was funded by the Deutsche Forschungsgemeinschaft (DFG) within the GRK 1870.

Acknowledgments: The authors thank Sandra van der Auwera-Palitschka for statistical advice.

Conflicts of Interest: The authors declare no conflict of interest.

Appendix A

Members of the KoInfekt Study Group: Dörte Becher (University of Greifswald), Barbara M. Bröker (University Medicine Greifswald), Sven Hammerschmidt (University of Greifswald), Lars Kaderali (University Medicine Greifswald), Bernd Kreikemeyer (University Medicine Rostock), Michael Lalk (University of Greifswald), Thomas C. Mettenleiter (Friedrich-Loeffler-Institute Isle of Riems), Brigitte Müller-Hilke (University Medicine Rostock), Katharina Riedel (University of Greifswald), Jochen Schubert (University Medicine Rostock), Ulrike Seifert (University Medicine Greifswald), Tim Urich (University of Greifswald), Uwe Völker (University Medicine Greifswald).

References

1. Roth, G.; Abate, D.; Abate, K.H.; Abay, S.M.; Abbafati, C.; Abbasi, N.; Abbastabar, H.; Abd-Allah, F.; Abdela, J.; Abdelalim, A.; et al. Global, regional, and national age-sex-specific mortality for 282 causes of death in 195 countries and territories, 1980–2017: A systematic analysis for the Global Burden of Disease Study 2017. *Lancet* **2018**, *392*, 1736–1788. [CrossRef]
2. Reiner, R.C.; Blacker, B.F.; Khalil, I.A.; Zimsen, S.R.M.; Albertson, S.B.; Abate, D.; Abdela, J.; Adhikari, T.B.; Aghayan, S.A.; Agrawal, S.; et al. Mortality, morbidity, and hospitalisations due to influenza lower respiratory tract infections, 2017: An analysis for the Global Burden of Disease Study 2017. *Lancet Respir. Med.* **2019**, *7*, 69–89.
3. Aliberti, S.; Kaye, K.S. The Changing Microbiologic Epidemiology of Community-Acquired Pneumonia. *Postgrad. Med.* **2013**, *125*, 31–42. [CrossRef] [PubMed]
4. McCullers, J.A. The co-pathogenesis of influenza viruses with bacteria in the lung. *Nat. Rev. Genet.* **2014**, *12*, 252–262. [CrossRef]
5. Tam, V.; Quehenberger, O.; Oshansky, C.M.; Suen, R.; Armando, A.M.; Treuting, P.M.; Thomas, P.G.; Dennis, E.A.; Aderem, A. Lipidomic profiling of influenza infection identifies mediators that induce and resolve inflammation. *Cell* **2013**, *154*, 213–227. [CrossRef]
6. Duffney, P.F.; Falsetta, M.L.; Rackow, A.R.; Thatcher, T.; Phipps, R.; Sime, P.J. Key roles for lipid mediators in the adaptive immune response. *J. Clin. Investig.* **2018**, *128*, 2724–2731. [CrossRef]
7. García-Sastre, A. Lessons from lipids in the fight against influenza. *Cell* **2013**, *154*, 22–23. [CrossRef]
8. Tam, V. Lipidomic profiling of bioactive lipids by mass spectrometry during microbial infections. *Semin. Immunol.* **2013**, *25*, 240–248. [CrossRef]
9. Arita, M. Mediator lipidomics in acute inflammation and resolution. *J. Biochem.* **2012**, *152*, 313–319. [CrossRef]
10. Masoodi, M.; Eiden, M.; Koulman, A.; Spaner, D.; Volmer, D.A. Comprehensive Lipidomics Analysis of Bioactive Lipids in Complex Regulatory Networks. *Anal. Chem.* **2010**, *82*, 8176–8185. [CrossRef]

11. Serhan, C.N. Pro-resolving lipid mediators are leads for resolution physiology. *Nature* **2014**, *510*, 92–101. [CrossRef] [PubMed]
12. Holtzman, M.J. Arachidonic acid metabolism in airway epithelial cells. *Annu. Rev. Physiol.* **1992**, *54*, 303–329. [CrossRef] [PubMed]
13. Peters-Golden, M.; Gleason, M.M.; Togias, A. Cysteinyl leukotrienes: Multi-functional mediators in allergic rhinitis. *Clin. Exp. Allergy* **2006**, *36*, 689–703. [CrossRef] [PubMed]
14. Obinata, H.; Izumi, T. G2A as a receptor for oxidized free fatty acids. *Prostaglandins Other Lipid Mediat.* **2009**, *89*, 66–72. [CrossRef] [PubMed]
15. Schwab, J.M.; Chiang, N.; Arita, M.; Serhan, C.N. Resolvin E1 and protectin D1 activate inflammation-resolution programmes. *Nature* **2007**, *447*, 869–874. [CrossRef] [PubMed]
16. Kronke, G.; Katzenbeisser, J.; Uderhardt, S.; Zaiss, M.M.; Scholtysek, C.; Schabbauer, G.; Zarbock, A.; Koenders, M.I.; Axmann, R.; Zwerina, J.; et al. 12/15-lipoxygenase counteracts inflammation and tissue damage in arthritis. *J. Immunol.* **2009**, *183*, 3383–3389. [CrossRef]
17. Thomson, S.J.; Askari, A.; Bishop-Bailey, D. Anti-Inflammatory Effects of Epoxyeicosatrienoic Acids. *Int. J. Vasc. Med.* **2012**, *2012*, 605101. [CrossRef]
18. Sanak, M. Eicosanoid Mediators in the Airway Inflammation of Asthmatic Patients: What is New? *Allergy, Asthma Immunol. Res.* **2016**, *8*, 481–490. [CrossRef]
19. Barnig, C.; Bezema, T.; Calder, P.C.; Charloux, A.; Frossard, N.; Garssen, J.; Haworth, O.; Dilevskaya, K.; Levi-Schaffer, F.; Lonsdorfer, E.; et al. Activation of Resolution Pathways to Prevent and Fight Chronic Inflammation: Lessons From Asthma and Inflammatory Bowel Disease. *Front. Immunol.* **2019**, *10*, 1699. [CrossRef]
20. Chiang, N.; Fredman, G.; Bäckhed, F.; Oh, S.F.; Vickery, T.; Schmidt, B.A.; Serhan, C.N. Infection regulates pro-resolving mediators that lower antibiotic requirements. *Nature* **2012**, *484*, 524–528. [CrossRef]
21. Blaho, V.A.; Buczynski, M.W.; Brown, C.; A Dennis, E. Lipidomic Analysis of Dynamic Eicosanoid Responses during the Induction and Resolution of Lyme Arthritis*. *J. Boil. Chem.* **2009**, *284*, 21599–21612. [CrossRef] [PubMed]
22. Morello, E.; Pérez-Berezo, T.; Boisseau, C.; Baranek, T.; Guillon, A.; Bréa, D.; Lanotte, P.; Carpena, X.; Pietrancosta, N.; Hervé, V.; et al. Pseudomonas aeruginosa Lipoxygenase LoxA Contributes to Lung Infection by Altering the Host Immune Lipid Signaling. *Front. Microbiol.* **2019**, *10*, 1826. [CrossRef] [PubMed]
23. Morita, M.; Kuba, K.; Ichikawa, A.; Nakayama, M.; Katahira, J.; Iwamoto, R.; Watanebe, T.; Sakabe, S.; Daidoji, T.; Nakamura, S.; et al. The Lipid Mediator Protectin D1 Inhibits Influenza Virus Replication and Improves Severe Influenza. *Cell* **2013**, *153*, 112–125. [CrossRef] [PubMed]
24. Schultz, D.; Methling, K.; Rothe, M.; Lalk, M.; KoInfekt Study Group. Eicosanoid Profile of Influenza A Virus Infected Pigs. *Metabolites* **2019**, *9*, 130. [CrossRef] [PubMed]
25. Salina, A.C.; Souza, T.P.; Serezani, C.; Medeiros, A.I. Efferocytosis-induced prostaglandin E2 production impairs alveolar macrophage effector functions during Streptococcus pneumoniae infection. *Innate Immun.* **2016**, *23*, 219–227. [CrossRef] [PubMed]
26. Krause, J.; Geginat, G.; Tammer, I. Prostaglandin E2 from Candida albicans Stimulates the Growth of Staphylococcus aureus in Mixed Biofilms. *PLoS ONE* **2015**, *10*, e0135404. [CrossRef]
27. Sheppe, A.E.F.; Kummari, E.; Walker, A.; Richards, A.; Hui, W.W.; Lee, J.H.; Mangum, L.; Borazjani, A.; Ross, M.K.; Edelmann, M.J. PGE2 Augments Inflammasome Activation and M1 Polarization in Macrophages Infected With Salmonella Typhimurium and Yersinia enterocolitica. *Front. Microbiol.* **2018**, *9*, 2447. [CrossRef]
28. Ikeh, M.A.C.; Fidel, P.L.; Noverr, M.C. Identification of Specific Components of the Eicosanoid Biosynthetic and Signaling Pathway Involved in Pathological Inflammation during Intra-abdominal Infection with Candida albicans and Staphylococcus aureus. *Infect. Immun.* **2018**, *86*, e00144-18. [CrossRef]
29. Shambat, S.M.; Chen, P.; Hoang, A.T.N.; Bergsten, H.; Vandenesch, F.; Siemens, N.; Lina, G.; Monk, I.R.; Foster, T.J.; Arakere, G.; et al. Modelling staphylococcal pneumonia in a human 3D lung tissue model system delineates toxin-mediated pathology. *Dis. Model. Mech.* **2015**, *8*, 1413–1425. [CrossRef]
30. Marks, L.; Parameswaran, G.I.; Hakansson, A.P. Pneumococcal Interactions with Epithelial Cells Are Crucial for Optimal Biofilm Formation and Colonization In Vitro and In Vivo. *Infect. Immun.* **2012**, *80*, 2744–2760. [CrossRef]

31. Blom, R.A.M.; Erni, S.T.; Krempaská, K.; Schaerer, O.; Van Dijk, R.M.; Amacker, M.; Moser, C.; Hall, S.R.R.; Von Garnier, C.; Blank, F. A Triple Co-Culture Model of the Human Respiratory Tract to Study Immune-Modulatory Effects of Liposomes and Virosomes. *PLoS ONE* **2016**, *11*, e0163539. [CrossRef] [PubMed]
32. Shirey, K.A.; Perkins, D.J.; Lai, W.; Zhang, W.; Fernando, L.R.; Gusovsky, F.; Blanco, J.C.G.; Vogel, S.; Arditi, M.; Kagan, J. Influenza "Trains" the Host for Enhanced Susceptibility to Secondary Bacterial Infection. *mBio* **2019**, *10*, 10. [CrossRef] [PubMed]
33. Ballinger, M.; Standiford, T.J. Postinfluenza Bacterial Pneumonia: Host Defenses Gone Awry. *J. Interf. Cytokine Res.* **2010**, *30*, 643–652. [CrossRef] [PubMed]
34. Obinata, H.; Hattori, T.; Nakane, S.; Tatei, K.; Izumi, T. Identification of 9-Hydroxyoctadecadienoic Acid and Other Oxidized Free Fatty Acids as Ligands of the G Protein-coupled Receptor G2A. *J. Boil. Chem.* **2005**, *280*, 40676–40683. [CrossRef] [PubMed]
35. Bittleman, D.B.; Casale, T.B. 5-Hydroxyeicosatetraenoic acid (HETE)-induced neutrophil transcellular migration is dependent upon enantiomeric structure. *Am. J. Respir. Cell Mol. Boil.* **1995**, *12*, 260–267. [CrossRef]
36. O'Flaherty, J.T.; Thomas, M.J.; Lees, C.J.; McCall, C.E. Neutrophil-aggregating activity of monohydroxyeicosatetraenoic acids. *Am. J. Pathol.* **1981**, *104*, 55–62.
37. Luo, M.; Lee, S.; Brock, T.G. Leukotriene synthesis by epithelial cells. *Histol. Histopathol.* **2003**, *18*, 587–595.
38. Neels, J. A role for 5-lipoxygenase products in obesity-associated inflammation and insulin resistance. *Adipocyte* **2013**, *2*, 262–265. [CrossRef]
39. Joshi, Y.B.; Praticò, D. The 5-lipoxygenase pathway: Oxidative and inflammatory contributions to the Alzheimer's disease phenotype. *Front. Cell. Neurosci.* **2015**, *8*, 8. [CrossRef]
40. Khan, R.; Spagnoli, V.; Tardif, J.-C.; L'Allier, P.L. Novel anti-inflammatory therapies for the treatment of atherosclerosis. *Atherosclerosis* **2015**, *240*, 497–509. [CrossRef]
41. Clementsen, P.F.; Bisgaard, H.; Pedersen, M.; Permin, H.; Struve-Christensen, E.; Milman, N.; Nüchel-Petersen, B.; Norn, S. Staphylococcus aureus and influenza A virus stimulate human bronchoalveolar cells to release histamine and leukotrienes. *Inflamm. Res.* **1989**, *27*, 107–109. [CrossRef] [PubMed]
42. De Vries, H. Eicosanoid production by rat cerebral endothelial cells: Stimulation by lipopolysaccharide, interleukin-1 and interleukin-6. *J. Neuroimmunol.* **1995**, *59*, 1–8. [CrossRef]
43. Cauley, L.S.; Vella, A.T. Why is coinfection with influenza virus and bacteria so difficult to control? *Discov. Med.* **2015**, *19*, 33–40. [PubMed]
44. Peltola, V.T.; Murti, K.G.; McCullers, J.A. Influenza virus neuraminidase contributes to secondary bacterial pneumonia. *J. Infect. Dis.* **2005**, *192*, 249–257. [CrossRef] [PubMed]
45. Han, S.W.; Inoue, H.; Flowers, L.C.; Sidell, N. Control of COX-2 gene expression through peroxisome proliferator-activated receptor gamma in human cervical cancer cells. *Clin. Cancer Res.* **2003**, *9*, 4627–4635. [PubMed]
46. Ricote, M.; Li, A.C.; Willson, T.M.; Kelly, C.J.; Glass, C.K. The peroxisome proliferator-activated receptor-γ is a negative regulator of macrophage activation. *Nature* **1998**, *391*, 79–82. [CrossRef]
47. Villapol, S. Roles of Peroxisome Proliferator-Activated Receptor Gamma on Brain and Peripheral Inflammation. *Cell. Mol. Neurobiol.* **2017**, *38*, 121–132. [CrossRef]
48. Solleti, S.K.; Simon, D.M.; Srisuma, S.; Arikan, M.C.; Bhattacharya, S.; Rangasamy, T.; Bijli, K.M.; Rahman, A.; Crossno, J.T., Jr.; Shapiro, S.D.; et al. Airway epithelial cell ppargamma modulates cigarette smoke-induced chemokine expression and emphysema susceptibility in mice. *Am. J. Physiol. Lung Cell. Mol. Physiol.* **2015**, *309*, L293–L304. [CrossRef]
49. Seki, T.; Ishimoto, T.; Sakurai, T.; Yasuda, Y.; Taniguchi, K.; Doi, M.; Sato, M.; Roman, R.J.; Miyata, N. Increased excretion of urinary 20-HETE in rats with cyclosporine-induced nephrotoxicity. *J. Pharmacol. Sci.* **2005**, *97*, 132–137. [CrossRef]
50. Shambat, S.M.; Haggar, A.; Vandenesch, F.; Lina, G.; Van Wamel, W.J.B.; Arakere, G.; Svensson, M.; Norrby-Teglund, A. Levels of Alpha-Toxin Correlate with Distinct Phenotypic Response Profiles of Blood Mononuclear Cells and with agr Background of Community-Associated Staphylococcus aureus Isolates. *PLoS ONE* **2014**, *9*, e106107.

51. Mairpady Shambat, S.; Siemens, N.; Monk, I.R.; Mohan, D.B.; Mukundan, S.; Krishnan, K.C.; Prabhakara, S.; Snall, J.; Kearns, A.; Vandenesch, F.; et al. A point mutation in agrc determines cytotoxic or colonizing properties associated with phenotypic variants of st22 mrsa strains. *Sci. Rep.* **2016**, *6*, 31360. [CrossRef] [PubMed]
52. Eisfeld, A.J.; Neumann, G.; Kawaoka, Y. Influenza a virus isolation, culture and identification. *Nat. Protoc.* **2014**, *9*, 2663–2681. [CrossRef] [PubMed]

Article II

16HBE Cell Lipid Mediator Responses to Mono and Co-Infections with Respiratory Pathogens

Daniel Schultz, Surabhi Surabhi, Nicolas Stelling, Michael Rothe, KoInfekt Study Group, Karen Methling, Sven Hammerschmidt, Nikolai Siemens and Michael Lalk

Metabolites

2020 Mar; 10(3): 113.

Published: March 10, 2020

For supplementary information see DOI: 10.3390/metabo10030113

Author Contributions: Conceptualization, **D.S.**, S.S., N.S. (Nicolas Stelling), and N.S. (Nikolai Siemens); methodology, **D.S.**, S.S., N.S. (Nicola Stelling), K.M., and M.R.; software, **D.S.** and K.M.; validation, **D.S.** and K.M.; formal analysis, **D.S.**; investigation, **D.S.**; resources, M.L., N.S. (Nikolai Siemens), and S.H.; data curation, **D.S.**; writing—original draft preparation, **D.S.**; writing—review and editing, K.M., M.L., M.R., and N.S. (Nikolai Siemens); visualization, **D.S.**; supervision, K.M. and M.L.; project administration, M.L. and N.S. (Nikolai Siemens); funding acquisition, M.L., S.H. and KoInfekt Study Group. All authors have read and agreed to the published version of the manuscript.

_____ _____

Daniel Schultz **Michael Lalk**

frontiers in Immunology

ORIGINAL RESEARCH
published: 07 October 2020
doi: 10.3389/fimmu.2020.579475

Inflammatory Joint Disease Is a Risk Factor for Streptococcal Sepsis and Septic Arthritis in Mice

Johann Volzke[1], Daniel Schultz[2], Marcel Kordt[1], Michael Müller[1], Wendy Bergmann[1], Karen Methling[2], Bernd Kreikemeyer[3] and Brigitte Müller-Hilke[1†] and KoInfekt Study Group*

[1] Core Facility for Cell Sorting and Cell Analysis, University Medical Center Rostock, Rostock, Germany, [2] Institute of Biochemistry, University of Greifswald, Greifswald, Germany, [3] Institute of Medical Microbiology, Virology and Hygiene, University Medical Center Rostock, Rostock, Germany

OPEN ACCESS

Edited by:
Stefano Caserta, University of Hull, United Kingdom

Reviewed by:
Timothy Barnett, University of Western Australia, Australia
Rille Pullerits, University of Gothenburg, Sweden

***Correspondence:**
Johann Volzke
johann.volzke@med.uni-rostock.de

†This author is the senior author

Specialty section:
This article was submitted to Inflammation, a section of the journal Frontiers in Immunology

Received: 02 July 2020
Accepted: 14 September 2020
Published: 07 October 2020

Citation:
Volzke J, Schultz D, Kordt M, Müller M, Bergmann W, Methling K, Kreikemeyer B, Müller-Hilke B, and KoInfekt Study Group (2020) Inflammatory Joint Disease Is a Risk Factor for Streptococcal Sepsis and Septic Arthritis in Mice. Front. Immunol. 11:579475. doi: 10.3389/fimmu.2020.579475

Septic arthritis is a medical emergency associated with high morbidity and mortality, yet hardly any novel advances exist for its clinical management. Despite septic arthritis being a global health burden, experimental data uncovering its etiopathogenesis remain scarce. In particular, any interplay between septic arthritis and preceding joint diseases are unknown as is the contribution of the synovial membrane to the onset of inflammation. Using C57BL/6 mice as a model to study sepsis, we discovered that Group A Streptococcus (GAS) – an important pathogen causing septic arthritis - was able to invade the articular microenvironment. Bacterial invasion resulted in the infiltration of immune cells and detrimental inflammation. *In vitro* infected fibroblast-like synoviocytes induced the expression of chemokines (*Ccl2*, *Cxcl2*), inflammatory cytokines (*Tnf*, *Il6*), and integrin ligands (ICAM-1, VCAM-1). Apart from orchestrating immune cell attraction and retention, synoviocytes also upregulated mediators impacting on bone remodeling (*Rankl*) and cartilage integrity (*Mmp13*). Using collagen-induced arthritis in DBA/1 × B10.Q F1 mice, we could show that an inflammatory joint disease exacerbated subsequent septic arthritis which was associated with an excessive release of cytokines and eicosanoids. Importantly, the severity of joint inflammation controlled the extent of bone erosions during septic arthritis. In order to ameliorate septic arthritis, our results suggest that targeting synoviocytes might be a promising approach when treating patients with inflammatory joint disease for sepsis.

Keywords: immunology, infection, sepsis, septic arthritis, group A streptococcus, rheumatoid arthritis, collagen-induced arthritis, bone erosion

INTRODUCTION

Streptococcus pyogenes (Group A Streptococcus, GAS) is a gram-positive pathogen causing a wide variety of usually non-severe disorders like impetigo and pharyngitis (1). However, GAS can also turn into a severe threat. Among many others, it uses lipoteichoic acid and the M protein as virulence factors to recognize host matrix molecules and thereby adheres to and breaches host tissue

barriers (2–4). Moreover, GAS can proficiently subvert the immune response of the host by, for example, inducing apoptosis in immune cells (5) and degrading neutrophil extracellular traps (6). Thus, it causes severe bacteremia resulting in a broad collection of critical conditions (7). Indeed, invasive GAS infections are estimated to cause more than 18 million cases worldwide leading to 517,000 deaths and an approximated 1.78 million new cases per year (8). As there is no vaccine against this pathogen (9), therapies need to be improved which in turn requires a better understanding of the pathological manifestations leading to severe disease courses like streptococcal toxic shock syndrome, necrotizing fasciitis, and septic arthritis (SA).

GAS is the second leading cause of SA and responsible for roughly 8%–16% of all cases reported (10–13). SA includes GAS invading the joint and thereby stimulating a local immune response that in turn results in irreversible and aggressively progressing erosions of bone and cartilage. In fact, it has been estimated that 30 percent of all patients surviving SA suffer from chronic joint damage eventually causing invalidity (14, 15). The mortality of this disorder remains continuously high and research data defining the pathogenesis of SA are limited (11, 16–18). In particular, the significance of pre-existing joint disorders for the onset and progression of SA remains obscure, despite epidemiological studies pointing toward autoimmune joint diseases as risk factors (13, 16, 19, 20).

Indeed, treatment regimen for autoimmune diseases like rheumatoid arthritis (RA) often include immunosuppression and are therefore being considered an elevated risk for invasive bacterial infections (18). Likewise, the application of monoclonal anti-TNFα antibodies has been reportedly associated with aggravated infections (21, 22). However, alternative hypotheses imply that autoimmune disorders by themselves predispose for SA due to an impaired ability to resist infections (16, 23, 24).

In order to investigate both, autoimmunity as a facilitator of aggravated sepsis and pre-existing inflammatory joint disease as risk factors for septic arthritis, we here turned to the mouse model of collagen induced arthritis (CIA). CIA shares important homologies with rheumatoid arthritis like synovial hyperplasia and articular immune cell infiltration (25–27). Triggering CIA prior to GAS infection therefore allowed for the analysis of the immune response, bone metabolism and the contribution of the synovial lining of the joint and the stromal cells to the disease process of septic arthritis.

MATERIALS AND METHODS

Animals

C57Bl/6J (B6) mice were initially purchased from Charles River (Wilmington, MA, USA). DBA/1 and B10.Q from Harlan Winkelmann (Borchen, Germany). The F1 generation resulting from a cross between female DBA/1 and male B10.Q mice was used for experiments. All strains were bred continuously in our animal care facility under specific germ-free conditions and were housed in individually ventilated cages at a 12-h light/dark cycle and an ambient temperature of 21 ± 2°C with 60 ± 10% humidity. Mice were given water and ssniff R/M-H diet (ssniff Spezialdiäten GmbH, Soest, Germany) ad libitum. Animal experiments were reviewed and approved by the federal state's animal ethics committee (State Department for Agriculture, Food Safety and Fishery in Mecklenburg-Western Pomerania) with the file reference number 7221.3-1.1-063/17.

Induction of Invasive Streptococcal Infection and Septic Arthritis

For all infection experiments, the *emm1* Group A Streptococcus (GAS) strain AP1 was used which was originally received from the World Health Organization Collaborating Center for Reference and Research on Streptococci (Prague, Czech Republic). Due to selection in the original human host, AP1 contains inactivating mutations in the *covS* gene that decrease repression of streptococcal virulence factors (28). As a result, AP1 is associated with invasive infections and is reportedly highly pathogenic in mice (29, 30). Bacteria were suspended into Todd-Hewitt broth (THB, Becton Dickinson, Franklin Lakes, NJ, USA) and cultured for about 16 h until stationary phase of growth was reached. A 20-fold dilution of the suspension was performed with THB and bacteria were cultured until mid-log phase of growth was attained as confirmed by an optical density (600 nm) of 0.4-0.6. Bacteria were washed twice and the OD was adjusted to 0.5 which corresponded to 0.9–1.1 × 10^8 CFU/ml as confirmed by blood agar cultures. Mice were restrained and the tail was disinfected. 100 µl of the diluted bacterial suspension was then injected intravenously with a 30 G needle at doses of 0.5 × 10^6 and 2.0 × 10^6 bacteria for B6 and F1 mice, respectively. Mice were subsequently monitored for 14 days post infection (p.i.). Animals with severely progressed disease were sacrificed at strictly defined clinical endpoints (see *Clinical Scoring*). At these endpoints, mice were anaesthetized and blood was collected by cardiac puncture. Animals were subsequently sacrificed by cervical dislocation. Afterwards, a medial arthrotomy was performed on both knee joints and swabs of the synovial fluid were performed for bacterial load determination. Hind- and forelimbs were extracted for fixation in 4% formaldehyde (Formafix, Düsseldorf, Germany) and snap frozen for storage at -80°C, respectively. The spleen, half of the liver and whole blood were determined for bacterial load. The residual liver was snap frozen and stored at -80°C for further analysis. The remaining anticoagulated blood samples were used for separation of plasma.

Collagen-Induced Arthritis

Male F1 mice at the age of 6–8 weeks were subjected to collagen-induced arthritis (CIA) by subcutaneous injection of 140 µg bovine type II collagen (Chondrex, Redmond, WA, USA) dissolved in 0.1 M acetic acid and emulsified with an equivalent volume of complete Freund's adjuvant (Becton Dickinson). The injection site for the primary immunization was located 5 mm distal from the base of the tail. For secondary immunization 3 weeks later, 140 µg collagen was emulsified in incomplete Freund's adjuvant and was applied slightly distal from the prior injection site. Mice were monitored for 11 weeks after the booster injection at which time point they were infected with GAS. For analgesia, mice were given Tramadol

(Ratiopharm, Ulm, Germany) at a final concentration of 1 mg/ml with the drinking water.

Clinical Scoring

Macroscopic scoring of hind and fore limbs for signs of arthritis was carried out every other day starting at boost. Severity of CIA was quantified as described previously (31): 1 point for redness and/or swelling for each affected digit, 5 points for redness and/or swelling for each affected palmar or plantar paw area and likewise, 5 points for redness and/or swelling for each affected wrist or ankle joint. Scoring for signs of septic arthritis was conducted once every day after GAS injection in a similar fashion. Additional 5 scoring points were added for each knee if bacteria were isolated from the joint capsule. The occurrence of an arthritis score of ≥ 1 was considered a disease incidence event for CIA and SA, alike. Severity of sepsis was scored at least once a day after bacterial infection using macroscopic burden manifestations as a proxy based on a previously described method (32) with few alterations. In brief, sepsis scoring was subdivided into four categories (weight loss, appearance, consciousness, respiration) each with a maximum score of 25 (**Table 1**). A sepsis score ≥ 5 was defined as sepsis occurrence. Animals with a total score of ≥ 25 were considered at septic shock (humane endpoint) and were sacrificed. Sacrifice at septic shock was implemented into the analysis of survival probability.

X-Ray Micro-Computed Tomography (μCT)

Hind limbs were excised and fixed and were then washed with tap water for 30 min. Thereafter, hind limbs were stored overnight in 154 mM NaCl which acted as the scanning medium. X-ray image acquisition was performed using a voxel size of 9 μm^3 on a SkyScan 1076 (Bruker, Antwerp, Belgium) with the source operated at 49 kVp and 200 μA. Beam hardening was reduced using a 0.5 mm Aluminum-filter. Rotation steps were set at 0.6°. Frame averaging was performed by 3 repetitions for each projection with an integration time of 1,700 ms. Attenuation coefficient calibration for bone mineral density (BMD) analysis was prepared by associated measurements of two phantoms with densities of 0.25 and 0.75 g/cm^3, respectively. Image processing was performed in the software pipeline from Bruker as described previously (33). Reconstruction of X-ray images and subdivision of hind limbs into femur, tibia, and paw was conducted with NRecon using a Gaussian filter, smoothing kernel of 2, defect pixel masking of ≤ 20%, ring artifact reduction of 6, beam hardening correction of 30%, and a misalignment compensation depending on image quality. Bones were spatially aligned within the DataViewer software. Selection of volumes and regions of interest were conducted in the CTAn software. For the femur, the proximal reference level was at the fusion site between the greater trochanter and the femoral head. The distal metaphyseal growth plate was set as the second reference point. For analysis of paws, the whole area containing Cuboid, Navicular and Cuneiform bones was analyzed. This region was chosen for the determination of cortical bone parameters and BMD. The cortical bone of the femur was analyzed in the diaphysis and in the epiphyses in proximity to the knee joint. Trabecular bone parameters were also determined at the distal epiphysis. Built-in algorithms were utilized for the determination of parameters of binarized images by 2D plate model for cortical bone (global threshold 64–255) and 3D model for trabecular bone (global threshold 75–255). Three-dimensional reconstructions of knee joints were performed using the CTVol software.

Histology and Immunohistochemistry

Paws were decalcified using USEDECALC (MEDITE, Burgdorf, Germany). Samples were subsequently dehydrated and embedded into paraffin. Serial sections of 5 μm thickness were then generated from the plantar plane of the paws. For the investigation of immune cell infiltration and tissue deterioration, H&E staining of deparaffinized and rehydrated sections was performed. Verification of bacterial colonization was performed *via* immunohistochemistry. Sections were equilibrated in TBS-T (50 mM TRIS-HCl, pH 7.6, 150 mM NaCl, 0.2% Tween 20). Endogenous peroxidases were inactivated using 3% H_2O_2 (Bio-Rad) for 15 min with subsequent rinsing in tap water and TBS-T. Unspecific antibody binding sites were blocked by incubation with

TABLE 1 | Murine Sepsis Score for disease severity using signs of burden after Group A Streptococcus (GAS) infection as a proxy.

Category	Score and description
Relative body weight	0 - no reduction or increase 5 - reduction ≥ 5% 10 - reduction ≥ 10% 25 - reduction ≥ 20%
Appearance	0 - smooth and gleaming fur, clean body orifices 5 - piloerection, badly groomed body orifices, eyes cloudy 10 - clotty and moist orifices, high myotonos, eyes with secretions 25 - convulsions, paralysis, animal appears cold/moribund
Level of consciousness	0 - mouse is active, normal behavior 5 - suppressed activity, motor deficit, limited reaction to stimuli 10 - self-isolation, lethargy, coordination disturbance 25 - pain vocalization at slight touch, apathy
Inflammation, respiration rate and quality	0 - no saliences 5 - redness/swelling on small body areas 10 - disseminated swellings, labored breathing, low breathing rate 25 - open wounds, gasping, extremely reduced respiration

5% normal rabbit serum (Thermo Fisher Scientific, Waltham, MA, USA) for 2 h. After washing with TBS-T, the sections were incubated with 0.5 µg/ml primary polyclonal Goat IgG anti-*Streptococcus pyogenes* Group A carbohydrate (ab9191, abcam, Cambridge, UK) overnight at 4°C. Goat IgG (abcam) was used as an isotype control at the same concentration. On the following day, 0.5 µg/ml secondary Rabbit IgG anti-Goat IgG (Thermo) conjugated with horseradish peroxidase (HRP) was applied for 1 h at room temperature. Subsequently, the sections were stained with the DAB Substrate Kit (Cell Signaling Technology, Danvers, MA, USA) and haematoxylin (Merck Millipore, Burlington, MA, USA). All histological sections were imaged using the Axioplan 2 (Carl Zeiss, Oberkochen, Germany).

Lipidomics

Eicosanoid Extraction

Frozen paw and liver samples were pulverized using a CP02 automated cryoPREP (Covaris, Woburn, MA, USA). The samples were transferred in a Covaris tissue tube, cooled down in liquid nitrogen and then pulverized. From the resulting powder 50 mg was taken, weighed for data normalization and immediately immersed in 500 µl ice cold methanol containing 0.1% butylated hydroxytoluene, 30 nM AUDA (liver samples only) and 500 µl ice cold water. 100 µl of deuterated internal standard mixture was added to each sample. The internal standard consisted of 12-HETE-d_8, 13-HODE-d_4, PG E_2-d_4, Resolvin D1-d_5, and AA-d_{11} (Cayman Chemicals, Ann Arbor, MI, USA). For paw samples, an extra lysis step was performed using Fastprep™ (MP Biomedicals, Irvine, CA, USA) with lysing matrix B for 45 s and 6 m/s. For the liver samples, an alkaline hydrolysis step was performed using 300 µl sodium hydroxide (10 M) for 30 min at 60°C. Immediately thereafter, 300 µl sodium acetate solution (1 M) was added on ice and the pH was adjusted for both paw and liver samples to 6 using 10 M acetic acid. Subsequently, solid phase extraction (SPE) was performed using Agilent (Santa Clara, CA, USA) SPE cartridges Bond Elut Certify II. SPE cartridges were conditioned with 3 ml methanol and then with 3 ml 0.1 sodium acetate buffer at pH 6 containing 5% methanol. The samples were loaded and washed with 3 ml of 50% methanol. Eicosanoids were eluted using 2 ml of hexane/ethyl acetate (75/25) containing 0.1 M acetic acid.

Eicosanoid Measurement

Extracts were dried under nitrogen flow (TurboVap® from Biotage, Uppsala, Sweden) and reconstituted in 70 µl 80% acetonitrile for liver or 70 µl 25% acetonitrile for paw samples. Dynamic multiple reaction monitoring LC-MS/MS analysis was performed using an Agilent HPLC system (1200 series), coupled to an Agilent 6460 Triple quadrupole mass spectrometer with electrospray ionization source in negative mode. The separation was done with a Gemini® (Phenomenex, Torrance, CA, USA) NX-C18 column (3 µm, 100 × 2 mm) and equivalent pre-column. Calibration curves with MS-certified standards for absolute quantification (range between 0.5 ng/ml and 50 ng/ml for HETEs and EETs; for prostaglandins 0.25 ng/ml to 50 ng/ml and 5 ng/ml to 1,000 ng/ml for precursors, curve type quadratic, weighting 1/x) and deuterated internal standard were used. Eicosanoids classes without appropriate MS-certified standards (HEPE, HODE; HDHA) were normalized to the response of the internal standard and stated in arbitrary units (AU) in the plots. Agilent Mass Hunter Qualitative Analysis software and Agilent Mass Hunter Quantitative Analysis software (both version B.07.00) were used for MS data analysis.

Serology

For the determination of mouse IgG anti-GAS titers, an in-house enzyme linked immunosorbent assay (ELISA) was performed. 1 ml bacteria suspension (~ 10^8 CFU/ml) in 6 Well plates was irradiated for 5 min in a GS Gene Linker UV Chamber (Bio-Rad). Complete inactivation of GAS was confirmed using blood agar plates. Suspensions were centrifuged at 4,000 × g for 10 min. Pellets were suspended in 50 mM CO_3^{2-}/HCO_3^- buffer (pH 9.4) and 100 µl of this suspension containing 10^7 inactivated bacteria was coated onto Nunc MaxiSorp plates (Thermo Fisher Scientific) overnight at 4°C. After washing with PBS-T (DPBS, 0.05% Tween-20), 200 µl blocking solution (DPBS, 2% BSA) was applied for 1 h at room temperature. Plasma samples were diluted 1:800 and subsequently incubated for 1.5 h at room temperature. 100 µl Rabbit $F(ab')_2$ anti-mouse IgG : HRP detection antibody (Bio-Rad) was then applied at a concentration of 0.5 µg/ml. For color reaction, 100 µl of the TMB Substrate Set was used (BioLegend, San Diego, CA, USA) and incubated for 10 min. Enzyme activity was then quenched using 100 µl H_2SO_4 (0.5 M). Absorbance signals at 450 nm were obtained by the automated plate reader HT3 (Anthos Mikrosysteme, Krefeld, Germany). For the determination of cytokine concentrations in plasma samples, the LEGENDplex Mouse Inflammation panel (BioLegend) was used containing capture beads and detection antibodies for Interleukin (IL-)1α, IL-1β, IL-6, IL-10, IL-12p70, IL-17A, IL-23, MCP-1, IFNβ, IFNγ, TNFα, and GM-CSF. The protocol was followed using the manufacturer's instructions. Data acquisition was performed using a FACSVerse (Becton Dickinson).

Osteoclastogenesis

Bone marrow cells were obtained as described (34). In short, mouse hind and fore limbs were excised and soft tissue was completely removed. Bone marrow cells were acquired by centrifuging long bones at 10,000 × g for 15 s in a perforated 0.5 ml tube nested in a 1.5 ml tube. Cells were counted and then suspended in αMEM with 10% FCS and 1% Penicillin/Streptomycin (Thermo Fisher Scientific). Bone marrow cells were seeded into 6 or 12 well culture plates at a density of 2 × 10^5 cells/cm^2 and incubated with 30 ng/ml M-CSF (R&D Systems, Minneapolis, MN, USA) for 24 h at 37°C and 5% CO_2. Cells were then stimulated using 50 ng/ml RANKL (R&D Systems) along with 100 ng/ml of the TLR2 agonistic lipopeptide Pam2CSK4 (InvivoGen, San Diego, CA, USA) and UV-inactivated GAS, respectively. For coculture experiments, osteoblasts were isolated as described previously (35). In brief, 2-3 days old mice were sacrificed by decapitation. After rinsing the heads with 70% Ethanol and DPBS, Calvaria were excised and cut into 4 mm^2 pieces. After washing thrice with DPBS, calvaria fragments were immersed in 4 ml digestion solution containing 280 U/ml collagenase type II and 0.25% Trypsin in HBSS (Thermo Fisher Scientific). Bones were subsequently

incubated at 37°C for 20 min with vigorous shaking in-between. Bone cells containing supernatants were then separated from the calvaria and the enzyme reaction was quenched by adding 700 µl FCS. The digestion was repeated three times and all supernatants were pooled thereafter. Calvaria cells were seeded into cell culture plates at a density of 0.2×10^5 cells/cm^2 and were cultured for 24 h. Afterwards, bone marrow cells isolated from long bones as described above were added at a density of 3.8×10^5 cells/cm^2. Then, the coculture was incubated for 48 h until stimulation with 10 nm 1α,25-Dihydroxyviatmin (D_3, Sigma-Aldrich, St. Louis, MO, USA) and 1 µM PGE_2 (Cayman Chemicals) with or without UV-inactivated GAS and Pam2CSK, respectively. Culture was continued for 10 days while adding D_3 and PGE_2 every 24 h. Multinucleated osteoclasts were identified using the tartrate resistant acid phosphatase (TRAcP) kit (Sigma-Aldrich).

Fibroblast-Like Synoviocytes Culture and Infection

Fibroblast-like synoviocytes (FLS) were extracted from murine paws. In brief, mice were sacrificed and rinsed with 70% Ethanol. Hind and forelimbs were removed and put into cold FLS-Medium composed of DMEM, 10% FCS, 1% Penicillin/Streptomycin, 2 mM L-Glutamine (Thermo Fisher Scientific), 10 mM HEPES, and 1 mM pyruvate (PAN-Biotech, Aidenbach, Germany). The following steps were conducted under sterile conditions. The skin was removed and the tendons of the digits were transected. After removal of any soft tissue, paws were isolated by overflexing ankle and wrist joints, respectively. Afterwards, paws from each animal were individually immersed in 240 U/ml collagenase type IV (STEMCELL Technologies, Vancouver, Canada) and digested for 1 h at 37°C with gentle agitation. Organ debris was then removed using a 70 µm cell strainer (Greiner Bio-One, Kremsmünster, Austria) and cells were suspended in FLS-Medium. After quantification of cell numbers, 10^6 FLS were cultured in T75 cell culture flasks (TPP, Trasadingen, Switzerland) until full confluency. Purification of cell cultures was achieved by using the CD45 S-pluriBead (pluriSelect, Leipzig, Germany) separation technique after the manufacturer's instructions. Purity of FLS was verified using a characterization panel consisting of anti-CD106:PerCP-Cy5.5 (clone 429), anti-CD11b:PE (M1/70), anti-CD31:APC (390), anti-CD45:FITC (30-F11), anti-CD54:APC/Fire750 (YN1/1.7.4), anti-CD90.2:BV605 (30-H12), anti-Gr-1:PE-Cy7 (RB-8C5), and DAPI for discrimination of dead cells (all from BioLegend). Cells were counted and suspended in autoMACS Running Buffer (Miltenyi Biotec, Bergisch Gladbach, Germany). TruStain FcX (BioLegend) was used for blocking CD16 and CD32 by incubation for 10 min on ice. The antibody cocktail was subsequently applied for 20 min at room temperature. After washing and suspending in 200 µl Running Buffer, cells were analyzed on a FACSAria IIIu utilizing the FACSDiva Software v8.0.2 (Becton Dickinson). All $CD31^-CD45^-$ cells were considered FLS. Flow cytometry data was analyzed using the FlowJo software (Becton Dickinson). Purified FLS were then again cultured until full confluency was reached and after washing thrice with DPBS, 3×10^5 cells in 2 ml αMEM (Thermo) with 10% FCS were subsequently seeded into 6 well plates. On the following day cells were infected with 3×10^6 bacteria (≈ MOI 10) for 4, 8, or 12 h. Non-infected cells served as a control along with cells incubated with UV-inactivated bacteria. For subsequent transcription analyses, cells were immersed in 700 µl Buffer RLT (Qiagen, Hilden, Germany) and lyzed using a cell scraper and vigorous vortexing. Suspensions were then snap frozen and stored at -80°C. Preparation for flow cytometry included washing of the cells with warm DPBS and digestion with trypsin at 37°C for 1 min. After quenching with medium, cells were suspended in autoMACS running buffer and put on ice until labeling as described above.

Gene Expression Analysis

RNA was isolated using the RNeasy Plus Mini Kit (Qiagen) to the manufacturer's instructions. RNA quantities were determined spectrophotometrically using the NanoDrop ND1000 (Thermo Fisher Scientific) and 500 ng were submitted to cDNA synthesis utilizing the High-capacity cDNA Reverse Transcription Kit (Applied Biosystems, Foster City, CA, USA). For qPCR analysis TaqMan primer pairs and probes were used for *Ccl2* (Assay ID: Mm00441242_m1), *Cxcl2* (Mm00436450_m1), *Il1b* (Mm00434228_m1), *Il6* (Mm00446190_m1), *Il10* (Mm00439614_m1), *Mmp13* (Mm00439491_m1), *Opg* (Mm01205928_m1), *Rank* (Mm00437132_m1), *Rankl* (Mm00441906_m1), *Tnf* (Mm00443258_m1), and *Gapdh* (Mm05724508_g1) as a reference gene (Applied Biosystems). All reactions were amplified using TaqMan Gene expression Master Mix and analyzed on the Applied Biosystems 7900 Fast Real-Time PCR System.

Statistical Analysis

Data visualization and statistics were performed using R (v3.6.3). For survival and probability of incidence analyses, groups were compared using the logrank test. Bivariate correlation was evaluated using the Pearson product-moment correlation coefficient (R). Variables with $R \geq 0.6$ were considered to correlate strongly. Univariate statistical analyses were performed under the assumption of non-normally distributed data. Medians were visualized using boxplots depicting interquartile ranges (IQR) within the box and whiskers for values within 1.5 × IQR. Comparisons of multiple groups were conducted using the Kruskal-Wallis test combined with the post-hoc Mann-Whitney U test for pairwise comparison including adjustments of p values with the Bonferroni-Holm method. When comparing medians to a standard value, the one-sample Wilcoxon signed rank test was performed. For sample sizes of n = 3 the Student's t-test was applied. P values of ≤ 0.05 were considered statistically significant. Significance levels are abbreviated as follows: $^*p < 0.05$, $^{**}p < 0.01$, $^{***}p < 0.001$.

RESULTS

GAS Infection Led to Sepsis and Septic Arthritis Characterized by Bacterial Colonization and Neutrophil Infiltration Into the Joints

We first explored the Group A Streptococcus (GAS) strain AP1 for its capacity to induce sepsis after intravenous infection in

C57BL/6 mice (**Figure 1A**). Sepsis was scored *via* assessment of clinical signs of burden as summarized in **Table 1**. Accordingly, macroscopic signs of animal stress that resulted in a sepsis score ≥ 5 were considered sepsis occurrence (*Materials and Methods*). Under this scoring, over 80% (16/19) of mice infected with 5×10^5 colony-forming units (CFU) developed sepsis (**Figure 1B**, left panel) and about 40% (7/19) exhibited a distinct swelling of paws (**Figure 1C**). Of note, the development of swollen limbs was accompanied by a considerable decrease of survival rate to below 20% when compared to animals without macroscopic signs of arthritis ($p = 0.04$, **Figure 1B**, right panel). Surprisingly, infection with 4×10^5 CFU resulted in less than 20% of mice developing septic arthritis and a 90% survival rate. Reducing the infectious dose further to 1×10^5 CFU neither induced septic arthritis nor mortality (**Figure S1A**). **Figure S1B** compares the sepsis scores resulting from the various infectious doses and **Figure S1C** confirms for the survivors of sepsis an immune response characterized by the production of GAS specific IgG. Altough the bacterial burden in the blood was increased at 5×10^5 CFU, it did not reach statistical significance when compared to lower doses of infection due to high a variance in the data. Also, the bacterial counts in liver and spleen did not change with varying doses of pathogens (**Figure S1D**).

Hematoxylin-Eosin stained thin sections of swollen paws revealed cellular infiltrates in the periarticular soft tissue surrounding the tarsal joints (**Figure 1D**). In order to prove the presence of GAS *in situ*, we established an immunohistochemistry assay using anti-Group A Carbohydrate antibodies and indeed detected bacteria directly within the joint microenvironment (**Figure 1E**). As we predicted that bacterial invasion into the joints would attract immune cells, we were interested in the particular type of cell and identified neutrophilic granulocytes - recognized by their segmented nuclei - co-localizing with GAS (**Figure 1F**). Taken together, we here established an *in vivo* model of sepsis that led to septic arthritis characterized by bacterial invasion and neutrophil infiltration into the joints.

GAS Infection Was Associated With Increased Eicosanoid Levels in the Paws

In order to monitor eicosanoids as prime mediators of immune activation and resolution, we employed HPLC-MS/MS on lipid extracts of the paws from C57BL/6J mice. We could thus show

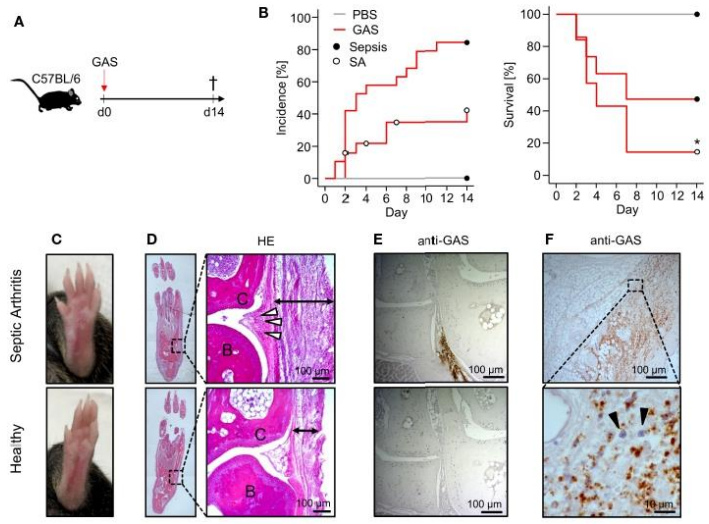

FIGURE 1 | Mice infected with Group A Streptococcus (GAS) show signs of rapidly progressing septic arthritis (SA) including immune cell infiltration and bacterial colonization of joint areas. **(A)** Experimental scheme for the infection of 20-22 week old male C57BL/6 mice with 5×10^5 CFU of GAS (n = 19). **(B)** Left panel: Kaplan-Meier estimator of incidence functions for sepsis and SA of infected animals (n = 19) and PBS controls (n = 4). Right panel: Survival rates of mice not affected by SA (n = 12) compared to mice with SA (n = 7). Open and closed circles denominate censored data, respectively. **(C)** Representative pictures showing swollen paw (top) after GAS infection in contrast to healthy paw (bottom). **(D)** Hematoxylin and eosin (HE)-stained sections in the frontal plane of the paws showing that the infection-related swelling of paws is a result of immune cell migration into the subcutaneous (black arrows) and periarticular soft tissue (white arrowheads). Upper panel: paw affected by septic arthritis. Lower panel: healthy paw. B: bone, C: cartilage. **(E, F)** Immunohistochemistry using the anti-Group A Carbohydrate antibody revealing the bacterial colonization in paw sections. **(E)** Areas around transverse tarsal joints are shown. Upper panel: goat anti-Group A Carbohydrate. Lower Panel: goat IgG isotype control. (**F**) Bacterial colonization of subcutaneous tissue accompanied by neutrophil infiltration (black arrowheads) identified by their nuclei's morphology in the hematoxylin staining. Images of histological sections are representative for mice with macroscopic swellings (n = 5).

that GAS infection led to a marked elevation of the pro-inflammatory prostaglandins (PG) E_2 and D_2 (**Figure 2**) resulting from cyclooxygenase activity. Likewise, GAS induced a significant increase in lipoxygenase catalyzed conversion to hydroxyeicosatrienoic acids (HETEs) and in particular 15-HETE, while the increase in 5-HETE did not quite reach statistical significance. Lastly, GAS also led to an increase in 13- and 14-HDHA derived from docosahexaenoic acid (DHA). Of note, the outliers of our data correspond to paws showing macroscopic signs of arthritis (**Figure 2**). In summary, we here showed for the first time that GAS infection resulted in a significant increase of eicosanoids in the paws.

UV-Inactivated GAS Inhibited Osteoclastogensis *In Vitro*

In order to monitor whether GAS infection, sepsis or septic arthritis impacted on bone morphometry, we employed micro-computed tomography (µCT). To that extent, we compared PBS treated animals to those infected. While all of the control animals reached experimental day 14 as endpoint, 47% of the infected mice had to be sacrificed between experimental days 2 and 4, due to high sepsis scores. To avoid a selection bias in our data, samples from all time points were used and combined into one GAS group. µCT analysis was performed on femora and paws. As for the femora, we concentrated on the distal epiphysis and differentiated trabecular from cortical bone while for the paws, we analyzed the cortical bone of the tarsus, only. As shown in **Figure S2**, we did not detect any alterations to the bone morphometry associated with GAS infection.

As the time frame for developing *in vivo* bone erosions may have been too short, we went on to investigate if GAS had any potential to manipulate bone homeostasis by impacting on the balance of bone resorbing osteoclasts and bone synthesizing osteoblasts. To that extent, we set up *in vitro* experiments and analyzed how GAS influenced on osteoclastogenesis. For that, we stimulated murine bone marrow cells with RANKL - a cytokine essential for osteoclast development - and UV-inactivated bacteria (UV-GAS) and subsequently identified multinucleated Osteoclasts (OCs) *via* TRAcP-staining, which is selective for the target cells (**Figure S3A**). Indeed, the application of UV-GAS dose-dependently led to a significant reduction in OC counts and resulted in mononucleated yet TRAcP-positive progenitors, only. In contrast, simple TLR2 activation *via* its agonist Pam2CSK4 significantly promoted OC differentiation (**Figures S3B, C**). As

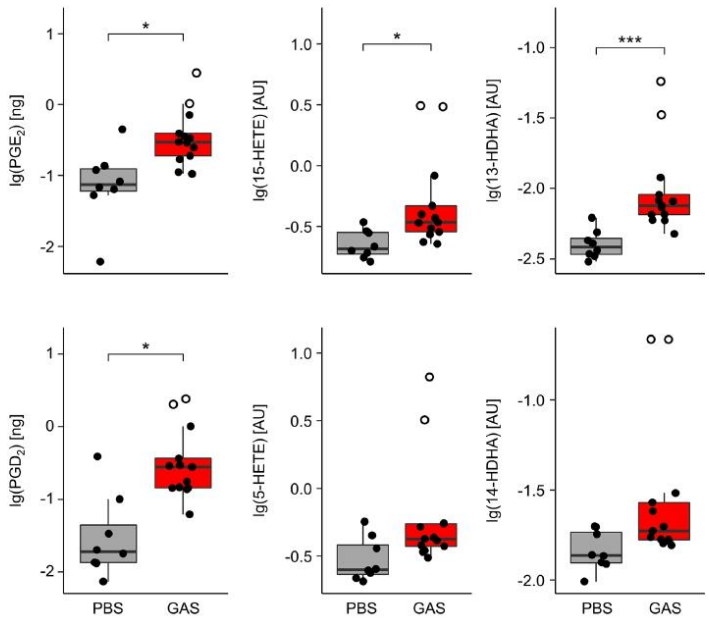

FIGURE 2 | Group A Streptococcus (GAS) infection stimulates the overproduction of paw eicosanoids in infected mice. Paws from C57BL/6J mice were homogenized and eicosanoids were extracted for lipidomics analyses by HLPC-MS/MS using dynamic multiple reaction monitoring. Samples from infected animals (n = 13) showed significantly elevated levels of prostaglandins (PG) E_2, D_2, 15-hydroxyeicosatrienoic acid (15-HETE), and 13-hydroxydocosahexaenoic acid (13-HDHA) when compared to samples from uninfected controls (n = 8). Open circles represent paws with septic arthritis. lg: common logarithm, AU, arbitrary units. *$p < 0.05$, ***$p < 0.001$, Mann-Whitney U test.

expected, the application of M-CSF on BM cultures without RANKL stimulation did not yield any TRAcP-positve precursor cells (**Figure S3B**).

To address the cross-talk between osteoblasts and osteoclasts, we established an *in vitro* co-culture model of calvaria-derived osteoblastogenic cells and mononuclear cells from the bone marrow. RANKL production by osteoblastogenic cells was initiated by stimulating with a bioactive Vitamin D_3 derivate and PGE_2 (**Figure S4A**). Under these conditions, multinucleated and TRAcP-positive osteoclasts developed and again, stimulation with the TLR2 agonist Pam2CSK4 enhanced this development. However, as was the case for single osteoclast cultures, UV-GAS inhibited osteoclast development (**Figure S4B**). Gene-expression analyses of these co-cultures yielded decreased expression levels of *Rankl*, *Rank*, and *Opg* as well as *Tnf*, *Il1b*, and *Il10* in the presence of UV-GAS (**Figure S4C**). In summary we did not observe any changes to the bone mass following GAS infection *in vivo*, even if GAS can perturb the RANK-RANKL-OPG axis and prevent osteoclastogenesis *in vitro*.

GAS-Infected FLS Upregulated Mediators of Immune Cell Attraction and Retention

To further address how GAS led to septic arthritis, we investigated the contribution of the synovial membrane to the disease process. To that extend, we isolated fibroblast-like synoviocytes (FLS) - the dominant cell type of the synovial membrane - and infected them *in vitro* with GAS at a multiplication of infection (moi) of 10 for 4, 8 or 12 h (**Figure 3A**). Transcription analyses at 4 h post infection revealed an over 30- and 1,000-fold increment in the transcription of the chemokine genes *Ccl2* and *Cxcl2*, respectively (**Figure 3B**). Likewise, the expression of the genes encoding pro-inflammatory cytokines *Il6* and *Tnf* were increased 40- and 200-fold, respectively. UV-inactivated GAS on the other hand was also capable of inducing an upregulation of *Ccl2*, *Cxcl2* and *Tnf* however, to a lesser extent than live bacteria and had only a negligible impact on *Il6* transcription. Infection with live GAS also promoted a 3-fold increase in *Rankl* expression whereas the level of *Opg*, whose protein product opposes the action of RANKL, remained apparently unaffected. Likewise, live GAS also augmented the transcription of the gene encoding for the matrix metalloprotease *Mmp13*. Levels of secreted proteins were almost consistently confirmed for CCL2, CXCL2, TNF, and IL-6. These cytokines were time-dependently increased in supernatants from infected cultures with the exception of CXCL2 at 8 h and IL-6 at 24 h p.i., respectively, due to low sample sizes and high variances (**Figure S5**). The capacity of FLS to adjust the expression of integrin ligands in response to GAS infection was assessed *via* flow cytometric analyses (**Figure S6**). Within 12 h of infection, we observed an almost complete shift of the $CD31^-CD45^-$ FLS population towards ICAM-1^+VCAM-1^+ cells (**Figure 3C**), indicating that more than 90% of all FLS expressed these adhesion molecules at a high level (**Figures 3C, D**). Together, these results suggest that FLS are involved in the initiation and

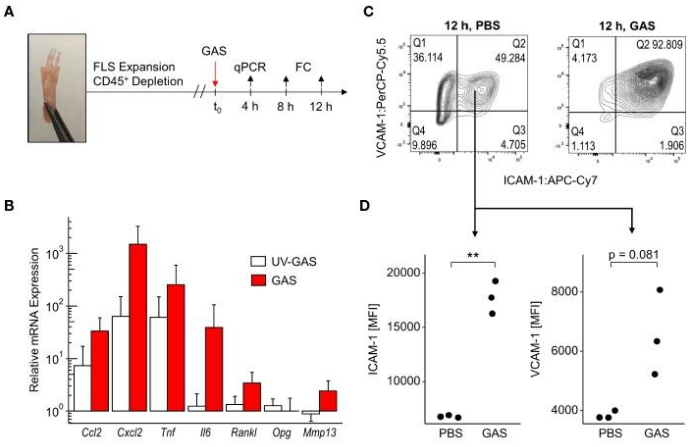

FIGURE 3 | Fibroblast-like synoviocytes (FLS) are triggered after Group A Streptococcus (GAS) infection to upregulate chemokines, pro-inflammatory cytokines and integrin ligands. **(A)** Experimental design of the *in vitro* infection model. FLS were isolated from murine paws by digestion with collagenase type IV and were purified by depleting leukocytes. GAS was applied at a multiplication of infection of 10. FC: flow cytometry. **(B)** Relative mRNA expression levels measured by quantitative PCR 4 h after GAS infection. Ct values were normalized to uninfected FLS and the housekeeping gene *Gapdh* by the $2^{-(\Delta\Delta Ct)}$-Method. Means + SD are depicted in bar plots. The bar graph shows gene-expression levels from infected cells (n = 4) and FLS stimulated with an equivalent number of UV-inactivated bacteria (UV-GAS, n = 3). **(C)** Representative contour plots of flow cytometry data 12 h into the infection experiment depicting subpopulations of $CD31^-CD45^-$ FLS. GAS infection promotes the shift to ICAM-1^+VCAM-1^+ fibroblasts. **(D)** Expression of ICAM-1 and VCAM-1 represented by mean fluorescence intensities (MFI) of $CD31^-CD45^-$ICAM-1^+VCAM-1^+ FLS. **p < 0.01, Mann-Whitney U test.

perpetuation of an immune response against GAS. Furthermore, they are possibly able to modulate bone remodeling by increasing *Rankl* production while maintaining *Opg* expression consistent, which would benefit amplified osteoclastogenesis.

Pre-Existing Inflammatory Joint Disease Exacerbated Sepsis and Promoted the Incidence of Septic Arthritis

To investigate whether chronic inflammatory joint disease promoted the incidence and severity of SA, we combined GAS infection with collagen-induced arthritis (CIA). To that extent, CIA was induced in genetically susceptible DBA/1 × B10.Q (F1) mice by primary and secondary immunization with bovine collagen type II (**Figure 4A**). Thereafter, the development of CIA was monitored until the start of the remission phase, 11 weeks post immunization, when mice were infected by GAS. By the time of the infection, the swelling of paws induced by CIA had subsided, hence allowing subsequent detection of SA signs (**Figure S7**). When comparing naïve controls to CIA mice, the incidence of SA significantly increased from 30 to 90% (**Figure 4B**). Moreover, SA developed in paws formerly affected by CIA but was not restricted to these sites. Of note, higher numbers of bacteria were isolated from the knee joints of mice with pre-existing CIA and likewise, bacteremia was facilitated as demonstrated by increased bacterial burdens in the blood, liver and spleen (**Table 2**). Thus, sepsis was exacerbated in CIA mice, reducing the survival rate to 10% within 5 days after infection (**Figure 4B**).

To further investigate if exacerbated sepsis was paralleled by a cytokine storm, we analyzed plasma cytokines using a multiplexed flow cytometry approach. Sepsis scores were thus found to be in strong linear correlation with the concentrations of IL-6, IFNγ, and TNFα and again, higher sepsis scores in mice with pre-existing CIA correlated with elevated levels of these cytokines (**Figure 4C**). Notably, mice suffering from CIA only did not display elevated levels of pro-inflammatory cytokines and were comparable to PBS controls and mice infected with GAS only (**Figure S8**).

Lipidomic analyses of the paws demonstrated correlations of the anti-inflammatory lipid mediators 13-HODE, 13-HDHA, and

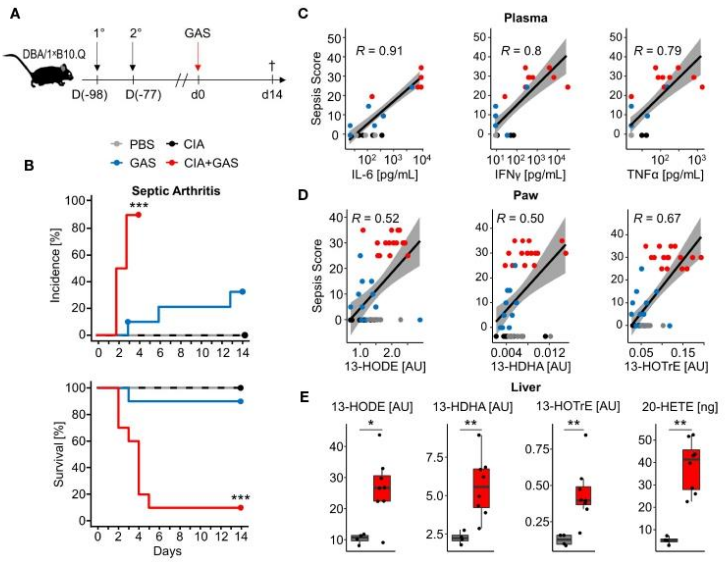

FIGURE 4 | Preceding collagen-induced arthritis (CIA) aggravates sepsis and septic arthritis. **(A)** Scheme for experimental procedure. 6-8 week old DBA/1 ˣ B10.Q mice of the F1 generation were immunized with bovine collagen type II in complete Freund's adjuvant (1°) and were boosted 3 weeks later (2°). CIA developed and was monitored for 11 weeks prior to infection with 2×10^6 colony-forming units of Group A Streptococcus (GAS). **(B)** Kaplan-Meier estimator curves of septic arthritis incidence (top) and survival (bottom) illustrate that preceding CIA (n = 10) exacerbates disease severity which is accompanied by a significant increase of septic arthritis occurrence when compared to mice without a previous CIA (n = 10). ***p < 0.001, logrank test. **(C, D)** Bivariate linear correlation of sepsis scores with plasma levels of pro-inflammatory cytokines in plasma **(C)** and amounts of eicosanoids in paws **(D)**. Mice with combined CIA and GAS infection show the highest sepsis scores which moderately to strongly correlate with Interleukin (IL-)6, Interferon (IFN)γ, Tumor Necrosis Factor (TNF)α, 13-Hydroxyoctadecadienoic acid (13-HODE), 13-Hydrodxydocosahexaenoic acid (13-HDHA) and 13-Hydroxyoctadecatrienoic acid (13-HOTrE). Gray areas depict the 0.95 confidence interval of the regression line. *R*: Pearson product-moment correlation coefficient. **(E)** Boxplots showing the increased eicosanoid levels in liver from mouse with CIA and GAS infection (red boxes, n = 8) compared to PBS controls (gray boxes, n = 4). *p < 0.05, **p < 0.01, Mann-Whitney U test.

13-HOTrE with the respective sepsis scores. As was the case for cytokines, CIA itself did not cause an increase in eicosanoid levels (**Figure 4D**). Moreover, eicosanoid levels in paws correlated positively with systemic IL-6 concentrations, suggesting interdependencies between immunologically relevant mediators during aggravated sepsis (**Figure S9**). Analysis of the lipid profiles in the liver again confirmed an increase in 13-HODE, 13-HDHA and 13-HOTrE together with pro-inflammatory 20-HETE in mice that were subjected to CIA and GAS infection when compared to PBS controls (**Figure 4E**). In summary, we demonstrated that pre-existing inflammatory joint disease promoted the incidence and severity of SA and increased sepsis scores were paralleled by elevated cytokines and eicosanoids.

Arthritis Scores Determine Bone Erosion in Septic Arthritis

In order to investigate if exacerbation of sepsis and SA following GAS infection in CIA mice also involved bone erosion, we here performed μCT analysis and evaluated the resulting bone morphometric data. To that extent, we concentrated on the distal femoral epiphysis for assessment of trabecular bone parameters and found a significant reduction in the bone volume fraction (BV/TV: bone volume [BV] divided by tissue volume [TV]) in CIA+GAS mice compared to PBS controls (**Figure 5A**). This reduction in BV/TV was paralleled by a significant reduction of trabecular numbers (Tb.N). Likewise, there was a significant increase in the structure model index (SMI), which is a measure for trabecular geometry, confirming a more osteoporotic phenotype. Cortical bone parameters were assessed again at the distal femoral epiphysis, the femoral diaphysis and at the tarsus. We observed a decreased cortical area fraction (Ct.Ar/Tt.Ar) - which is defined as the quotient of the cortical bone area and the total cross-sectional area inside the periosteal envelope - close to the knee joints of the CIA+GAS mice. In fulminant cases the deleterious changes in morphology parameters cumulatively led to a grossly deteriorated bone structure of the tibiofemoral joints (**Figure 5B**). However, the cortical bone in the femoral diaphysis was also most affected in the CIA+GAS compared to the PBS control mice. This was shown by reduced cortical thickness (Ct.Th) and polar moment of inertia (MMI) (**Figure 5A**). The latter describes the resistance of the bone to torsional deformation. As for the cortical bone of the tarsus, CIA mice showed comparable parameters to the CIA +GAS mice that were characterized by an increase in the MMI and a reduction in the bone mineral density (BMD). To assess if the severity of joint inflammation determined the magnitude of bone erosion, we correlated arthritis scores to bone parameters. Indeed, **Figure 6** shows a representative correlation analysis between arthritis scores and the corresponding structure model index (SMI). **Table 3** summarizes further correlations. Of note, when analyzing plasma samples from infected mice, concentrations of soluble RANKL where not altered between groups, suggesting that bone erosion was possibly mediated by membrane-bound RANKL (data not shown). In summary, the severity of on-going arthritis determined the magnitude of bone erosions resulting from GAS infection, especially in CIA mice.

DISCUSSION

We here demonstrated that inflammatory joint disease posed a risk for Streptococcal sepsis and septic arthritis in mice. Pre-existing CIA significantly reduced survival of subsequent GAS infection and significantly increased incidence of SA with both, synovial fibroblasts and immune cells contributing to the disease process.

Our immune histologic analyses of SA revealed neutrophils co-localizing with bacteria in the joints. Although neutrophils are unconditionally indispensable for reducing the bacterial load during infection, they are also suspected to be involved in the pathogenesis of SA (36). They express high densities of pattern recognition receptors and these receptors may be rapidly activated upon encounter with streptococcal components (37–39). Receptor activation leads to the discharge of inflammatory mediators, thereby attracting further cells and feeding into the derailment of the immune response in SA (40, 41). CIA on the other hand is characterized by continuous proliferation and accumulation of synovial fibroblasts in the joints (42, 43). Our *in vitro* data demonstrated that these FLS are stimulated by GAS to release cytokines and upregulate the expression of integrin ligands, thereby attracting immune cells. In summary our data suggest that, in the case of pre-existing CIA, within the pannus, FLS may encounter invading bacteria, activate and upregulate the expression of cytokines that attract/retain innate immune cells. FLS and neutrophils then act in concert and promote inflammation entailing joint deterioration.

Inflammation in SA has been postulated to manipulate the RANKL/RANK/OPG axis and promote the differentiation of bone osteoclasts thereby accelerating bone resorption (44–47).

TABLE 2 | Pre-existing collagen induced arthritis (CIA) promoted bacteremia and colonization of tibiofemoral joints.

	Median bacterial burden (IQR) [CFU/ml ^{x} 10^{5}]		
	GAS	CIA+GAS	p
Knee (left)	<0.005 (0.005 – 0.005)	0.010 (0.005 – 0.52)	0.036*
Knee (right)	<0.005 (0.005 – 0.005)	0.015 (0.005 – 0.18)	0.058
Blood	<0.001 (0.001 – 0.001)	10 (0.51 – 10)	0.012*
Liver	<0.002 (0.002 – 0.002)	532 (38 – 800)	0.0039**
Spleen	<0.001 (0.001 – 0.001)	194 (2 – 800)	0.0039**

*GAS were isolated, selected and counted on blood agar. p values depict significance levels when comparing bacterial counts of the CIA+GAS group with the respective limits of detection. *p < 0.05, **p < 0.01, one-sample Wilcoxox signed rank test.*

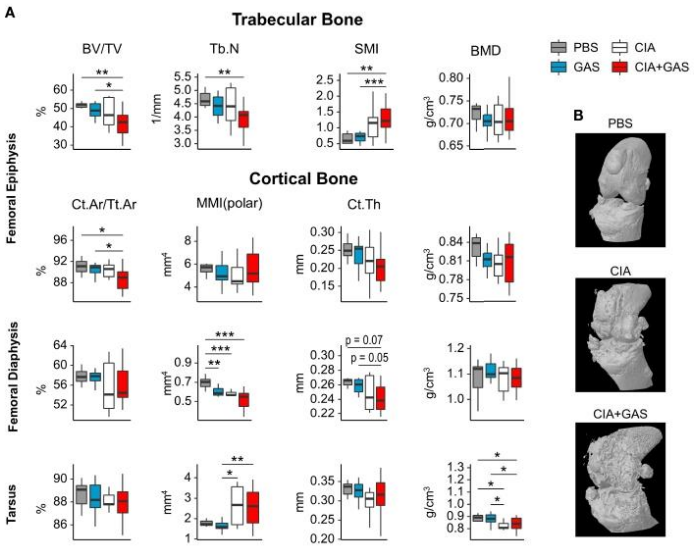

FIGURE 5 | Deterioration of bone morphology due to collagen induced arthritis (CIA) becomes significant when combining the chronic inflammatory joint disease with Group A Streptococcus (GAS) infection. **(A)** Femora and paws were morphometrically assessed by micro-computed tomography. A panel of bone morphology parameters is shown for trabecular bone in the femoral epiphysis and cortical bone in the femur and the tarsus, respectively. Bone volume fraction (BV/TV), structure model index (SMI) and trabecular number (Tb.N) of trabecular bone are affected in the CIA+GAS group. In this Group cortical area fraction (Ct.Ar/Tt.Ar), polar moment of inertia (MMI), cortical thickness (Ct.Th) and bone mineral density (BMD) of certain areas of cortical bone are also modified. **(B)** Representative 3-dimensional reconstructions of the knee joint areas show bone erosion caused by CIA and CIA+GAS, respectively, as a result of detrimentally changed morphology parameters. *$p < 0.05$, **$p < 0.01$, ***$p < 0.001$, Kruskal-Wallis test combined with posthoc Mann-Whitney U test and type I error rate corrections with the Bonferroni-Holm method.

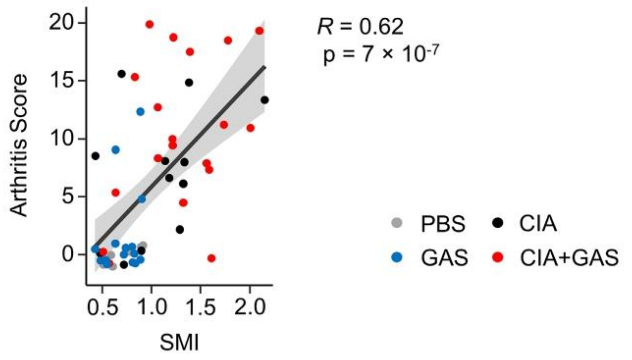

FIGURE 6 | Elevated Arthritis Scores are associated with an osteoporotic phenotype. Dot plot depicting the bivariate correlation analysis of Arthritis Scores and the Structure Model Index (SMI) of the femoral epiphysis. The gray area shows the 0.95 confidence interval of the regression line. *R*: Pearson product-moment correlation coefficient.

TABLE 3 | Arthritis scores determine bone erosion in septic arthritis.

Location	Parameter	Arthritis Score	
		R	p
Femural Epiphysis	BV/TV	-0.47	***0.00033
	Tb.N	-0.34	*0.013
	BMD	-0.32	*0.017
	Ct.Ar/Tt.Ar	-0.37	**0.005
	MMI(polar)	0.15	0.29
	Ct.Th	-0.33	*0.016
	BMD	-0.40	**0.0026
Femural Diaphysis	Ct.Ar/Tt.Ar	-0.45	***0.00071
	MMI(polar)	-0.21	0.14
	Ct.Th	**-0.60**	***2.0×10^{-6}
	BMD	-0.33	*0.014
Tarsus	Ct.Ar/Tt.Ar	-0.32	*0.017
	MMI(polar)	0.56	***5.8×10^{-6}
	Ct.Th	-0.26	*0.050
	BMD	-0.49	***0.00012

*The bold value depicts a strong correlation. *p < 0.05, **p < 0.01, ***p < 0.001, Pearson product-moment correlation coefficient (R).*

However, the cellular source of RANKL, the master switch of osteoclast differentiation, has not yet been unambiguously identified. A previous *in vitro* study demonstrated that osteoblastogenic bone cells were able to upregulate RANKL upon GAS infection (48). Interestingly, our *in vitro* data demonstrated that GAS infection of bone cells inhibited RANKL-mediated osteoclastogensis rather than promoting it, which supports the notion that bone erosion is a consequence of the host's reaction to the infection and not a result of the infection itself (12). However, for an infection of bone cells to occur *in vivo*, an active osteomyelitis is required which was not observed in the present experiments.

We suggest that FLS may be the primary cellular source of RANKL during SA for two reasons: (i) our histological analyses suggested that FLS were in direct contact with GAS during SA and (ii) GAS triggered the upregulation of RANKL (*Tnfsf11*) in FLS cultures to some degree. Furthermore, it has been shown that the inflammatory cytokines TNFα and IL-6 support RANKL production in FLS (49–51). We here confirmed that both, TNFα and IL-6 were markedly increased in CIA mice after infection and this was accompanied by severe bone loss within a few days of SA progression. Mice without the preceding joint condition neither displayed such high cytokine levels nor exhibited any apparent changes in bone morphometry. We therefore suggest that rapid onset of excessive inflammation expedited joint destruction. Similarly, Matsui et al. demonstrated that mice expressing human CD46 - which facilitates GAS infection and therefore promotes a disproportionate inflammatory response (52, 53) - were suffering from pronounced bone lesions within three days after infection (54). The bone mass of infected wild type mice, however, did not change significantly when compared to healthy animals. Another argument supporting FLS as a source for RANKL is our observation of bone loss positively correlating with arthritis severity scores. These account for joint swelling, a result of hyperplasia mostly driven by FLS during inflammation. Yet, we did not detect RANKL production and presentation by FLS *in situ*. To test our hypothesis, future studies must therefore investigate the mechanisms of RANKL-induced bone erosion during SA and the contribution of FLS to osteoclastogenisis *in vivo*.

The combination of GAS with pre-existing CIA led to an increase of several lipid mediators in paws and liver. In detail, the oxylipin 13-HOTrE was also found to be augmented in sera samples of patients with psoriatic arthritis (55). Both 15-lipoxygenase metabolites 13-HODE and 13-HOTrE are able to inhibit the NLRP3 inflammasome complex (56) and increased levels of 13-HODE were also discovered in patients suffering from sepsis (57). Furthermore, the lipid mediator 20-HETE is known to be involved in both sepsis and arthritis. This metabolite is able to influence vasoconstriction and vasodilation by release of nitric oxide (58, 59), to induce cardiac protection in sepsis (60) and inhibit synthesis of prostanoids like PG E_2 (61). We suggest that high levels of 20-HETE in the liver from CIA+GAS animals (fold change > 7) was a result of the combined disorders.

Despite our novel insights into the etiopathogenesis of SA, there are limitations to our study. We used an animal model for a strictly human pathogen, as GAS is primarily adapted to this host to the extent that many of its substantial virulence factors have activities exclusively against human cells and proteins (62, 63). Yet, our mouse model was sufficiently adequate in representing the haematogenous dissemination of the bacteria, which is the main prerequisite for SA occurrence. Accordingly, we not only observed bacterial load in liver and spleen, but also were able to isolate vital GAS from tibiofemoral joints. On the other hand, GAS infection seemed to have exacerbated pre-existing autoimmunity. Although CIA had entered a remission phase by week 11, uninfected CIA mice showed signs of undergoing autoimmune bone-pathology (e.g., in the femoral diaphysis and tarsus) that became more evident in GAS-infected CIA mice. Therefore, our data support the hypothesis that pre-existing autoimmunity promotes SA, which was derived from epidemiological studies on human cohorts. A minor limitation of this study is the selection of a relatively short observation period of 14 days post infection and animals suffering from SA

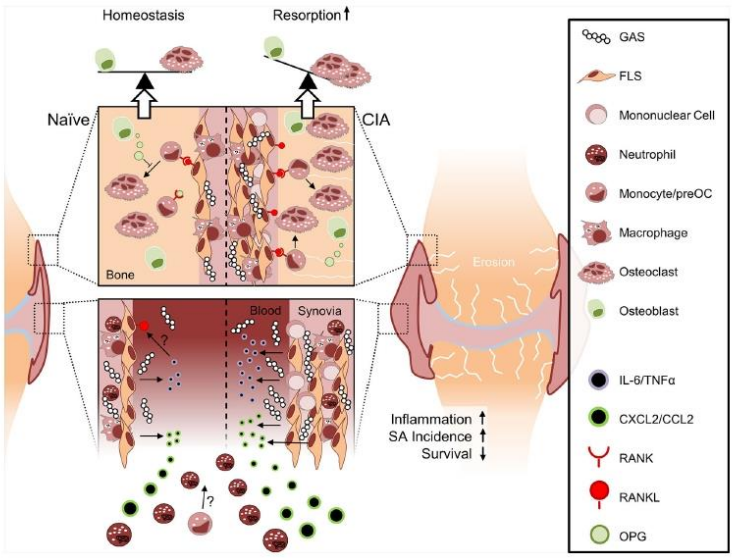

FIGURE 7 | Collagen-induced arthritis facilitates sepsis and septic arthritis after Group A Streptococcus (GAS) infection: a model proposition. The synovial membrane of the naïve joint consists of a thin layer of fibroblast-like synoviocytes (FLS) and few macrophages. In collagen induced arthritis (CIA), however, FLS are highly proliferative and the synovial membrane is infiltrated by mononuclear cells. Compared to the naïve joint, the chronically inflamed synovia or pannus may facilitate the rapid discharge of increased amounts of cytokines and chemokines upon GAS encounter. Consequently, newly infiltrating neutrophils and possibly also monocytes further promote inflammation. Although it is not yet clear how CIA determines impaired bacterial clearance, the pre-existing disease entails a cytokines storm which is paralleled by an increased incidence of septic arthritis and a decreased survival probability. Certain sepsis-related cytokines, especially IL-6, are able to induce the presentation of RANKL on FLS at the interface between synovia and bone. RANKL consequently induces the differentiation of hematopoietic cells into osteoclasts. Bone forming osteoblasts can detain bone resorption by releasing OPG, a soluble RANKL surrogate, which impedes osteoclastogenesis. However, this homeostasis is vanquished by excessive RANKL expression that ultimately causes bone erosion.

even had to be sacrificed within a few days of disease progression. Human SA, however, may transit to a chronic disease state with irreversible joint damage and disability in surviving patients (14). We therefore are unable to assess any impact of an adaptive immune response on the perpetuation of joint inflammation.

In summary, SA in naïve mice led to acute inflammation that was insufficient to cause bone erosions. Mice with pre-existing CIA on the other hand were particularly susceptible to GAS infection and suffered from increased mortality and SA incidence. Aggravated SA was paralleled by excessive inflammation and significant bone destruction (**Figure 7**). Our results thus offer new insights into the interdependencies of different disease entities and point at inhibition of FLS activity in RA patients suffering from sepsis as a future potential avenue for intervention.

DATA AVAILABILITY STATEMENT

The raw data supporting the conclusions of this article will be made available by the authors upon reasonable request.

ETHICS STATEMENT

The animal study was reviewed and approved by State Department for Agriculture, Food Safety and Fishery in Mecklenburg-Western Pomerania with the file reference number 7221.3-1.1-063/17.

AUTHOR CONTRIBUTIONS

The following are members of the KoInfekt Study Group: Michael Lalk (Institute of Biochemistry, University of Greifswald), Sophia Müller, and Erik Weipert (both Core Facility for Cell Sorting and Cell Analysis, University Medical Center Rostock). BM-H, MM, WB, and JV contributed to conception and design of the study. DS, MK, and JV performed the statistical analysis. JV wrote the first draft of the manuscript. BM-H and DS wrote sections of the manuscript. All authors contributed to the article and approved the submitted version.

FUNDING

This research was funded by Federal Excellence Initiative of Mecklenburg-Western Pomerania and European Social Fund (ESF) Grant KoInfekt (ESF/14-BM-A55-0011/16 and ESF/14-BM-A55-0005/16).

ACKNOWLEDGMENTS

The authors sincerely give their thanks to all staff and students that took part in the scientific discussions and experimental conduct. We especially want to thank Daniel Wolter, Marlies Dettmer, and Yvonne Humboldt for their excellent experimental support. Moreover, we like to express our gratitude to Karin Gerber, Mareike Degner, and Ilona Klamfuß for their participation in the animal breeding and care at the animal core facility.

SUPPLEMENTARY MATERIAL

The Supplementary Material for this article can be found online at: https://www.frontiersin.org/articles/10.3389/fimmu.2020.579475/full#supplementary-material

REFERENCES

1. Cunningham MW. Pathogenesis of Group A Streptococcal Infections. *Clin Microbiol Rev* (2000) 13(3):470–511. doi: 10.1128/CMR.13.3.470-511.2000
2. Cue D, Lam H, Cleary PP. Genetic dissection of the Streptococcus pyogenes M1 protein: regions involved in fibronectin binding and intracellular invasion. *Microb Pathog* (2001) 31(5):231–42. doi: 10.1006/mpat.2001.0467
3. Nobbs AH, Lamont RJ, Jenkinson HF. Streptococcus Adherence and Colonization. *Microbiol Mol Biol Rev* (2009) 73(3):407–50. doi: 10.1128/MMBR.00014-09
4. Walker MJ, Barnett TC, McArthur JD, Cole JN, Gillen CM, Henningham A, et al. Disease manifestations and pathogenic mechanisms of group A Streptococcus. *Clin Microbiol Rev* (2014) 27(2):264–301. doi: 10.1128/CMR.00101-13
5. Timmer AM, Timmer JC, Pence MA, Hsu L-C, Ghochani M, Frey TG, et al. Streptolysin O Promotes Group A Streptococcus Immune Evasion by Accelerated Macrophage Apoptosis. *J Biol Chem* (2009) 284(2):862–71. doi: 10.1074/jbc.M804632200
6. Chang A, Khemlani A, Kang H, Proft T. Functional analysis of Streptococcus pyogenes nuclease A (SpnA), a novel group A streptococcal virulence factor. *Mol Microbiol* (2011) 79(6):1629–42. doi: 10.1111/j.1365-2958.2011.07550.x
7. Burlet E, HogenEsch H, Dunham A, Morefield G. Evaluation of the Potency, Neutralizing Antibody Response, and Stability of a Recombinant Fusion Protein Vaccine for Streptococcus pyogenes. *AAPS J* (2017) 19(3):875–81. doi: 10.1208/s12248-017-0069-5
8. World Health Organization. *The Current Evidence for the Burden of Group A Streptococcal Diseases Department of Child and Adolescent Health and Development World Health Organization*. World Health Organization (2005). pp. 52.
9. McKenna S, Malito E, Rouse SL, Abate F, Bensi G, Chiarot E, et al. Structure, dynamics and immunogenicity of a catalytically inactive CXC chemokine-degrading protease SpyCEP from Streptococcus pyogenes. *Comput Struct Biotechnol J* (2020) 18:650–60. doi: 10.1016/j.csbj.2020.03.004
10. Newman JH. Review of septic arthritis throughout the antibiotic era. *Ann Rheum Dis* (1976) 35(3):198–205. doi: 10.1136/ard.35.3.198
11. Morgan DS, Fisher D, Merianos A, Currie BJ. An 18 year clinical review of septic arthritis from tropical Australia. *Epidemiol Infect* (1996) 117:423–8. doi: 10.1017/S0950268800059070
12. Goldenberg DL. Septic arthritis. *Lancet* (1998) 351(9097):197–202. doi: 10.1016/S0140-6736(97)09522-6
13. Weston VC, Jones AC, Bradbury N, Fawthrop F, Doherty M. Clinical features and outcome of septic arthritis in a single UK Health District 1982-1991. *Ann Rheum Dis* (1999) 58(4):214–9. doi: 10.1136/ard.58.4.214
14. García-De La Torre I. Advances in the management of septic arthritis. *Rheum Dis Clin North Am* (2003) 29(1):61–75. doi: 10.1016/S0889-857X(02)00080-7
15. García-Arias M, Balsa A, Mola EM. Septic arthritis. *Best Pract Res Clin Rheumatol* (2011) 25(3):407–21. doi: 10.1016/j.berh.2011.02.001
16. Gupta MN, Sturrock RD, Field M. A prospective 2-year study of 75 patients with adult-onset septic arthritis. *Rheumatology* (2001) 40(1):24–30. doi: 10.1093/rheumatology/40.1.24
17. Mathews CJ, Weston VC, Jones A, Field M, Coakley G. Bacterial septic arthritis in adults. *Lancet* (2010) 375(9717):846–55. doi: 10.1016/S0140-6736(09)61595-6
18. Singh JA, Yu S. Septic arthritis in the Emergency Departments in the U.S.: A National Study of healthcare utilization and time-trends. *Arthritis Care Res (Hoboken)* (2017) 70(2):320–6. doi: 10.1002/acr.23270
19. Kaandorp CJE, Van Schaardenburg D, Krijnen P, Habbema JDF, Van De Laar MAFJ. Risk factors for septic arthritis in patients with joint disease. *Arthritis Rheumatol* (1995) 38(12):1819–25. doi: 10.1002/art.1780381215
20. Al-Nammari S, Gulati V, Patel R, Bejjanki N, Wright M. Septic Arthritis in Haemodialysis Patients: A Seven-Year Multi-Centre Review. *J Orthop Surg* (2008) 16(1):54–7. doi: 10.1177/230949900801600114
21. Galloway JB, Hyrich KL, Mercer LK, Dixon WG, Ustianowski AP, Helbert M, et al. Risk of septic arthritis in patients with rheumatoid arthritis and the effect of anti-TNF therapy: results from the British Society for Rheumatology Biologics Register. *Ann Rheum Dis* (2011) 70(10):1810–4. doi: 10.1136/ard.2011.152769
22. Ali T, Bronze, Kaitha, Mahmood, Ftaisi, Stone. Clinical use of anti-TNF therapy and increased risk of infections. *Drug Healthc Patient Saf* (2013) 5:79–99. doi: 10.2147/DHPS.S28801
23. Myllykangas-Luosujärvi R, Aho K, Kautiainen H, Isomäki H. Shortening of life span and causes of excess mortality in a population-based series of subjects with rheumatoid arthritis. *Clin Exp Rheumatol* (1995) 13(2):149–53.
24. Doran MF, Crowson CS, Pond GR, O'Fallon WM, Gabriel SE. Frequency of infection in patients with rheumatoid arthritis compared with controls: A population-based study. *Arthritis Rheumatol* (2002) 46(9):2287–93. doi: 10.1002/art.10524
25. Rooney M, Condell D, Quinlan W, Daly L, Whelan A, Feighery C, et al. Analysis of the histologic variation of synovitis in rheumatoid arthritis. *Arthritis Rheumatol* (1988) 31(8):956–63. doi: 10.1002/art.1780310803
26. Brand DD, Latham KA, Rosloniec EF. Collagen-induced arthritis. *Nat Protoc* (2007) 2(5):1269–75. doi: 10.1038/nprot.2007.173
27. Oh BR, Suh D, Bae D, Ha N, Choi YII, Yoo HJ, et al. Therapeutic effect of a novel histone deacetylase 6 inhibitor, CKD-L, on collagen-induced arthritis in vivo and regulatory T cells in rheumatoid arthritis in vitro. *Arthritis Res Ther* (2017) 19(1):154. doi: 10.1186/s13075-017-1357-2
28. Fiebig A, Loof TG, Babbar A, Itzek A, Koehorst JJ, Schaap PJ, et al. Comparative Genomics of Streptococcus pyogenes M1 isolates differing in virulence and propensity to cause systemic infection in mice. *Int J Med Microbiol* (2015) 305(6):532–43. doi: 10.1016/j.ijmm.2015.06.002
29. Oehmcke S, Shannon O, von Köckritz-Blickwede M, Mörgelin M, Linder A, Olin AI, et al. Treatment of invasive streptococcal infection with a peptide derived from human high-molecular weight kininogen. *Blood* (2009) 114(2):444–51. doi: 10.1182/blood-2008-10-182527
30. Oehmcke S, Westman J, Malmström J, Mörgelin M, Olin AI, Kreikemeyer B, et al. A Novel Role for Pro-Coagulant Microvesicles in the Early Host Defense against Streptococcus pyogenes. *PloS Pathog* (2013) 9(8):e1003529. doi: 10.1371/journal.ppat.1003529
31. Ebbers M, Lübcke PM, Volzke J, Kriebel K, Hieke C, Engelmann R, et al. Interplay between P. gingivalis, F. nucleatum and A. actinomycetemcomitans in murine alveolar bone loss, arthritis onset and progression. *Sci Rep* (2018) 8(1):15129. doi: 10.1038/s41598-018-33129-z
32. Shrum B, Anantha RV, Xu SX, Donnelly M, Haeryfar S, McCormick JK, et al. A robust scoring system to evaluate sepsis severity in an animal model. *BMC Res Notes* (2014) 7(1):233. doi: 10.1186/1756-0500-7-233

33. Hollinski R, Osterberg A, Polei S, Lindner T, Cantré D, Mittlmeier T, et al. Young and healthy C57BL/6 J mice performing sprint interval training reveal gender- and site-specific changes to the cortical bone. *Sci Rep* (2018) 8 (1):1529. doi: 10.1038/s41598-018-19547-z
34. Amend SR, Valkenburg KC, Pienta KJ. Murine Hind Limb Long Bone Dissection and Bone Marrow Isolation. *J Vis Exp* (2016) 110:e53936. doi: 10.3791/53936
35. Bakker AD, Klein-Nulend J. Osteoblast Isolation from Murine Calvaria and Long Bones. *Methods Mol Biol (Clifton N J)* (2012) 816:19–29. doi: 10.1007/978-1-61779-415-5_2
36. Boff D, Oliveira VLS, Queiroz Junior CM, Silva TA, Allegretti M, Verri WA, et al. CXCR2 is critical for bacterial control and development of joint damage and pain in Staphylococcus aureus -induced septic arthritis in mouse. *Eur J Immunol* (2018) 48(3):454–63. doi: 10.1002/eji.201747198
37. Hayashi F, Means TK, Luster AD. Toll-like receptors stimulate human neutrophil function. *Blood* (2003) 102(7):2660–9. doi: 10.1182/blood-2003-04-1078
38. Navarini AA, Lang KS, Verschoor A, Recher M, Zinkernagel AS, Nizet V, et al. Innate immune-induced depletion of bone marrow neutrophils aggravates systemic bacterial infections. *Proc Natl Acad Sci U S A* (2009) 106(17):7107–12. doi: 10.1073/pnas.0901162106
39. Hafner A, Kolbe U, Freund I, Castiglia V, Kovarik P, Poth T, et al. Crucial Role of Nucleic Acid Sensing via Endosomal Toll-Like Receptors for the Defense of Streptococcus pyogenes in vitro and in vivo. *Front Immunol* (2019) 10:198 (FEB). doi: 10.3389/fimmu.2019.00198
40. Joosten LAB, Koenders MI, Smeets RL, Heuvelmans-Jacobs M, Helsen MMA, Takeda K, et al. Toll-Like Receptor 2 Pathway Drives Streptococcal Cell Wall-Induced Joint Inflammation: Critical Role of Myeloid Differentiation Factor 88. *J Immunol* (2003) 171(11):6145–53. doi: 10.4049/jimmunol.171.11.6145
41. Joosten LAB, Abdollahi-Roodsaz S, Heuvelmans-Jacobs M, Helsen MMA, Van Den Bersselaar LAM, Oppers-Walgreen B, et al. T cell dependence of chronic destructive murine arthritis induced by repeated local activation of toll-like receptor-driven pathways: Crucial role of both interleukin-1?? and interleukin-17. *Arthritis Rheumatol* (2008) 58(1):98–108. doi: 10.1002/art.23152
42. Nasu K, Kohsaka H, Nonomura Y, Terada Y, Ito H, Hirokawa K, et al. Adenoviral Transfer of Cyclin-Dependent Kinase Inhibitor Genes Suppresses Collagen-Induced Arthritis in Mice. *J Immunol* (2000) 165(12):7246–52. doi: 10.4049/jimmunol.165.12.7246
43. Matsuo Y, Mizoguchi F, Saito T, Kawahata K, Ueha S, Matsushima K, et al. Local fibroblast proliferation but not influx is responsible for synovial hyperplasia in a murine model of rheumatoid arthritis. *Biochem Biophys Res Commun* (2016) 470(3):504–9. doi: 10.1016/j.bbrc.2016.01.121
44. Sakurai A, Okahashi N, Nakagawa I, Kawabata S, Amano A, Ooshima T, et al. Streptococcus pyogenes Infection Induces Septic Arthritis with Increased Production of the Receptor Activator of the NF-κB Ligand. *Infect Immun* (2003) 71(10):6019–26. doi: 10.1128/IAI.71.10.6019-6026.2003
45. Leite FRM, de Aquino SG, Guimarães MR, Cirelli JA, Zamboni DS, Silva JS, et al. Relevance of the Myeloid Differentiation Factor 88 (MyD88) on RANKL, OPG, and Nod Expressions Induced by TLR and IL-1R Signaling in Bone Marrow Stromal Cells. *Inflammation* (2015) 38(1):1–8. doi: 10.1007/s10753-014-0001-4
46. Kassem A, Lindholm C, Lerner UH. Toll-Like receptor 2 stimulation of osteoblasts mediates staphylococcus aureus induced bone resorption and osteoclastogenesis through enhanced RANKL. *PloS One* (2016) 11(6):1–20. doi: 10.1371/journal.pone.0156708
47. Staurengo-Ferrari L, Ruiz-Miyazawa KW, Pinho-Ribeiro FA, Domiciano TP, Fattori V, Mizokami SS, et al. The nitroxyl donor Angeli's salt ameliorates Staphylococcus aureus-induced septic arthritis in mice. *Free Radic Biol Med* (2017) 108(April):487–99. doi: 10.1016/j.freeradbiomed.2017.04.016
48. Okahashi N, Sakurai A, Nakagawa I, Fujiwara T, Kawabata S, Amano A, et al. Infection by Streptococcus pyogenes induces the receptor activator of NF-kappaB ligand expression in mouse osteoblastic cells. *Infect Immun* (2003) 71 (2):948–55. doi: 10.1128/IAI.71.2.948
49. Hashizume M, Hayakawa N, Mihara M. IL-6 trans-signalling directly induces RANKL on fibroblast-like synovial cells and is involved in RANKL induction by TNF- and IL-17. *Rheumatology* (2008) 47(11):1635–40. doi: 10.1093/rheumatology/ken363
50. Choe J-Y, Park K-Y, Park S-H, Lee S-I, Kim S-K. Regulatory effect of calcineurin inhibitor, tacrolimus, on IL-6/sIL-6R-mediated RANKL expression through JAK2-STAT3-SOCS3 signaling pathway in fibroblast-like synoviocytes. *Arthritis Res Ther* (2013) 15(1):R26. doi: 10.1186/ar4162
51. Gao Q-F, Zhang X-H, Yuan F-L, Zhao M-D, Li X. Recombinant human endostatin inhibits TNF-alpha-induced receptor activator of NF-κB ligand expression in fibroblast-like synoviocytes in mice with adjuvant arthritis. *Cell Biol Int* (2016) 40(12):1340–8. doi: 10.1002/cbin.10689
52. Lövkvist L, Sjölinder H, Wehelie R, Aro H, Norrby-Teglund A, Plant L, et al. CD46 contributes to the severity of group A streptococcal infection. *Infect Immun* (2008) 76(9):3951–8. doi: 10.1128/IAI.00109-08
53. Matsui H, Sekiya Y, Nakamura M, Murayama SY, Yoshida H, Takahashi T, et al. CD46 transgenic mouse model of necrotizing fasciitis caused by Streptococcus pyogenes infection. *Infect Immun* (2009) 77(11):4806–14. doi: 10.1128/IAI.00577-09
54. Matsui H, Nakatani Y, Yoshida H, Takizawa A, Takeuchi O, Øverby A, et al. Flesh-eating Streptococcus pyogenes triggers the expression of receptor activator of nuclear factor-κB ligand. *Cell Microbiol* (2016) 18(10):1390–404. doi: 10.1111/cmi.12581
55. Coras R, Kavanaugh A, Boyd T, Huynh Q, Pedersen B, Armando AM, et al. Pro- and anti-inflammatory eicosanoids in psoriatic arthritis. *Metabolomics* (2019) 15(4):65. doi: 10.1007/s11306-019-1527-0
56. Kumar N, Gupta G, Anilkumar K, Fatima N, Karnati R, Reddy GV, et al. 15-Lipoxygenase metabolites of α-linolenic acid, [13-(S)-HPOTrE and 13-(S)-HOTrE], mediate anti-inflammatory effects by inactivating NLRP3 inflammasome. *Sci Rep* (2016) 6:31649. doi: 10.1038/srep31649
57. Hamaguchi M, Wu HN, Tanaka M, Tsuda N, Tantengco OAG, Matsushima T, et al. A case series of the dynamics of lipid mediators in patients with sepsis. *Acute Med Surg* (2019) 6:413–8. doi: 10.1002/ams2.443
58. Cuez T, Korkmaz B, Buharalioglu CK, Sahan-Firat S, Falck J, Malik KU, et al. A synthetic analogue of 20-HETE, 5,14-HEDGE, reverses endotoxin-induced hypotension via increased 20-HETE levels associated with decreased iNOS protein expression and vasodilator prostanoid production in rats. *Basic Clin Pharmacol Toxicol* (2010) 106(5):378–88. doi: 10.1111/j.1742-7843.2009.00501.x
59. Jacobs ER, Zhu D, Gruenloh S, Lopez B, Medhora M. VEGF-induced relaxation of pulmonary arteries is mediated by endothelial cytochrome P-450 hydroxylase. *Am J Physiol Lung Cell Mol Physiol* (2006) 291(3):L369–77. doi: 10.1152/ajplung.00265.2004
60. Chen J, Hamers AJP, Finsterbusch M, Massimo G, Zafar M, Corder R, et al. Endogenously generated arachidonate-derived ligands for TRPV1 induce cardiac protection in sepsis. *FASEB J* (2018) 32(7):3816–31. doi: 10.1096/fj.201701303R
61. Tunctan B, Korkmaz B, Sari AN, Kacan M, Unsal D, Serin MS, et al. Contribution of iNOS/sGC/PKG pathway, COX-2, CYP4A1, and gp91 (phox) to the protective effect of 5,14-HEDGE, a 20-HETE mimetic, against vasodilation, hypotension, tachycardia, and inflammation in a rat model of septic shock. *Nitric Oxide* (2013) 33:18–41. doi: 10.1016/j.niox.2013.05.001
62. Kasper KJ, Zeppa JJ, Wakabayashi AT, Xu SX, Mazzuca DM, Welch I, et al. Bacterial Superantigens Promote Acute Nasopharyngeal Infection by Streptococcus pyogenes in a Human MHC Class II-Dependent Manner. DeLeo FR, editor. *PloS Pathog* (2014) 10(5):e1004155. doi: 10.1371/journal.ppat.1004155
63. Reglinski M, Sriskandan S. The contribution of group A streptococcal virulence determinants to the pathogenesis of sepsis. *Virulence* (2014) 5 (1):127–36. doi: 10.4161/viru.26400

Conflict of Interest: The authors declare that the research was conducted in the absence of any commercial or financial relationships that could be construed as a potential conflict of interest.

Article III

Inflammatory Joint Disease Is a Risk Factor for Streptococcal Sepsis and Septic Arthritis in Mice

Johann Volzke, Daniel Schultz, Marcel Kordt, Michael Müller, Wendy Bergmann, Karen Methling, Bernd Kreikemeyer, Brigitte Müller-Hilke, KoInfekt Study Group

Frontiers in Immunology

2020 Oct 7;11:579475

Published: October 11, 2020

For supplementary information see DOI: 10.3389/fimmu.2020.579475

Author contributions: BM-H, MM, WB, and JV contributed to conception and design of the study. **DS**, MK, and JV performed the statistical analysis. JV wrote the first draft of the manuscript.BM-H and **DS** wrote sections of the manuscript. All authors contributed to the article and approved the submitted version. The following are members of the KoInfekt Study Group: Michael Lalk (Institute of Biochemistry, University of Greifswald), Sophia Müller, and Erik Weipert (both Core Facility for Cell Sorting and Cell Analysis, University Medical Center Rostock).

_____ _____

Daniel Schultz **Michael Lalk**

Bioactive lipid screening during respiratory tract infections with bacterial and viral pathogens in mice

Daniel Schultz[1], Fabian Cuypers[2], Sebastian Skorka[2], Jan Rockstroh[1] Manuela Salazar[3], Jakob Krieger[4], Dirk Albrecht[5], KoInfekt Study Group, Michael Lalk[1], Nikolai Siemens[2] and Karen Methling[1]

[1] Institute of Biochemistry, University of Greifswald, Greifswald, Germany
[2] Department of Molecular Genetics and Infection Biology, University of Greifswald, Germany
[3] Department of Functional Genomics, University Medicine Greifswald, Greifswald, Germany
[4] Zoological Institute and Museum, Cytology and Evolutionary Biology, University of Greifswald, Greifswald, Germany
[5] Institute of Microbiology, University of Greifswald, Greifswald, Germany
* Email: methling@uni-greifswald.de

Abstract

Introduction: Respiratory tract infections are an emerging worldwide health problem for humans and animals. Lipid mediators are host-derived eicosanoids like hydroxyeicosatetraenoic acids (HETEs) and oxylipins like hydroxydocosahexaenoic acids (HDHAs) that activate immune system and resolution consisting out of eicosanoids like hydroxyeicosatetraenoic acids (HETEs) and oxylipins like hydroxydocosahexaenoic acids (HDHAs). Little is known about their role in infections with pathogens like *S. pneumoniae* and *S. aureus* as well as co-infection with Influenza A virus (IAV).

Objectives: We infected C57BL/6 mice with *S. pneumoniae*, *S. aureus*, IAV and additionally performed pneumonoccal-viral co-infection. Subsequently different sample types were screened to identify lipid mediator perturbations.

Methods: Lipid mediators from lung, spleen and blood plasma samples were analyzed using HPLC-MS/MS. Tissue samples were additionally investigated using MALDI-MS-Imaging to reveal the spatial-resolution of sphingosine 1-phosphate (S1P) and ceramide 1-phosphate (C1P). The appearance of bacterial pathogens in the lung was confirmed by immune fluorescent staining.

Results: We found IAV specific changes in the mice lungs for different HDHAs and HETEs as well as enhanced levels of 20-HETE for severe *S. aureus* infection. Moreover, MALDI-MS-Imaging analysis showed an accumulation of S1P and C1P during co-infection in lung and spleen. Long chain C1P was enriched in the red and not in the white pulp of the spleen.

Conclusion: Lipid mediator analysis showed that host response on bioactive level is in part specific for a certain pathogen, in particular for IAV infection. Furthermore, MS-Imaging showed great potential to study infections and revealed rise of S1P and C1P, which was not described before in context of co-infection.

1 Introduction

Infections of the respiratory tract are an emerging global problem for human health [1], which is strikingly apparent in the actual coronavirus crisis [2]. Besides coronavirus, airway infections can be caused by different bacterial and viral pathogens like *Staphylococcus aureus* (*S. aureus*), *Streptococcus pneumoniae* (*S. pneumoniae*) [3] and influenza A virus (IAV) [4]. In addition to infection with a single pathogen, bacterial-viral co-infections frequently occur, which can even aggravate the course of disease [5]. Host-derived bioactive lipids including eicosanoids and oxylipins are a group of lipids that are able to influence the immune system and therefore interesting metabolites in the analysis of host-pathogen interactions. They are derived from different ω-3 and ω-6 polyunsaturated fatty acids (PUFAs), and these PUFAs can be released from cell membranes by phospholipases. The most important PUFAs regarding oxylipin biosynthesis are arachidonic acid (AA), docosahexaenoic acid (DHA) and eicosapentaenoic acid (EPA). The main enzymes responsible for the biosynthesis of these oxylipins are lipoxygenases (LOX), cyclooxygenases (COX) and cytochrome P450 enzymes (CYPs). Additionally, some of the oxylipins can be synthesized by transcellular biosynthesis [6], non-enzymatic reactions or during lipid peroxidation processes [7]. These intermediates can have pro-inflammatory properties like immune cell attraction [8,9] or increased microvascular permeability [10]. The anti-inflammatory properties of lipid mediators include for instance inhibition of interleukin-6 secretion from macrophages [11], activation of peroxisome proliferator-activated receptor (PPAR) [12] or inhibition of immune cell migration [13]. For the separation and detection of these lipid mediators, HPLC-MS/MS techniques are widely used [14,15].

In addition to the described bioactive lipids originated from PUFA conversion, also mediators from the sphingolipids, sphingosine 1-phosphate (S1P) and ceramide 1-phosphate (C1P) in particular, are involved in immune system related processes like cell migration, cell survival, cell growth and the biosynthesis of eicosanoids [16-18]. The bioactive

lipids S1P and C1P are able to induce eicosanoid synthesis through the activation of cytosolic phospholipase A_2 [19] and COX-2 [20] respectively. The sphingolipid derivative C1P has further pro-inflammatory properties like mast cell degranulation [21] or activation of cell migration. The latter have been described for murine macrophages [22] and human monocytes [17]. High amounts of S1P are found in blood plasma and lymph, whereas the concentration is very low in the secondary lymphatic organs. This S1P gradient is important for lymphocyte traffic. According to lipid maps structure database, 14 derivatives of C1P with different acyl chain length are described [23]. Little is known about the distribution of C1P and S1P in immune system related organs. Matrix-assisted laser ionization MS imaging (MALDI-MS-Imaging) enables the measurement of the spatial distribution of metabolites or proteins within cryo sections of tissue samples.
The aim of this study was to analyze alterations in the eicosanoid profile of infected C57BL/6 mice. Therefore, mice were infected with IAV H1N1 (A/Bayern/74/2009), *S. aureus* strains LUG2012 (high pathogenic) and 113 (low pathogenic), *S. pneumoniae* 19F and co-infected with *S. pneumoniae* followed by an IAV infection. Lipid mediators from the sample types lung, spleen and blood plasma were detected using HPLC-MS/MS and additionally the spatial distribution of the bioactive lipids C1P and S1P were measured by MALDI-MS-Imaging. The presence of bacterial pathogens in the lung tissue was confirmed using immune fluorescent staining. Additionally, proteome analysis of important enzymes involved in oxylipin biosynthesis was performed. The investigation of the pathogen-mediated changes in the bioactive lipid profile could help us to understand pathogen-specific host immune responses in viral and bacterial single as well as co-infections.

2 Material and Methods

2.1 Animals and pathogens

2.2 Infection experiments

2.3 Lipid mediator extraction

Whole frozen lung and spleen samples were pulverized using a CP02 automated cryoPREP® (Covaris). The frozen tissue was transferred in a tissue tube (Covaris, extra thick) and cooled down by dipping in liquid nitrogen for 60 s. Then the sample was pulverized with an impact level of four and afterwards cooling and pulverization was repeated once as described above. 50 mg of organ powder was immediately extracted with 500 µL ice cold methanol (Roth®) containing 0.1 % 3,5-Di-*tert*-4-butylhydroxytoluene (Sigma-Aldrich) and 500 µL ice cold water. Then the internal standard consisting of 12-HETE-d_8 and 13-HODE-d_4 (both 100 ng/ml in acetonitrile; Cayman chemicals) was added. An alkaline hydrolysis step was performed using 300 µL sodium hydroxide (10 mol/L; Sigma-Aldrich) for 30 min at 60 °C. Immediately after hydrolysis, the pH was adjusted to a value of 6 using acetic acid (10 mol/L, VWR®). For EDTA plasma samples, an aliquot of 100 µL was hydrolyzed and extracted as described for the tissue material. Afterwards, solid phase extraction was done as previously described [24].

2.4 LC-MS/MS measurement of lipid mediators

Extracts were dried under nitrogen flow (TurboVap® from Biotage®) and reconstituted in 70 µL 80% acetonitrile (Th. Geyer®). Dynamic multiple reaction monitoring LC-MS/MS analysis was performed using an Agilent® HPLC system (1200 series), coupled to an Agilent® 6460 Triple quadrupole mass spectrometer with electrospray ionization source in negative mode. The separation was done with a Gemini® (Phenomenex, Torrance, CA, USA) NX-C18 column (3 µm, 100 × 2 mm) and equivalent pre-column. The separation and used MS parameters were described previously [25]. Calibration curves with MS-certified standards (purchased from Cayman chemicals) for absolute quantification (range between 0.5 ng/mL and 50 ng/ml for HETEs and EETs, curve type quadratic, weighting 1/x) and deuterated internal standards were used. Eicosanoids classes without appropriate MS-certified standards (HEPE, HODE; HDHA) were normalized to the response of the internal standard and stated in arbitrary units (AU) in the plots. Agilent Mass Hunter Qualitative Analysis software and Agilent Mass Hunter Quantitative Analysis software (both version B.07.00) were used for MS data analysis.

2.5 MALDI-FTICR-MS imaging

2.5.1 Tissue Preparation

Before cutting, the complete mice lung was embedded in 1% carboxymethylcellulose (high viscosity, Sigma-Aldrich) in ice cube trays and frozen for 24 hours at -80 °C. The carboxymethylcellulose was solved under stirring at 60 °C for three hours and cooled down at 4 °C before usage. The cryosections of lung (20 µm thickness) and spleen (10 µm thickness) were prepared using a Leica CM 1950 cryostat. Organs were partially glued with OCT embedding matrix (Roth®) for cutting and only OCT-free sections were transferred on cooled ITO coated glass slides (Bruker). After cutting, the sections were immediately lyophilized for 30 min. The MALDI matrix 9-aminoacridine (10 mg/mL from Sigma-Aldrich in 70% ethanol from Roth®) was spread on tissue sections using a HTX TM-Sprayer™ with the following parameters: N_2 pressure 10 psi, nozzle temperature: 65 °C, solvent flow: 0.125 mL/min, drying time: 10 s, track space: 2 mm and 4 passes.

2.5.2 Measurement

For MALDI-MS imaging, a solarix XR (Bruker) mass spectrometer (FT-ICR-MS) operating in negative ionization mode was used**.** The analyzed mass range was between 150-1000 m/z and the mass of 9-aminoacridin was used for online calibration. The following ion transfer parameters were used: time of flight of 0,750 ms, 4 MHz frequency and RV amplitude of 350 Vpp. The capillary exit was -150 V and Funnel 1 was set to 150 V. The laser focus was small with a frequency of 1000 Hz, 200 shots and a raster of 50 µm. An imaging run was done using flexImaging software (Bruker) and lipids were identified using the HMDB and lipid maps® database with a mass tolerance of 5 ppm. Additionally, identification of ceramide-1 phosphate and sphingosine-1 phosphate was done with standard compounds (both from Cayman chemicals).

2.6 Histology

2.6.1 H&E staining

After MALDI-MS imaging measurements, the slides with the tissue sections were transferred in a cuvette containing 60% ethanol to remove MALDI matrix. The H&E was done using a standard protocol. Histological scans were done using Reflecta MF5000 scanner.

2.6.2 IF staining

Lung cryosections (20 µm) were fixed in an ice-cold 4% formaldehyde (Roti®-Histofix) solution for 20 min and subsequently washed three times for 20 min with PBS. Afterwards, the sections were incubated for 60 min with PBS-TX (PBS containing 1% BSA (Sigma-Aldrich), 0.01% sodium azide and 0.3% Triton™ X-100). After buffer removal, 30 µl of primary antibody solution (rabbit anti-S. aureus ab20920 from Abcam and rabbit anti-*S. pneumoniae* from the lab of Prof. Dr. Sven Hammerschmidt) was added to the lung sections and incubated for 60 min in a humidity chamber. Slides were then washed five times for 2 min with PBS-TX. 30 µl of the secondary antibody (goat anti-rabbit IgG (H+L) with Alexa Fluor 488 from Thermo Fisher) together with phalloidin atto 550 (Sigma-Aldrich) and bisBenzimide H33258 (Sigma-Aldrich) was added and samples were incubated for 60 min. Finally, the sections were washed three times with PBS-TX and two times with PBS before embedding with mowiol 4-88 (Roth®).

2.7 Proteome analysis

2.8 Statistics

Infection experiments including lipid mediator analysis were performed in 8-10 biological replicates and in at least 13 replicates for PBS control experiments (non-infection). Statistics were done using the Kruskal-Wallis-test and Dunn´s multiple comparison test with Graph Pad Prism (version 7.05). The p-values obtained after Dunn´s correction were

compared to a significance level α of 0.05. MALDI-MS-imaging was performed with three replicates and discriminative m/z signals were analyzed using receiver operating characteristics (ROC) analysis tool (area under curve > 0.75) from SCiLS Lab software. Image data were normalized using total ion count normalization.

3 Results

3.1 Clinical scoring and lung infiltration

Mouse infection with the high-pathogenic *S. aureus* strain LUG2012 led to the highest observed clinical score eight hours post infection (hpi) for all tested infection experiments (Fig S1B) and the animals had to be sacrificed. Therefore, this strain seemed not suitable for long-term co-infection experiments. The infection with the low pathogenic *S. aureus* strain 113 resulted in lower scores (Fig S1A). A dose dependent response on pathogenic burden was also observed for both *S. pneumoniae* 19F infections leading to a colonization (1E07 CFU) or a pneumonia (1E08 CFU) as shown in Fig S1C. The administration of a higher pneumococcal dose to induce pneumonia led to higher clinical scores compared to pneumococcal colonization with a peak at two days post infection (dpi). The IAV infection led a maximum score at five dpi, which was comparable to the maximum of the pneumococcal score (Fig S1D). For a co-infection experiment, a colonization with *S. pneumoniae* 19F was performed followed by IAV infection for 2 days. A difference in scoring between the colonized mouse and co-infected animals was not observed. The IF staining confirmed the presence of the bacterial pathogens *S. aureus* and *S. pneumoniae* in the lungs of infected animals (Figure S1F). The high-pathogenic *S. aureus* strain LUG2012 showed a strong invasion of the lung at eight hpi, which was not observed for the staphylococcal strain 113 at 3 dpi in the analyzed tissue sections. The presence of bacterial pathogens in all lung samples used for MALDI-MS-Imaging was confirmed by separate IF staining from sections of the same tissue samples.

3.2 Eicosanoid analysis of the lungs

Oxylipin analysis of the lungs revealed increased amounts of lipid mediators from mainly LOX conversion during IAV infection (5 dpi) namely pro-inflammatory 5-and 20-HETE as well as anti-inflammatory 12-and 15-HETE as shown in Figure 1. Furthermore, we measured enhanced levels of anti-inflammatory 13-, 14-and 17-HDHA in accordance with IAV infection. The amount of the pro-inflammatory 20-HETE was moreover enhanced (5 ng/100 mg) in samples infected with the high-pathogenic strain *S. aureus* LUG2012. Besides, *S. aureus* LUG2012 infection led to increased levels of the EPA metabolite 18-HEPE. In general, infections with *S. pneumoniae* and *S. aureus* 113 had only little influence on analyzed lipid mediators. Another EPA-derived oxylipin is 15-HEPE and it showed alterations for infection with both *S. aureus* strains, *S. pneumoniae* induced pneumonia (1E08 CFU) as well as IAV infections.

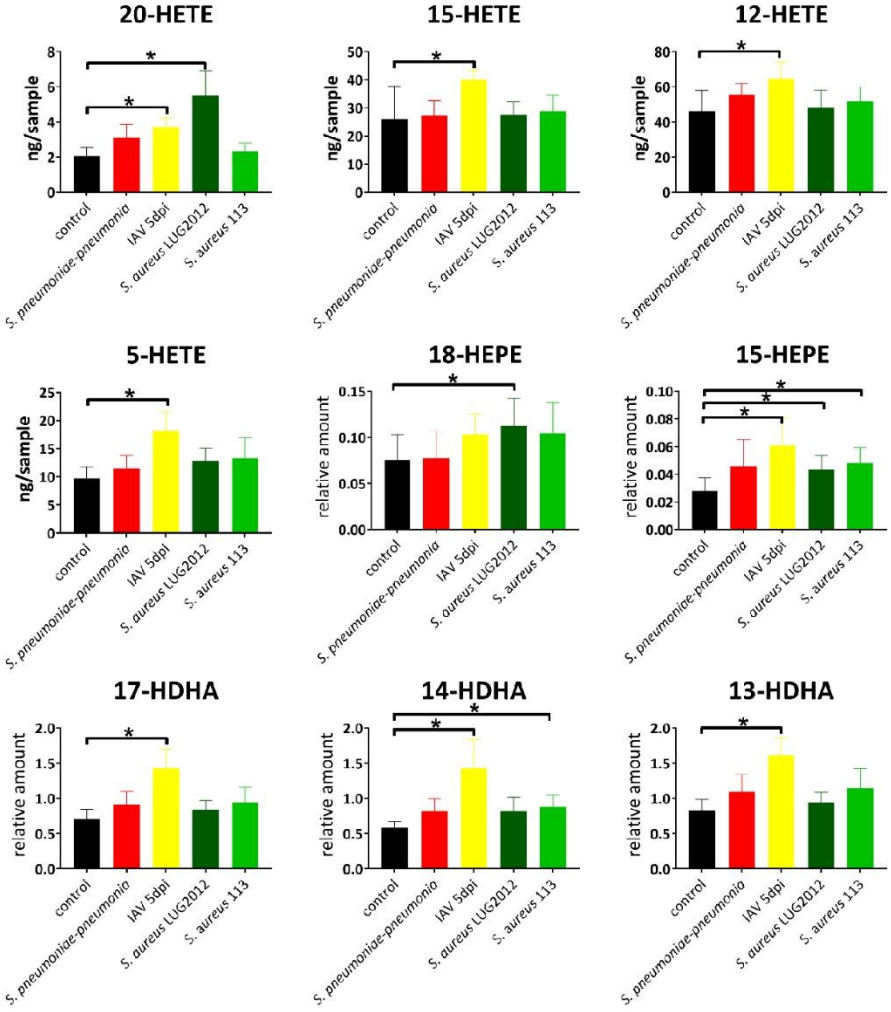

Figure 1: Lung oxylipin amounts in response to bacterial and virus mono-infections: control (black), *S. pneumoniae* induced pneumonia (red), IAV (yellow), infection with *S. aureus* strain LUG2012 (dark green) and strain 133 (light green). The bars denote mean values ± standard deviations. For statistical analysis, Kruskal-Wallis test with Dunn´s multiple comparison test for n =13 replicates (control) and n = 8-10 replicates (infections). The p-values were compared to a significance level α of 0.05 and significant changes were marked using asterisk. The oxylipin amounts were normalized to sample weights of 100 mg.

We used IAV and *S. pneumoniae* for co-infection experiments starting with bacterial colonization for 7 days followed by IAV infection for 4 days with slight modifications for long-term experiments: the bacterial burden was reduced (from 1E08 CFU for pneumonia to 1E07 CFU for colonization) and the following viral infection was shortened to two

days. As shown in Figure 2, co-infection led to decreased amounts of 20-HETE and 12-HETE as well as increased 18-HEPE level compared to control and to corresponding mono-infection. The level of 15-HETE in co-infection samples was reduced compared to control and 5-HETE was affected negatively during co-infection compared to IAV infected animals. A further decrease in the amount of oxylipins in co-infection samples compared to IAV mono-infection could be detected for 14-and 17-HDHA. Moreover, for the pro-inflammatory oxylipin 9-HODE an increased amount during co-infection compared to mono-infections could be observed.

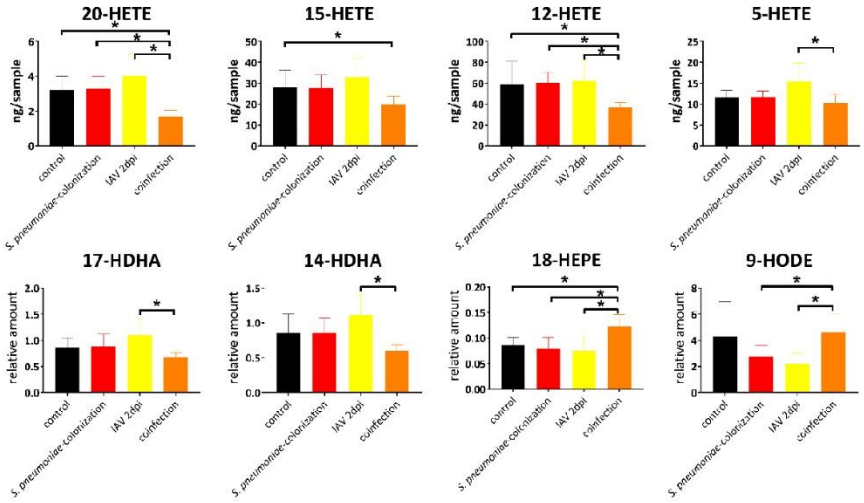

Figure 2: Lung oxylipin amounts in response to co-infection with *S. pneumoniae* and IAV: control (black), *S. pneumoniae* induced lung colonization (red), IAV (yellow) and co-infection (orange). The bars denote mean values ± standard deviations. For statistical analysis, Kruskal-Wallis test with Dunn´s multiple comparison test for n =14 replicates (control), n = 9 replicates (mono-infections) and n = 6 (co-infection). The p-values were compared to a significance level α of 0.05 and significant changes were marked using asterisk. The oxylipin amounts were normalized to sample weights of 100 mg.

In addition to oxylipin measurement, the proteome of infected lungs was analyzed from separate infection experiments including all tested IAV and S. *pneumoniae* conditions. Perturbations were found for several enzymes involved in lipid mediator biosynthesis like cytosolic phospholipase A2 (cPLA$_2$), which is responsible for the release of lipid mediator precursors from plasma membrane. Indeed, increased cPLA$_2$ levels were detected for IAV infection at 5 dpi (Tab S1) together with enhanced amounts of the 5-LOX-activating protein (FLAP), which were both in accordance with augmented amounts of the corresponding HETEs, HEPEs and HDHAs during IAV infection. Moreover, the comparison of samples from IAV infection obtained from the two different time points 2 and 5 dpi showed enhanced levels of cPLA$_2$ at 5 dpi together with increased amounts of HDHAs at 5 dpi compared to 2 dpi. Other significant changes in protein levels like increased FLAP levels during *S. pneumoniae* related pneumonia or reduced amounts of glutathione peroxidase 1 needed for 5-HETE synthesis during co-infection accorded with the tendency of oxylipin levels, but the changes in this lipid mediators were not significant compared to control.

3.3 Eicosanoid analysis of the blood plasma and spleen

Analysis of plasma samples from infected mice revealed significant perturbations in particular for *S. aureus* LUG2012 and *S. pneumoniae* infections as shown in Figure 3. All anti-inflammatory EETs were detected in increased amounts under pneumoncoccal induced pneumonia and 14,15-EET was the most affected one. The baseline EET levels were significantly lower in plasma samples than in spleen and lung samples. Moreover, enhanced levels of 12-, 15-and 20-HETE as well as 14-and 17-HDHA could be measured for mice infected with *S. aureus* LUG2012. In contrast to *S. pneumoniae* related pneumonia, the colonization had no impact on levels of EETs in plasma. The co-infection led to decreased amounts of 12-, 15- and 20-HETE as well as 13-HODE and 17-HDHA in comparison to control and pneumococcal related colonization. As for lung samples, a rise of 18-HEPE could be measured under co-infection conditions. For both analyzed time points during IAV infection (2 dpi and 5 dpi) a decrease in the amount of 9-HODE and 13-HODE could be observed and these levels were also reduced under co-infection compared to control plasma levels.

Lipid mediators analyzed in the spleen showed increased level of 20-HETE for *S. aureus* LUG2012 infection in blood plasma and lung samples. The amount of 11,12-EET measured in the spleen was enhanced under infection with the staphylococcal 113 strain. Moreover, the anti-inflammatory metabolite 13-HODE and pro-inflammatory 5-HETE were detected in decreased amounts under *S. aureus* 113 infection. The co-infection led to reduced EET levels compared to control for all measured anti-inflammatory EETs. The same effect was investigated during IAV infection (2 dpi) for 14,15 -EET; 11,12-EET and 8,9-EET. Moreover, changes in the oxylipin levels with exception of 11,12-EET observed for pneumococcal colonization or related pneumonia were not statistically significant.

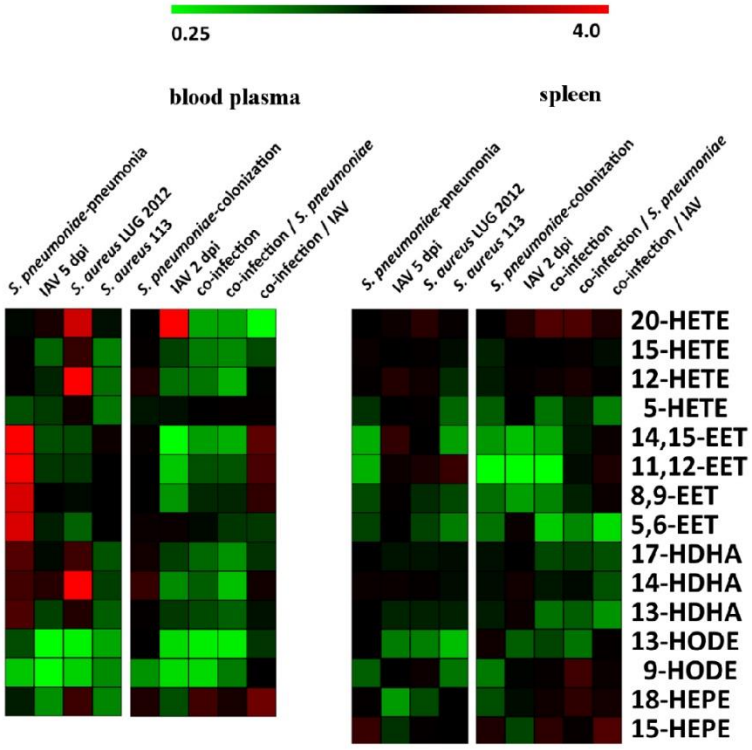

Figure 3: Heatmap displaying fold change (infection/control or co-infection/corresponding mono-infection) of lipid mediator amounts from blood plasma (left side) and spleen (right side). Decreased levels are shown in green, increased amounts in red and comparable amounts in black. The oxylipin amounts were normalized to sample weights of 100 mg (spleen) or 100 µL (blood plasma). 15-HEPE was not detected in plasma samples.

3.4 Ratio of 13-HODE/9-HODE

The anti-inflammatory 13-HODE and the pro-inflammatory 9-HODE are both products of linoleic acid oxidation. Their ratio is possibly useful to describe the immune status of the mouse during infection [26]. We calculated the ratio for all sample types (Figure 4) and observed similar relations independent of sample type even if the single 9-and 13-HODE levels differ in the different organs or plasma. A colonization with *S. pneumoniae* led to increased ratios in both organ types suggesting an anti-inflammatory state. An IAV infection had no impact on HODE ratio, Moreover, the 13-HODE/9-HODE relation decreased during co-infection compared to bacterial mono-infection and to a lower extend in comparison to control.

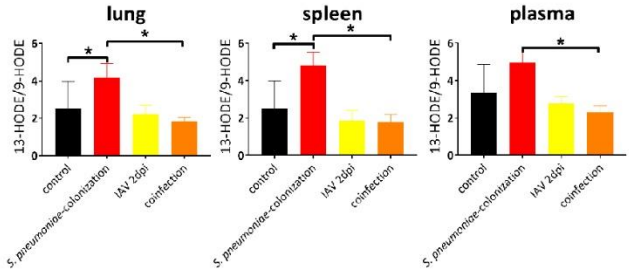

Figure 4: Ratio of 13-HODE/9-HODE calculated for all samples types in response to co-infection with *S. pneumoniae* and IAV: control (black), *S. pneumoniae* induced lung colonization (red), infection with IAV (yellow) and co-infection (orange).

3.4 MALDI-MS-Imaging reveals rise of S1P and C1P under co-infection

We additionally analyzed the spatial resolution of bioactive S1P and C1P (CerP) in lung and spleen samples. For statistical evaluation, ROC analysis was used and the resulting AUC values are listed in Table S2. This method can be used to identify m/z values discriminating different conditions [27,28]. The measurements of the spleen samples revealed that the amount of S1P decreased during mono-infection with *S. aureus* 113, IAV and co-infection (Figure 5). Several derivatives of C1P exist with different acyl chain lengths. Three of these different derivatives (C18:0, C24:1 and C26:1) decreased in amounts under IAV infection and an increase under co-infection compared to control and corresponding mono-infection. Moreover, we were able to show, that the distribution of the long chain C1P (d18:1/26:1(17*Z*)) was higher in the red pulp (pink area of the HE stains, Figure 5) than in the white pulp (dark purple areas of the HE staining). The co-infection led to increased amounts of all three C1P derivatives in the red pulp, whereas, the infection with *S. aureus* LUG2012 or *S. pneumoniae* alone didn´t seem to affect the amount of S1P or C1P.

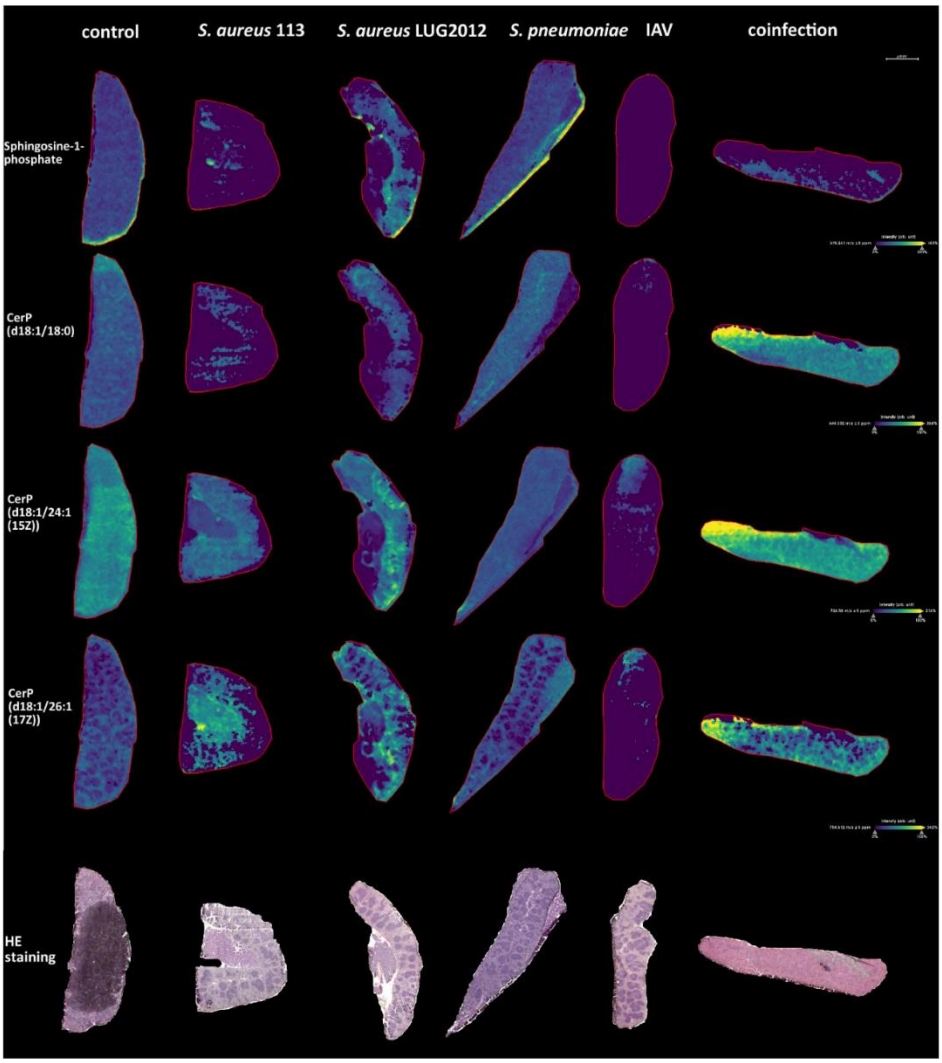

Figure 5: MALDI-MS-Imaging and HE staining of spleen samples. Representative images from three replicates per condition are shown. The measurements include samples of infections with *S. aureus* strains 113 and LUG2012, *S. pneumoniae* (colonization), IAV (5 dpi) and co-infection. The compound-related heatmaps illustrate high intensities in yellow and low abundances in purple normalized to total ion count.

The MALDI-MS-Imaging analysis of the lungs with direct pathogen colonization showed several similarities to the spleen. As for the spleen, an accumulation of C1Ps could be observed (Figure 6). Furthermore, enhanced amounts of C1P (d18:1/18:0) and C1P (d18:1/24:1(15Z)) compared to control and mono-infection could be measured in co-infected lungs. However, the pneumococcal infection caused a drop in C1P (d18:1/18:0), which differs from spleen samples. Additionally, a decrease in S1P concentration under *S. pneumoniae* infection was observed different to the spleen. A further difference to the results of the analysis of the spleen was the impact of IAV on S1P levels. Whereas splenic levels decreased, we observed an increased amount in the lung. Furthermore, lung S1P and C1P amounts didn´t show alterations due to infection with both *S. aureus* strains.

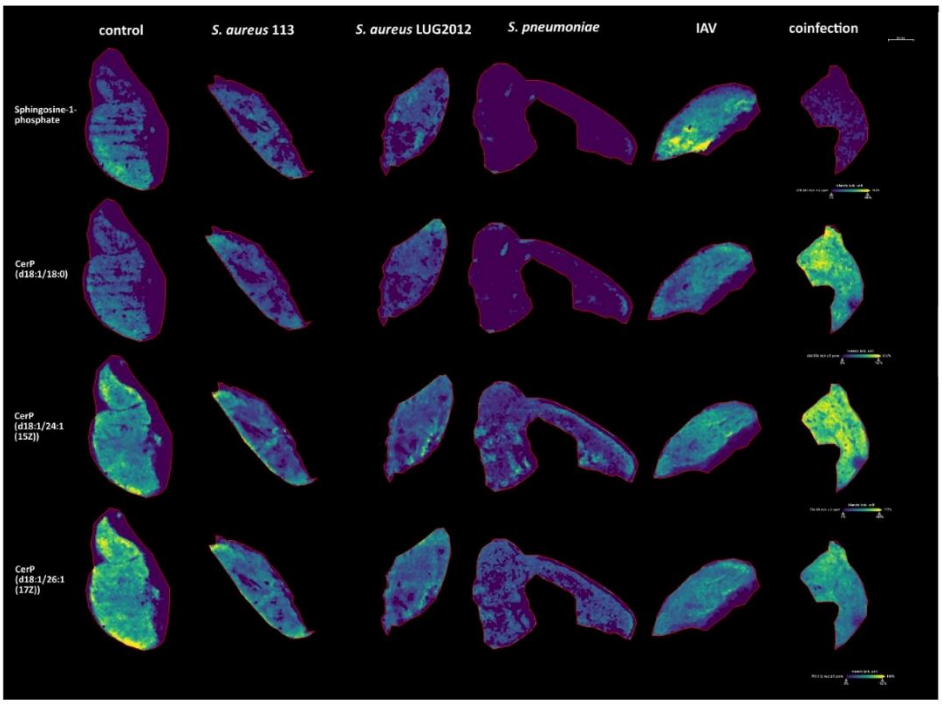

Figure 6*:* MALDI-MS-Imaging of lung samples. Representative images from three replicates per condition are shown. The measurements include samples from infection with *S. aureus* strains 113 and LUG2012, *S. pneumoniae* (colonization), IAV (5 dpi) and co-infection. The compound-related heatmaps illustrate high intensities in yellow and low abundances in purple normalized to total ion count.

4 Conclusions

The oxylipin analysis through HPLC-MS/MS combined with MALDI-MS-Imaging of different sample types from respiratory tract infected mice revealed that mainly IAV, *S. aureus* LUG2012 and co-infection with both *S. pneumoniae* and IAV are responsible for the majority of changes in the bioactive lipid levels. Perturbations focusing on eicosanoids were observed for lung with direct pathogen contact as well as for blood plasma. The spleen as part of the immune system showed an increase of C1Ps with different chain length during co-infection. On the one hand, C1P has pro-inflammatory properties including activation of cell migration, which is described for murine macrophages [22] and human monocytes [17]. On the other hand, C1P seems to prevent the biosynthesis of pro-inflammatory ceramides during respiratory infection [29]. To our knowledge, this is the first report of a splenic red pulp-specific distribution for long-chain C1P. The accumulation of C1Ps during a pneumococcal infection followed by IAV infection was not described before. This impact of the co-infection on C1P levels could be confirmed for two of three detected C1Ps through similar accumulations in the lung and may suggest a local and systemic host immune reaction.

An opposite behavior was observed for S1P levels in lung and spleen, which both showed a decrease under co-infection conditions. S1P is mainly known for its pro-inflammatory properties including the activation of eicosanoid synthesis through activation of COX-2 [20]. S1P is not distributed equally among organs and body fluids. High amounts of S1P are found in blood plasma and lymph, whereas the concentration in the secondary lymphatic organs is very low. This S1P gradient is important for lymphocyte traffic [30]. The decrease during infection with IAV and corresponding co-infection may be beneficial for facilitating immune cell migration into the spleen which seems to be independent from pneumococcal infection. Lung S1P levels showed an increase for IAV infection. Indeed, the enzyme sphingosine kinase SphK, which is responsible for S1P biosynthesis can be upregulated by the IAV to promote virus propagation [31]. An accumulation of S1P in the lung was not detected upon co-infection. This could be due to the pneumococcal influence or due to reduced IAV infection time.

Moreover, IAV infection for five days led to strong increase in levels of HETEs and HDHAs, which was previously detected for lungs of infected pigs using the same IAV strain [24] or mice infection with other IAV strains [26,32]. The obtained proteome data confirmed this observation. In particular, 17-HDHA is known for its positive effect on host antibody production against IAV [33]. Beside its positive effect on host B cell activation, 17-HDHA is able to inhibit viral nucleoprotein mRNA expression in human lung epithelial cells [28]. The same effect was reported for 12- and 15-HETE [32]. Furthermore, 12-and 15-HETE are anti-inflammatory and able to inhibit the interleukin-6 secretion from macrophages [11], whereas 5-HETE is a potent chemoattractant for immune cells [9]. Under co-infection conditions, the HDHAs and HETEs were not found to be elevated and moreover the clinical scores were unobtrusive. For 17-HDHA this phenomenon is also described for IAV infected children with bacterial co-infection [34]. This could be a sign for a dampened host reaction towards infection, but the reason is still unclear.

A prominent role was detected for 20-HETE in all sample types during infection with the high invasive and strong pathogenic *S. aureus* LUG2012 leading to high clinical scores. Besides locally affected 20-HETE level from lungs samples, also a systemic reaction with alterations of 20-HETE amounts in spleen and blood plasma was visible. This lipid mediator is found to be associated with sepsis and arthritis and can influence vasoconstriction and vasodilation by release of nitric oxide [35], induce cardiac protection in sepsis (60) and inhibit synthesis of prostanoids like PG E_2 [36,37]. We have evidence, that the rise of 20-HETE may be associated not only with *S. aureus* but also with severe infections [38] and this aspect was also observed in other studies [35,39].

The analysis of lipid mediators reveals broad perturbations for sample material localized close to infection site (lung) and for sample material common for diagnostics (plasma). Our results showed that the lung material is a promising sample type to study respiratory tract infections. Some of the detected changes were IAV-specific like for 17-, 14-and 13-HDHA or related to severe infection with *S. aureus* LUG2012, which was the case for increased levels of 20-HETE in all sample types. An infection with *S. pneumoniae* only affected EET levels in plasma when oxylipin amounts were considered individually. Additionally, the 13-HODE/9-HODE ratio showed changes in all sample materials and could be a helpful extension to evaluate pneumococcal infections. Moreover, MALDI-MS-Imaging showed great potential to study host reaction to infection within the organ. The spatial resolution revealed accumulation of different C1P derivatives in lung and spleen during co-infection and furthermore high levels of long chain C1P in the red pulp of the spleen.

Acknowledgement: The authors thank Katharina Riedel, Gabriele Uhl, Heidi Land, Steffen Harzsch, Jan-Peter Hildebrandt and Elvira Lutjanov (all University of Greifswald) for their support concerning tissue imaging. We further thank Sven Hammerschmidt (University of Greifswald) for the kindly donation of anti-*S. pneumoniae* antibody.

Funding: This study was funded by Federal Excellence Initiative of Mecklenburg Western Pomerania and European Social Fund (ESF) Grant KoInfekt (ESF_14-BM-A55-00xx_16). Moreover, this research was funded by the Deutsche Forschungsgemeinschaft (DFG) within the GRK 1870.

Conflict of Interest: The authors declare no conflict of interest.

Author Contributions

ML, NS, DS and KM conceived and designed research. FC, SS and NS conducted infection experiments. DS and KM performed oxylipin measurement and analyzed data. DS and DA conducted MALDI-MS-Imaging. JK and DS performed IF staining and imaging. MS conducted proteome analysis. DS analyzed data and wrote the manuscript. All authors read and approved the manuscript.

Ethical Statements

All applicable international, national, and/or institutional guidelines for the care and use of animals were followed.

Data Availability The metabolomics and metadata reported in this paper are available via [insert repository and URL] study identifier [insert study identifier/project ID etc]

References

1. Collaborators, G.B.D.C.o.D. Global, regional, and national age-sex-specific mortality for 282 causes of death in 195 countries and territories, 1980-2017: A systematic analysis for the global burden of disease study 2017. *Lancet* **2018**, *392*, 1736-1788.
2. Huang, C.; Wang, Y.; Li, X.; Ren, L.; Zhao, J.; Hu, Y.; Zhang, L.; Fan, G.; Xu, J.; Gu, X., *et al.* Clinical features of patients infected with 2019 novel coronavirus in wuhan, china. *Lancet* **2020**, *395*, 497-506.
3. Aliberti, S.; Kaye, K.S. The changing microbiologic epidemiology of community-acquired pneumonia. *Postgraduate medicine* **2013**, *125*, 31-42.
4. Collaborators, G.B.D.I. Mortality, morbidity, and hospitalisations due to influenza lower respiratory tract infections, 2017: An analysis for the global burden of disease study 2017. *The Lancet. Respiratory medicine* **2019**, *7*, 69-89.
5. McCullers, J.A. The co-pathogenesis of influenza viruses with bacteria in the lung. *Nature reviews. Microbiology* **2014**, *12*, 252-262.
6. Fabre, J.E.; Goulet, J.L.; Riche, E.; Nguyen, M.; Coggins, K.; Offenbacher, S.; Koller, B.H. Transcellular biosynthesis contributes to the production of leukotrienes during inflammatory responses in vivo. *The Journal of clinical investigation* **2002**, *109*, 1373-1380.
7. Hall, L.M.; Murphy, R.C. Electrospray mass spectrometric analysis of 5-hydroperoxy and 5-hydroxyeicosatetraenoic acids generated by lipid peroxidation of red blood cell ghost phospholipids. *Journal of the American Society for Mass Spectrometry* **1998**, *9*, 527-532.
8. Nakayama, T.; Mutsuga, N.; Yao, L.; Tosato, G. Prostaglandin E2 promotes degranulation-independent release of MCP-1 from mast cells. *Journal of leukocyte biology* **2006**, *79*, 95-104.
9. Bittleman, D.B.; Casale, T.B. 5-hydroxyeicosatetraenoic acid (HETE)-induced neutrophil transcellular migration is dependent upon enantiomeric structure. *American journal of respiratory cell and molecular biology* **1995**, *12*, 260-267.
10. Funk, C.D. Prostaglandins and leukotrienes: Advances in eicosanoid biology. *Science* **2001**, *294*, 1871-1875.
11. Kronke, G.; Katzenbeisser, J.; Uderhardt, S.; Zaiss, M.M.; Scholtysek, C.; Schabbauer, G.; Zarbock, A.; Koenders, M.I.; Axmann, R.; Zwerina, J., *et al.* 12/15-lipoxygenase counteracts inflammation and tissue damage in arthritis. *Journal of immunology* **2009**, *183*, 3383-3389.
12. Wray, J.A.; Sugden, M.C.; Zeldin, D.C.; Greenwood, G.K.; Samsuddin, S.; Miller-Degraff, L.; Bradbury, J.A.; Holness, M.J.; Warner, T.D.; Bishop-Bailey, D. The epoxygenases CYP2j2 activates the nuclear receptor ppar alpha in vitro and in vivo. *Plos One* **2009**, *4*.

13. Serhan, C.N. Pro-resolving lipid mediators are leads for resolution physiology. *Nature* **2014**, *510*, 92-101.
14. Levison, B.S.; Zhang, R.; Wang, Z.; Fu, X.; DiDonato, J.A.; Hazen, S.L. Quantification of fatty acid oxidation products using online high-performance liquid chromatography tandem mass spectrometry. *Free radical biology & medicine* **2013**, *59*, 2-13.
15. Astarita, G.; Kendall, A.C.; Dennis, E.A.; Nicolaou, A. Targeted lipidomic strategies for oxygenated metabolites of polyunsaturated fatty acids. *Biochimica et biophysica acta* **2015**, *1851*, 456-468.
16. Cuvillier, O.; Pirianov, G.; Kleuser, B.; Vanek, P.G.; Coso, O.A.; Gutkind, S.; Spiegel, S. Suppression of ceramide-mediated programmed cell death by sphingosine-1-phosphate. *Nature* **1996**, *381*, 800-803.
17. Arana, L.; Ordonez, M.; Ouro, A.; Rivera, I.G.; Gangoiti, P.; Trueba, M.; Gomez-Munoz, A. Ceramide 1-phosphate induces macrophage chemoattractant protein-1 release: Involvement in ceramide 1-phosphate-stimulated cell migration. *American journal of physiology. Endocrinology and metabolism* **2013**, *304*, E1213-1226.
18. Simanshu, D.K.; Kamlekar, R.K.; Wijesinghe, D.S.; Zou, X.; Zhai, X.; Mishra, S.K.; Molotkovsky, J.G.; Malinina, L.; Hinchcliffe, E.H.; Chalfant, C.E., *et al.* Non-vesicular trafficking by a ceramide-1-phosphate transfer protein regulates eicosanoids. *Nature* **2013**, *500*, 463-467.
19. Pettus, B.J.; Bielawska, A.; Subramanian, P.; Wijesinghe, D.S.; Maceyka, M.; Leslie, C.C.; Evans, J.H.; Freiberg, J.; Roddy, P.; Hannun, Y.A., *et al.* Ceramide 1-phosphate is a direct activator of cytosolic phospholipase a(2). *Journal of Biological Chemistry* **2004**, *279*, 11320-11326.
20. Pettus, B.J.; Kitatani, K.; Chalfant, C.E.; Taha, T.A.; Kawamori, T.; Bielawski, J.; Obeid, L.M.; Hannun, Y.A. The coordination of prostaglandin e2 production by sphingosine-1-phosphate and ceramide-1-phosphate. *Molecular pharmacology* **2005**, *68*, 330-335.
21. Mitsutake, S.; Kim, T.J.; Inagaki, Y.; Kato, M.; Yamashita, T.; Igarashi, Y. Ceramide kinase is a mediator of calcium-dependent degranulation in mast cells. *Journal of Biological Chemistry* **2004**, *279*, 17570-17577.
22. Granado, M.H.; Gangoiti, P.; Ouro, A.; Arana, L.; Gonzalez, M.; Trueba, M.; Gomez-Munoz, A. Ceramide 1-phosphate (C1P) promotes cell migration involvement of a specific C1P receptor. *Cell Signal* **2009**, *21*, 405-412.
23. Sud, M.; Fahy, E.; Cotter, D.; Brown, A.; Dennis, E.A.; Glass, C.K.; Merrill, A.H., Jr.; Murphy, R.C.; Raetz, C.R.; Russell, D.W., *et al.* Lmsd: Lipid maps structure database. *Nucleic acids research* **2007**, *35*, D527-532.
24. Schultz, D.; Methling, K.; KoInfekt Study, G.; Rothe, M.; Lalk, M. Eicosanoid profile of influenza A virus infected pigs. *Metabolites* **2019**, *9*.
25. Schultz, D.; Surabhi, S.; Stelling, N.; Rothe, M.; Group, K.S.; Methling, K.; Hammerschmidt, S.; Siemens, N.; Lalk, M. 16HBE cell lipid mediator responses to mono and co-infections with respiratory pathogens. *Metabolites* **2020**, *10*.
26. Tam, V.C.; Quehenberger, O.; Oshansky, C.M.; Suen, R.; Armando, A.M.; Treuting, P.M.; Thomas, P.G.; Dennis, E.A.; Aderem, A. Lipidomic profiling of influenza infection identifies mediators that induce and resolve inflammation. *Cell* **2013**, *154*, 213-227.
27. Klein, O.; Strohschein, K.; Nebrich, G.; Oetjen, J.; Trede, D.; Thiele, H.; Alexandrov, T.; Giavalisco, P.; Duda, G.N.; von Roth, P., *et al.* Maldi imaging mass spectrometry: Discrimination of pathophysiological regions in traumatized skeletal muscle by characteristic peptide signatures. *Proteomics* **2014**, *14*, 2249-2260.
28. Hajian-Tilaki, K. Receiver operating characteristic (ROC) curve analysis for medical diagnostic test evaluation. *Caspian journal of internal medicine* **2013**, *4*, 627-635.
29. Peng, H.M.; Li, C.; Kadow, S.; Henry, B.D.; Steinmann, J.; Becker, K.A.; Riehle, A.; Beckmann, N.; Wilker, B.; Li, P.L., *et al.* Acid sphingomyelinase inhibition protects mice from lung edema and lethal *staphylococcus aureus* sepsis. *J Mol Med* **2015**, *93*, 675-689.

30. Baeyens, A.; Fang, V.; Chen, C.; Schwab, S.R. Exit strategies: S1P signaling and t cell migration. *Trends in immunology* **2015**, *36*, 778-787.
31. Vijayan, M.; Hahm, B. Influenza viral manipulation of sphingolipid metabolism and signaling to modulate host defense system. *Scientifica* **2014**, *2014*, 793815.
32. Morita, M.; Kuba, K.; Ichikawa, A.; Nakayama, M.; Katahira, J.; Iwamoto, R.; Watanebe, T.; Sakabe, S.; Daidoji, T.; Nakamura, S., *et al.* The lipid mediator protectin D1 inhibits influenza virus replication and improves severe influenza. *Cell* **2013**, *153*, 112-125.
33. Ramon, S.; Baker, S.F.; Sahler, J.M.; Kim, N.; Feldsott, E.A.; Serhan, C.N.; Martinez-Sobrido, L.; Topham, D.J.; Phipps, R.P. The specialized proresolving mediator 17-HDHA enhances the antibody-mediated immune response against influenza virus: A new class of adjuvant? *Journal of immunology* **2014**, *193*, 6031-6040.
34. Anania, V.G.; Randolph, A.G.; Yang, X.; Nguyen, A.; Newhams, M.M.; Mathews, W.R.; Rosenberger, C.M.; McBride, J.M. Early amplified respiratory bioactive lipid response is associated with worse outcomes in pediatric influenza-related respiratory failure. *Open Forum Infect Dis* **2020**, *7*, ofaa122.
35. Cuez, T.; Korkmaz, B.; Buharalioglu, C.K.; Sahan-Firat, S.; Falck, J.; Malik, K.U.; Tunctan, B. A synthetic analogue of 20-HETE, 5,14-HEDGE, reverses endotoxin-induced hypotension via increased 20-HETE levels associated with decreased inos protein expression and vasodilator prostanoid production in rats. *Basic Clin Pharmacol* **2010**, *106*, 378-388.
36. Chen, J.M.; Hamers, A.J.P.; Finsterbusch, M.; Massimo, G.; Zafar, M.; Corder, R.; Colas, R.A.; Dalli, J.; Thiemermann, C.; Ahluwalia, A. Endogenously generated arachidonate-derived ligands for trpv1 induce cardiac protection in sepsis. *Faseb J* **2018**, *32*, 3816-3831.
37. Tunctan, B.; Korkmaz, B.; Sari, A.N.; Kacan, M.; Unsal, D.; Serin, M.S.; Buharalioglu, C.K.; Sahan-Firat, S.; Cuez, T.; Schunck, W.H., *et al.* Contribution of inos/sgc/pkg pathway, cox-2, cyp4a1, and gp91(phox) to the protective effect of 5,14-HEDGE, a 20-HETE mimetic, against vasodilation, hypotension, tachycardia, and inflammation in a rat model of septic shock. *Nitric Oxide-Biol Ch* **2013**, *33*, 18-41.
38. Volzke, J.; Schultz, D.; Kordt, M.; Muller, M.; Bergmann, W.; Methling, K.; Kreikemeyer, B.; Muller-Hilke, B.; KoInfekt Study, G. Inflammatory joint disease is a risk factor for streptococcal sepsis and septic arthritis in mice. *Front Immunol* **2020**, *11*, 579475.
39. Tunctan, B.; Korkmaz, B.; Sari, A.N.; Kacan, M.; Unsal, D.; Serin, M.S.; Buharalioglu, C.K.; Sahan-Firat, S.; Schunck, W.H.; Falck, J.R., *et al.* A novel treatment strategy for sepsis and septic shock based on the interactions between prostanoids, nitric oxide, and 20-hydroxyeicosatetraenoic acid. *Anti-inflammatory & anti-allergy agents in medicinal chemistry* **2012**, *11*, 121-150.

Supplemental Material

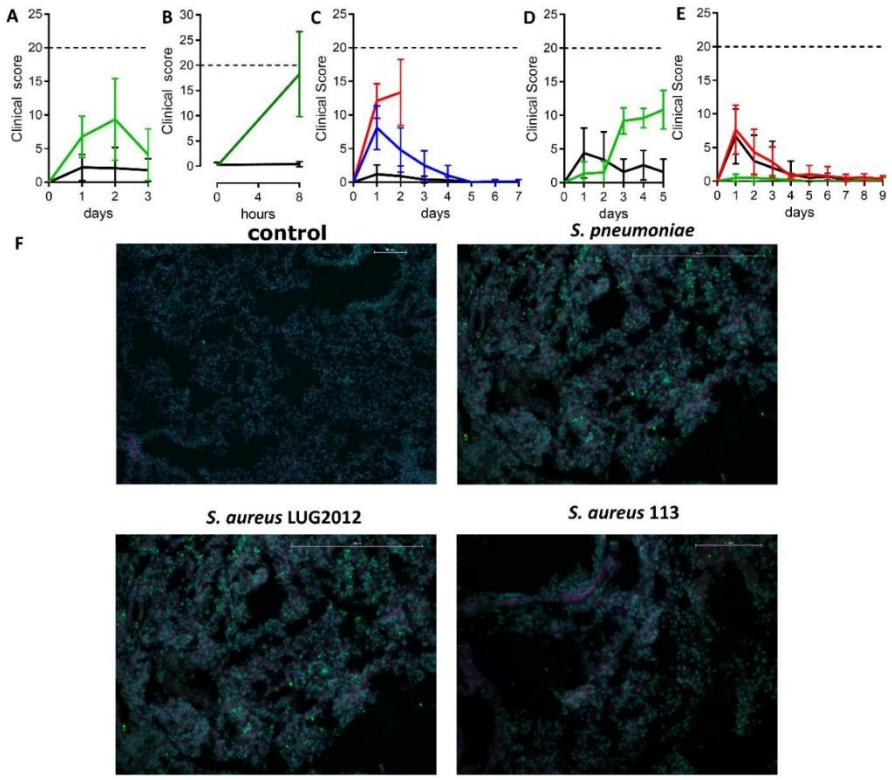

Figure S1: Clinical scores of mice infected with S. *aureus* strain 113 for three days (A) and strain LUG2012 for eight hours (B); *S. pneumoniae* colonization for seven days (C, blue) and induced pneumonia for two days (C, red), IAV for five days (D) and co-infection starting with colonization of *S. pneumoniae* for seven days (E, black) followed by IAV infection at seven dpi for a duration of two days (green) resulting in co-infected animals, which were challenged all in all for nine days with pathogens (red). With exception for (E), clinical scores of control (non-infected) animals are shown in black. Representative images of lungs from immune fluorescent staining are shown in (F). Lung infiltrating bacterial pathogens *S. aureus* and *S. pneumoniae* are illustrated in green, nuclei in cyan and actin filaments from lung tissue in purple.

Table S1: Log_2 ratio of altered proteins involved in oxylipin biosynthesis in the lungs. Glutathione peroxidase 1 (GPX1), 5-LOX-activating protein (FLAP), 12-lipoxygenating 15-LOX and cytosolic phospholipase A_2 ($cPLA_2$) were detected in lung samples from separate infection experiments. Displayed are significant ratios with a corrected *p*-value <0.5 from Benjamini- Hochberg correction. For pneumococcal infections, induced pneumonia was compared to control and colonization with co-infection.

	S. pneumoniae **vs control**	**IAV 5 dpi vs control**	**co-infection vs control**	**IAV 5 dpi vs *S. pneumoniae***	**IAV 5 dpi vs IAV 2 dpi**
GPX1	-	-	-0.23	-	-
FLAP	0.96	0.81	-	-	0.83
15-LOX	-	-	0.66	-	-
$cPLA_2$	-	0.84	-	0.54	0.92

Table S2: AUC values from ROC analysis of lung and spleen for S1P and CerPs for the different infection conditions.

	S1P	CerP (d18:1/18:0)	CerP (d18:1/24:1(15Z))	CerP (d18:1/26:1(17Z))
lung				
control vs *S. pneumoniae*	0.800	0.788	0.778	0.834
control vs IAV	0.248	0.272	-	-
control vs coinfection	-	0.096	0.128	-
IAV vs coinfection	0.834	0.181	0.168	-
spleen				
control vs IAV	0.916	0.950	0.892	0.793
control vs coinfection	0.912	0.165	0.207	0.249
IAV vs coinfection	-	0.060	0.100	0.218
S. pneumoniae vs coinfection	-	0.230	0.091	-

References

1. Kang, J.; Chapdelaine, P.; Parent, J.; Madore, E.; Laberge, P.Y.; Fortier, M.A. Expression of human prostaglandin transporter in the human endometrium across the menstrual cycle. *The Journal of clinical endocrinology and metabolism* **2005**, *90*, 2308-2313.
2. Jenkins, C.M.; Cedars, A.; Gross, R.W. Eicosanoid signalling pathways in the heart. *Cardiovascular research* **2009**, *82*, 240-249.
3. Minamizaki, T.; Yoshiko, Y.; Kozai, K.; Aubin, J.E.; Maeda, N. EP2 and EP4 receptors differentially mediate mapk pathways underlying anabolic actions of prostaglandin e2 on bone formation in rat calvaria cell cultures. *Bone* **2009**, *44*, 1177-1185.
4. Mairpady Shambat, S.; Chen, P.; Nguyen Hoang, A.T.; Bergsten, H.; Vandenesch, F.; Siemens, N.; Lina, G.; Monk, I.R.; Foster, T.J.; Arakere, G.*, et al.* Modelling staphylococcal pneumonia in a human 3d lung tissue model system delineates toxin-mediated pathology. *Disease models & mechanisms* **2015**, *8*, 1413-1425.
5. Tam, V.C. Lipidomic profiling of bioactive lipids by mass spectrometry during microbial infections. *Seminars in immunology* **2013**, *25*, 240-248.
6. Arita, M. Mediator lipidomics in acute inflammation and resolution. *J Biochem* **2012**, *152*, 313-319.
7. Fabre, J.E.; Goulet, J.L.; Riche, E.; Nguyen, M.; Coggins, K.; Offenbacher, S.; Koller, B.H. Transcellular biosynthesis contributes to the production of leukotrienes during inflammatory responses in vivo. *The Journal of clinical investigation* **2002**, *109*, 1373-1380.
8. Hall, L.M.; Murphy, R.C. Electrospray mass spectrometric analysis of 5-hydroperoxy and 5-hydroxyeicosatetraenoic acids generated by lipid peroxidation of red blood cell ghost phospholipids. *Journal of the American Society for Mass Spectrometry* **1998**, *9*, 527-532.
9. Serhan, C.N. Systems approach to inflammation resolution: Identification of novel anti-inflammatory and pro-resolving mediators. *J Thromb Haemost* **2009**, *7*, 44-48.
10. An, S.; Yang, J.; So, S.W.; Zeng, L.; Goetzl, E.J. Isoforms of the ep3 subtype of human prostaglandin E2 receptor transduce both intracellular calcium and camp signals. *Biochemistry* **1994**, *33*, 14496-14502.
11. Hirai, H.; Tanaka, K.; Yoshie, O.; Ogawa, K.; Kenmotsu, K.; Takamori, Y.; Ichimasa, M.; Sugamura, K.; Nakamura, M.; Takano, S.*, et al.* Prostaglandin D2 selectively induces chemotaxis in t helper type 2 cells, eosinophils, and basophils via seven-transmembrane receptor crth2. *The Journal of experimental medicine* **2001**, *193*, 255-261.
12. Wray, J.A.; Sugden, M.C.; Zeldin, D.C.; Greenwood, G.K.; Samsuddin, S.; Miller-Degraff, L.; Bradbury, J.A.; Holness, M.J.; Warner, T.D.; Bishop-Bailey, D. The epoxygenases CYP2j2 activates the nuclear receptor ppar alpha in vitro and in vivo. *Plos One* **2009**, *4*.
13. Morin, C.; Sirois, M.; Echave, V.; Gomes, M.M.; Rousseau, E. EET displays anti-inflammatory effects in TNF-alpha stimulated human bronchi: Putative role of cpi-17. *American journal of respiratory cell and molecular biology* **2008**, *38*, 192-201.
14. Serhan, C.N.; Chiang, N.; Dalli, J.; Levy, B.D. Lipid mediators in the resolution of inflammation. *Csh Perspect Biol* **2015**, *7*.
15. Park, C.K.; Lu, N.; Xu, Z.Z.; Liu, T.; Serhan, C.N.; Ji, R.R. Resolving Trpv1-and TNF-alpha-mediated spinal cord synaptic plasticity and inflammatory pain with neuroprotectin D1. *J Neurosci* **2011**, *31*, 15072-15085.

16. Esaki, Y.; Li, Y.; Sakata, D.; Yao, C.; Segi-Nishida, E.; Matsuoka, T.; Fukuda, K.; Narumiya, S. Dual roles of PGE2-EP4 signaling in mouse experimental autoimmune encephalomyelitis. *Proceedings of the National Academy of Sciences of the United States of America* **2010**, *107*, 12233-12238.
17. Vane, J.R. Inhibition of prostaglandin synthesis as a mechanism of action for aspirin-like drugs. *Nature-New Biol* **1971**, *231*, 232-&.
18. Birnbaum, Y.; Ye, Y.; Lin, Y.; Freeberg, S.Y.; Nishi, S.P.; Martinez, J.D.; Huang, M.H.; Uretsky, B.F.; Perez-Polo, J.R. Augmentation of myocardial production of 15-epi-lipoxin-A4 by pioglitazone and atorvastatin in the rat. *Circulation* **2006**, *114*, 929-935.
19. Cuvillier, O.; Pirianov, G.; Kleuser, B.; Vanek, P.G.; Coso, O.A.; Gutkind, S.; Spiegel, S. Suppression of ceramide-mediated programmed cell death by sphingosine-1-phosphate. *Nature* **1996**, *381*, 800-803.
20. Arana, L.; Ordonez, M.; Ouro, A.; Rivera, I.G.; Gangoiti, P.; Trueba, M.; Gomez-Munoz, A. Ceramide 1-phosphate induces macrophage chemoattractant protein-1 release: Involvement in ceramide 1-phosphate-stimulated cell migration. *American journal of physiology. Endocrinology and metabolism* **2013**, *304*, E1213-1226.
21. Simanshu, D.K.; Kamlekar, R.K.; Wijesinghe, D.S.; Zou, X.; Zhai, X.; Mishra, S.K.; Molotkovsky, J.G.; Malinina, L.; Hinchcliffe, E.H.; Chalfant, C.E.*, et al.* Non-vesicular trafficking by a ceramide-1-phosphate transfer protein regulates eicosanoids. *Nature* **2013**, *500*, 463-467.
22. Sanak, M. Eicosanoid mediators in the airway inflammation of asthmatic patients: What is new? *Allergy, asthma & immunology research* **2016**, *8*, 481-490.
23. Barnig, C.; Bezema, T.; Calder, P.C.; Charloux, A.; Frossard, N.; Garssen, J.; Haworth, O.; Dilevskaya, K.; Levi-Schaffer, F.; Lonsdorfer, E.*, et al.* Activation of resolution pathways to prevent and fight chronic inflammation: Lessons from asthma and inflammatory bowel disease. *Front Immunol* **2019**, *10*, 1699.
24. Dennis, E.A.; Norris, P.C. Eicosanoid storm in infection and inflammation. *Nat Rev Immunol* **2015**, *15*, 511-523.
25. Dalli, J.; Serhan, C.N. Identification and structure elucidation of the pro-resolving mediators provides novel leads for resolution pharmacology. *British journal of pharmacology* **2019**, *176*, 1024-1037.
26. Mogensen, T.H. Pathogen recognition and inflammatory signaling in innate immune defenses. *Clinical microbiology reviews* **2009**, *22*, 240-273, Table of Contents.
27. Lawrence, T.; Willoughby, D.A.; Gilroy, D.W. Anti-inflammatory lipid mediators and insights into the resolution of inflammation. *Nat Rev Immunol* **2002**, *2*, 787-795.
28. Funk, C.D. Prostaglandins and leukotrienes: Advances in eicosanoid biology. *Science* **2001**, *294*, 1871-1875.
29. Nakayama, T.; Mutsuga, N.; Yao, L.; Tosato, G. Prostaglandin E2 promotes degranulation-independent release of Mcp-1 from mast cells. *Journal of leukocyte biology* **2006**, *79*, 95-104.
30. Szymanski, K.V.; Toennies, M.; Becher, A.; Fatykhova, D.; N'Guessan, P.D.; Gutbier, B.; Klauschen, F.; Neuschaefer-Rube, F.; Schneider, P.; Rueckert, J.*, et al.* Streptococcus pneumoniae-induced regulation of cyclooxygenase-2 in human lung tissue. *The European respiratory journal* **2012**, *40*, 1458-1467.
31. Goldmann, O.; Hertzen, E.; Hecht, A.; Schmidt, H.; Lehne, S.; Norrby-Teglund, A.; Medina, E. Inducible cyclooxygenase released prostaglandin E2 modulates the severity of infection caused by streptococcus pyogenes. *Journal of immunology* **2010**, *185*, 2372-2381.
32. Ballinger, M.N.; Standiford, T.J. Postinfluenza bacterial pneumonia: Host defenses gone awry. *Journal of interferon & cytokine research : the official journal of the International Society for Interferon and Cytokine Research* **2010**, *30*, 643-652.

33. Eckmann, L.; Stenson, W.F.; Savidge, T.C.; Lowe, D.C.; Barrett, K.E.; Fierer, J.; Smith, J.R.; Kagnoff, M.F. Role of intestinal epithelial cells in the host secretory response to infection by invasive bacteria. Bacterial entry induces epithelial prostaglandin H synthase-2 expression and prostaglandin E2 and F2alpha production. *The Journal of clinical investigation* **1997**, *100*, 296-309.
34. Asakrah, S.; Nieves, W.; Mahdi, Z.; Agard, M.; Zea, A.H.; Roy, C.J.; Morici, L.A. Post-exposure therapeutic efficacy of cox-2 inhibition against burkholderia pseudomallei. *PLoS neglected tropical diseases* **2013**, *7*, e2212.
35. Uchiya, K.; Nikai, T. Salmonella enterica serovar typhimurium infection induces cyclooxygenase 2 expression in macrophages: Involvement of salmonella pathogenicity island 2. *Infection and immunity* **2004**, *72*, 6860-6869.
36. Peres-Buzalaf, C.; de Paula, L.; Frantz, G.; Soares, E.M.; Medeiros, A.I.; Peters-Golden, M.; Silva, C.L.; Faccioli, L.H. Control of experimental pulmonary tuberculosis depends more on immunostimulatory leukotrienes than on the absence of immunosuppressive prostaglandins. *Prostag Leukotr Ess* **2011**, *85*, 75-81.
37. Lisowska, B.; Kosson, D.; Domaracka, K. Lights and shadows of NSAIDs in bone healing: The role of prostaglandins in bone metabolism. *Drug design, development and therapy* **2018**, *12*, 1753-1758.
38. Matsuoka, T.; Hirata, M.; Tanaka, H.; Takahashi, Y.; Murata, T.; Kabashima, K.; Sugimoto, Y.; Kobayashi, T.; Ushikubi, F.; Aze, Y.*, et al.* Prostaglandin D-2 as a mediator of allergic asthma. *Science* **2000**, *287*, 2013-2017.
39. Soter, N.A.; Lewis, R.A.; Corey, E.J.; Austen, K.F. Local-effects of synthetic leukotrienes (LtC4, LtD4, LtE4, and LtB4) in human-skin. *J Invest Dermatol* **1983**, *80*, 115-119.
40. Basu, S.; Whiteman, M.; Mattey, D.L.; Halliwell, B. Raised levels of F-2-isoprostanes and prostaglandin F-2 alpha in different rheumatic diseases. *Ann Rheum Dis* **2001**, *60*, 627-631.
41. Boffa, J.J.; Just, A.; Coffman, T.M.; Arendshorst, W.J. Thromboxane receptor mediates renal vasoconstriction and contributes to acute renal failure in endotoxemic mice. *J Am Soc Nephrol* **2004**, *15*, 2358-2365.
42. Tam, V.C.; Quehenberger, O.; Oshansky, C.M.; Suen, R.; Armando, A.M.; Treuting, P.M.; Thomas, P.G.; Dennis, E.A.; Aderem, A. Lipidomic profiling of influenza infection identifies mediators that induce and resolve inflammation. *Cell* **2013**, *154*, 213-227.
43. Rouzer, C.A.; Samuelsson, B. On the nature of the 5-lipoxygenase reaction in human-leukocytes - enzyme-purification and requirement for multiple stimulatory factors. *Proceedings of the National Academy of Sciences of the United States of America* **1985**, *82*, 6040-6044.
44. Bittleman, D.B.; Casale, T.B. 5-hydroxyeicosatetraenoic acid (HETE)-induced neutrophil transcellular migration is dependent upon enantiomeric structure. *American journal of respiratory cell and molecular biology* **1995**, *12*, 260-267.
45. Dahlen, S.E.; Bjork, J.; Hedqvist, P.; Arfors, K.E.; Hammarstrom, S.; Lindgren, J.A.; Samuelsson, B. Leukotrienes promote plasma leakage and leukocyte adhesion in post-capillary venules - invivo effects with relevance to the acute inflammatory response. *P Natl Acad Sci-Biol* **1981**, *78*, 3887-3891.
46. Cuez, T.; Korkmaz, B.; Buharalioglu, C.K.; Sahan-Firat, S.; Falck, J.; Malik, K.U.; Tunctan, B. A synthetic analogue of 20-HETE, 5,14-HEDGE, reverses endotoxin-induced hypotension via increased 20-HETE levels associated with decreased inos protein expression and vasodilator prostanoid production in rats. *Basic Clin Pharmacol* **2010**, *106*, 378-388.
47. Jacobs, E.R.; Zhu, D.L.; Gruenloh, S.; Lopez, B.; Medhora, M. Vegf-induced relaxation of pulmonary arteries is mediated by endothelial Cytochrome P-450 hydroxylase. *Am J Physiol-Lung C* **2006**, *291*, L369-L377.

48. Chen, J.M.; Hamers, A.J.P.; Finsterbusch, M.; Massimo, G.; Zafar, M.; Corder, R.; Colas, R.A.; Dalli, J.; Thiemermann, C.; Ahluwalia, A. Endogenously generated arachidonate-derived ligands for Trpv1 induce cardiac protection in sepsis. *Faseb J* **2018**, *32*, 3816-3831.
49. Tunctan, B.; Korkmaz, B.; Sari, A.N.; Kacan, M.; Unsal, D.; Serin, M.S.; Buharalioglu, C.K.; Sahan-Firat, S.; Cuez, T.; Schunck, W.H*., et al.* Contribution of Inos/Sgc/Pkg pathway, cox-2, cyp4a1, and gp91(phox) to the protective effect of 5,14-HEDGE, a 20-HETE mimetic, against vasodilation, hypotension, tachycardia, and inflammation in a rat model of septic shock. *Nitric Oxide-Biol Ch* **2013**, *33*, 18-41.
50. Pettus, B.J.; Bielawska, A.; Subramanian, P.; Wijesinghe, D.S.; Maceyka, M.; Leslie, C.C.; Evans, J.H.; Freiberg, J.; Roddy, P.; Hannun, Y.A*., et al.* Ceramide 1-phosphate is a direct activator of cytosolic phospholipase a(2). *Journal of Biological Chemistry* **2004**, *279*, 11320-11326.
51. Pettus, B.J.; Kitatani, K.; Chalfant, C.E.; Taha, T.A.; Kawamori, T.; Bielawski, J.; Obeid, L.M.; Hannun, Y.A. The coordination of prostaglandin E2 production by sphingosine-1-phosphate and ceramide-1-phosphate. *Molecular pharmacology* **2005**, *68*, 330-335.
52. Mitsutake, S.; Kim, T.J.; Inagaki, Y.; Kato, M.; Yamashita, T.; Igarashi, Y. Ceramide kinase is a mediator of calcium-dependent degranulation in mast cells. *Journal of Biological Chemistry* **2004**, *279*, 17570-17577.
53. Granado, M.H.; Gangoiti, P.; Ouro, A.; Arana, L.; Gonzalez, M.; Trueba, M.; Gomez-Munoz, A. Ceramide 1-phosphate (C1P) promotes cell migration involvement of a specific C1P receptor. *Cell Signal* **2009**, *21*, 405-412.
54. Hattori, T.; Obinata, H.; Ogawa, A.; Kishi, M.; Tatei, K.; Ishikawa, O.; Izumi, T. G2a plays proinflammatory roles in human keratinocytes under oxidative stress as a receptor for 9-hydroxyoctadecadienoic acid. *J Invest Dermatol* **2008**, *128*, 1123-1133.
55. Obinata, H.; Hattori, T.; Nakane, S.; Tatei, K.; Izumi, T. Identification of 9-hydroxyoctadecadienoic acid and other oxidized free fatty acids as ligands of the g protein-coupled receptor G2a. *The Journal of biological chemistry* **2005**, *280*, 40676-40683.
56. Obinata, H.; Izumi, T. G2a as a receptor for oxidized free fatty acids. *Prostag Oth Lipid M* **2009**, *89*, 66-72.
57. Szczuko, M.; Kotlega, D.; Palma, J.; Zembron-Lacny, A.; Tylutka, A.; Golab-Janowska, M.; Drozd, A. Lipoxins, Revd1 and 9, 13 HODE as the most important derivatives after an early incident of ischemic stroke. *Scientific reports* **2020**, *10*, 12849.
58. Gilroy, D.W.; Edin, M.L.; De Maeyer, R.P.; Bystrom, J.; Newson, J.; Lih, F.B.; Stables, M.; Zeldin, D.C.; Bishop-Bailey, D. Cyp450-derived oxylipins mediate inflammatory resolution. *Proceedings of the National Academy of Sciences of the United States of America* **2016**, *113*, E3240-3249.
59. Waindok, P.; Janecek-Erfurth, E.; Lindenwald, D.; Wilk, E.; Schughart, K.; Geffers, R.; Balas, L.; Durand, T.; Rund, K.M.; Schebb, N.H*., et al.* Multiplex profiling of inflammation-related bioactive lipid mediators in toxocara canis- and toxocara cati-induced neurotoxocarosis. *PLoS neglected tropical diseases* **2019**, *13*, e0007706.
60. Levy, B.D.; Clish, C.B.; Schmidt, B.; Gronert, K.; Serhan, C.N. Lipid mediator class switching during acute inflammation: Signals in resolution. *Nature immunology* **2001**, *2*, 612-619.
61. Honda, A.; Sugimoto, Y.; Namba, T.; Watabe, A.; Irie, A.; Negishi, M.; Narumiya, S.; Ichikawa, A. Cloning and expression of a cDNA for mouse prostaglandin E receptor EP2 subtype. *The Journal of biological chemistry* **1993**, *268*, 7759-7762.
62. Bystrom, J.; Evans, I.; Newson, J.; Stables, M.; Toor, I.; van Rooijen, N.; Crawford, M.; Colville-Nash, P.; Farrow, S.; Gilroy, D.W. Resolution-phase macrophages possess a unique inflammatory phenotype that is controlled by camp. *Blood* **2008**, *112*, 4117-4127.
63. Gilroy, D.W.; Colville-Nash, P.R.; Willis, D.; Chivers, J.; Paul-Clark, M.J.; Willoughby, D.A. Inducible cyclooxygenase may have anti-inflammatory properties. *Nature medicine* **1999**, *5*, 698-701.

64. Ajuebor, M.N.; Singh, A.; Wallace, J.L. Cyclooxygenase-2-derived prostaglandin D-2 is an early anti-inflammatory signal in experimental colitis. *Am J Physiol-Gastr L* **2000**, *279*, G238-G244.
65. Joo, M.; Kwon, M.; Sadikot, R.T.; Kingsley, P.J.; Marnett, L.J.; Blackwell, T.S.; Peebles, R.S., Jr.; Urade, Y.; Christman, J.W. Induction and function of lipocalin prostaglandin D synthase in host immunity. *Journal of immunology* **2007**, *179*, 2565-2575.
66. Syed, M.A.; Joo, M.; Abbas, Z.; Rodger, D.; Christman, J.W.; Mehta, D.; Sadikot, R.T. Expression of trem-1 is inhibited by PGD(2) and PGJ(2) in macrophages. *Exp Cell Res* **2010**, *316*, 3140-3149.
67. Kronke, G.; Katzenbeisser, J.; Uderhardt, S.; Zaiss, M.M.; Scholtysek, C.; Schabbauer, G.; Zarbock, A.; Koenders, M.I.; Axmann, R.; Zwerina, J.*, et al.* 12/15-lipoxygenase counteracts inflammation and tissue damage in arthritis. *Journal of immunology* **2009**, *183*, 3383-3389.
68. Yoshimoto, T.; Suzuki, H.; Yamamoto, S.; Takai, T.; Yokoyama, C.; Tanabe, T. Cloning and sequence analysis of the cdna for arachidonate 12-lipoxygenase of porcine leukocytes. *Proceedings of the National Academy of Sciences of the United States of America* **1990**, *87*, 2142-2146.
69. Kuhn, H.; Banthiya, S.; van Leyen, K. Mammalian lipoxygenases and their biological relevance. *Bba-Mol Cell Biol L* **2015**, *1851*, 308-330.
70. Node, K.; Huo, Y.; Ruan, X.; Yang, B.; Spiecker, M.; Ley, K.; Zeldin, D.C.; Liao, J.K. Anti-inflammatory properties of Cytochrome P450 epoxygenase-derived eicosanoids. *Science* **1999**, *285*, 1276-1279.
71. Fang, X.; Moore, S.A.; Stoll, L.L.; Rich, G.; Kaduce, T.L.; Weintraub, N.L.; Spector, A.A. 14,15-epoxyeicosatrienoic acid inhibits prostaglandin E2 production in vascular smooth muscle cells. *The American journal of physiology* **1998**, *275*, H2113-2121.
72. Serhan, C.N. Pro-resolving lipid mediators are leads for resolution physiology. *Nature* **2014**, *510*, 92-101.
73. Serhan, C.N.; Krishnamoorthy, S.; Recchiuti, A.; Chiang, N. Novel anti-inflammatory--pro-resolving mediators and their receptors. *Current topics in medicinal chemistry* **2011**, *11*, 629-647.
74. Morita, M.; Kuba, K.; Ichikawa, A.; Nakayama, M.; Katahira, J.; Iwamoto, R.; Watanebe, T.; Sakabe, S.; Daidoji, T.; Nakamura, S.*, et al.* The lipid mediator protectin D1 inhibits influenza virus replication and improves severe influenza. *Cell* **2013**, *153*, 112-125.
75. Ramon, S.; Baker, S.F.; Sahler, J.M.; Kim, N.; Feldsott, E.A.; Serhan, C.N.; Martinez-Sobrido, L.; Topham, D.J.; Phipps, R.P. The specialized proresolving mediator 17-HDHA enhances the antibody-mediated immune response against influenza virus: A new class of adjuvant? *Journal of immunology* **2014**, *193*, 6031-6040.
76. Anania, V.G.; Randolph, A.G.; Yang, X.Y.; Nguyen, A.; Newhams, M.M.; Mathews, W.R.; Rosenberger, C.M.; McBride, J.M.; Influ, P.P.I.C. Early amplified respiratory bioactive lipid response is associated with worse outcomes in pediatric influenza-related respiratory failure. *Open Forum Infect Di* **2020**, *7*.
77. Endo, J.; Sano, M.; Isobe, Y.; Fukuda, K.; Kang, J.X.; Arai, H.; Arita, M. 18-HEPE, an n-3 fatty acid metabolite released by macrophages, prevents pressure overload-induced maladaptive cardiac remodeling. *The Journal of experimental medicine* **2014**, *211*, 1673-1687.
78. Liu, Y.; Fang, X.; Zhang, X.; Huang, J.; He, J.; Peng, L.; Ye, C.; Wang, Y.; Xue, F.; Ai, D.*, et al.* Metabolic profiling of murine plasma reveals eicosapentaenoic acid metabolites protecting against endothelial activation and atherosclerosis. *British journal of pharmacology* **2018**, *175*, 1190-1204.
79. Han, S.W.; Inoue, H.; Flowers, L.C.; Sidell, N. Control of cox-2 gene expression through peroxisome proliferator-activated receptor gamma in human cervical cancer cells. *Clin Cancer Res* **2003**, *9*, 4627-4635.
80. Ricote, M.; Li, A.C.; Willson, T.M.; Kelly, C.J.; Glass, C.K. The peroxisome proliferator-activated receptor-gamma is a negative regulator of macrophage activation. *Nature* **1998**, *391*, 79-82.
81. Villapol, S. Roles of peroxisome proliferator-activated receptor gamma on brain and peripheral inflammation. *Cell Mol Neurobiol* **2018**, *38*, 121-132.

82. Kumar, N.; Gupta, G.; Anilkumar, K.; Fatima, N.; Karnati, R.; Reddy, G.V.; Giri, P.V.; Reddanna, P. 15-lipoxygenase metabolites of alpha-linolenic acid, [13-(s)-HPOTrE and 13-(s)-HOTrE], mediate anti-inflammatory effects by inactivating NLRP3 inflammasome. *Scientific reports* **2016**, *6*, 31649.
83. Fang, R.D.; Uchiyama, R.; Sakai, S.; Hara, H.; Tsutsui, H.; Suda, T.; Mitsuyama, M.; Kawamura, I.; Tsuchiya, K. Asc and Nlrp3 maintain innate immune homeostasis in the airway through an inflammasome-independent mechanism. *Mucosal Immunol* **2019**, *12*, 1092-1103.
84. Hait, N.C.; Maiti, A. The role of sphingosine-1-phosphate and ceramide-1-phosphate in inflammation and cancer. *Mediators of inflammation* **2017**, *2017*, 4806541.
85. Nofer, J.R.; Bot, M.; Brodde, M.; Taylor, P.J.; Salm, P.; Brinkmann, V.; van Berkel, T.; Assmann, G.; Biessen, E.A.L. Fty720, a synthetic sphingosine 1 phosphate analogue, inhibits development of atherosclerosis in low-density lipoprotein receptor-deficient mice. *Circulation* **2007**, *115*, 501-508.
86. Blaho, V.A.; Galvani, S.; Engelbrecht, E.; Liu, C.; Swendeman, S.L.; Kono, M.; Proia, R.L.; Steinman, L.; Han, M.H.; Hla, T. Hdl-bound sphingosine-1-phosphate restrains lymphopoiesis and neuroinflammation. *Nature* **2015**, *523*, 342-+.
87. Peng, H.M.; Li, C.; Kadow, S.; Henry, B.D.; Steinmann, J.; Becker, K.A.; Riehle, A.; Beckmann, N.; Wilker, B.; Li, P.L*., et al.* Acid sphingomyelinase inhibition protects mice from lung edema and lethal staphylococcus aureus sepsis. *J Mol Med* **2015**, *93*, 675-689.
88. Kim, Y.I.; Park, K.; Kim, J.Y.; Seo, H.S.; Shin, K.O.; Lee, Y.M.; Holleran, W.M.; Elias, P.M.; Uchida, Y. An endoplasmic reticulum stress-initiated sphingolipid metabolite, ceramide-1-phosphate, regulates epithelial innate immunity by stimulating beta-defensin production. *Molecular and cellular biology* **2014**, *34*, 4368-4378.
89. Jozefowski, S.; Czerkies, M.; Lukasik, A.; Bielawska, A.; Bielawski, J.; Kwiatkowska, K.; Sobota, A. Ceramide and ceramide 1-phosphate are negative regulators of tnf-alpha production induced by lipopolysaccharide. *Journal of immunology* **2010**, *185*, 6960-6973.
90. Astarita, G.; Kendall, A.C.; Dennis, E.A.; Nicolaou, A. Targeted lipidomic strategies for oxygenated metabolites of polyunsaturated fatty acids. *Biochimica et biophysica acta* **2015**, *1851*, 456-468.
91. Lundstrom, S.L.; D'Alexandri, F.L.; Nithipatikom, K.; Haeggstrom, J.Z.; Wheelock, A.M.; Wheelock, C.E. HPLC/MS/MS-based approaches for detection and quantification of eicosanoids. *Methods in molecular biology* **2009**, *579*, 161-187.
92. Masoodi, M.; Eiden, M.; Koulman, A.; Spaner, D.; Volmer, D.A. Comprehensive lipidomics analysis of bioactive lipids in complex regulatory networks. *Anal Chem* **2010**, *82*, 8176-8185.
93. Levison, B.S.; Zhang, R.; Wang, Z.; Fu, X.; DiDonato, J.A.; Hazen, S.L. Quantification of fatty acid oxidation products using online high-performance liquid chromatography tandem mass spectrometry. *Free radical biology & medicine* **2013**, *59*, 2-13.
94. Bessard, J.; Cracowski, J.L.; Stanke-Labesque, F.; Bessard, G. Determination of isoprostaglandin F2alpha type III in human urine by gas chromatography-electronic impact mass spectrometry. Comparison with enzyme immunoassay. *Journal of chromatography. B, Biomedical sciences and applications* **2001**, *754*, 333-343.
95. Dahl, J.H.; van Breemen, R.B. Rapid quantitative analysis of 8-iso-prostaglandin-F(2alpha) using liquid chromatography-tandem mass spectrometry and comparison with an enzyme immunoassay method. *Analytical biochemistry* **2010**, *404*, 211-216.
96. Tsikas, D. Application of gas chromatography-mass spectrometry and gas chromatography-tandem mass spectrometry to assess in vivo synthesis of prostaglandins, thromboxane, leukotrienes, isoprostanes and related compounds in humans. *Journal of chromatography. B, Biomedical sciences and applications* **1998**, *717*, 201-245.
97. Tsukamoto, H.; Hishinuma, T.; Mikkaichi, T.; Nakamura, H.; Yamazaki, T.; Tomioka, Y.; Mizugaki, M. Simultaneous quantification of prostaglandins, isoprostane and thromboxane in cell-cultured

medium using gas chromatography-mass spectrometry. *Journal of chromatography. B, Analytical technologies in the biomedical and life sciences* **2002**, *774*, 205-214.

98. Tunctan, B.; Korkmaz, B.; Sari, A.N.; Kacan, M.; Unsal, D.; Serin, M.S.; Buharalioglu, C.K.; Sahan-Firat, S.; Schunck, W.H.; Falck, J.R.*, et al.* A novel treatment strategy for sepsis and septic shock based on the interactions between prostanoids, nitric oxide, and 20-hydroxyeicosatetraenoic acid. *Anti-inflammatory & anti-allergy agents in medicinal chemistry* **2012**, *11*, 121-150.
99. Koch, E.; Mainka, M.; Dalle, C.; Ostermann, A.I.; Rund, K.M.; Kutzner, L.; Froehlich, L.F.; Bertrand-Michel, J.; Gladine, C.; Schebb, N.H. Stability of oxylipins during plasma generation and long-term storage. *Talanta* **2020**, *217*, 121074.
100. Maddipati, K.R.; Zhou, S.L. Stability and analysis of eicosanoids and docosanoids in tissue culture media. *Prostaglandins Other Lipid Mediat* **2011**, *94*, 59-72.
101. Tripathi, N.; Paliwal, S.; Sharma, S.; Verma, K.; Gururani, R.; Tiwari, A.; Verma, A.; Chauhan, M.; Singh, A.; Kumar, D.*, et al.* Discovery of novel soluble epoxide hydrolase inhibitors as potent vasodilators. *Scientific reports* **2018**, *8*, 14604.
102. Gomolka, B.; Siegert, E.; Blossey, K.; Schunck, W.H.; Rothe, M.; Weylandt, K.H. Analysis of omega-3 and omega-6 fatty acid-derived lipid metabolite formation in human and mouse blood samples. *Prostaglandins Other Lipid Mediat* **2011**, *94*, 81-87.
103. Niehaus, M.; Soltwisch, J.; Belov, M.E.; Dreisewerd, K. Transmission-mode maldi-2 mass spectrometry imaging of cells and tissues at subcellular resolution. *Nat Methods* **2019**, *16*, 925-+.
104. Zavalin, A.; Yang, J.H.; Caprioli, R. Laser beam filtration for high spatial resolution maldi imaging mass spectrometry. *Journal of the American Society for Mass Spectrometry* **2013**, *24*, 1153-1156.
105. Potocnik, N.O.; Porta, T.; Becker, M.; Heeren, R.M.A.; Ellis, S.R. Use of advantageous, volatile matrices enabled by next-generation high-speed matrix-assisted laser desorption/ionization time-of-flight imaging employing a scanning laser beam. *Rapid Commun Mass Sp* **2015**, *29*, 2195-2203.
106. Geier, B.; Sogin, E.M.; Michellod, D.; Janda, M.; Kompauer, M.; Spengler, B.; Dubilier, N.; Liebeke, M. Spatial metabolomics of in situ host-microbe interactions at the micrometre scale. *Nat Microbiol* **2020**, *5*, 498-+.
107. Calvano, C.D.; Monopoli, A.; Cataldi, T.R.I.; Palmisano, F. Maldi matrices for low molecular weight compounds: An endless story? *Analytical and bioanalytical chemistry* **2018**, *410*, 4015-4038.
108. Kruger, R.; Pfenninger, A.; Fournier, I.; Gluckmann, M.; Karas, M. Analyte incorporation and ionization in matrix-assisted laser desorption/ionization visualized by ph indicator molecular probes. *Anal Chem* **2001**, *73*, 5812-5821.
109. Vermillion-Salsbury, R.L.; Hercules, D.M. 9-aminoacridine as a matrix for negative mode matrix-assisted laser desorption/ionization. *Rapid Commun Mass Sp* **2002**, *16*, 1575-1581.
110. Nielsen, M.M.B.; Lambertsen, K.L.; Clausen, B.H.; Meyer, M.; Bhandari, D.R.; Larsen, S.T.; Poulsen, S.S.; Spengler, B.; Janfelt, C.; Hansen, H.S. Mass spectrometry imaging of biomarker lipids for phagocytosis and signalling during focal cerebral ischaemia. *Scientific reports* **2016**, *6*.
111. Okutan, S.; Hansen, H.S.; Janfelt, C. Cryo-sectioning of mice for whole-body imaging of drugs and metabolites with desorption electrospray ionization mass spectrometry imaging - a simplified approach. *Proteomics* **2016**, *16*, 1633-1641.
112. Collaborators, G.B.D.C.o.D. Global, regional, and national age-sex-specific mortality for 282 causes of death in 195 countries and territories, 1980-2017: A systematic analysis for the global burden of disease study 2017. *Lancet* **2018**, *392*, 1736-1788.
113. Collaborators, G.B.D.I. Mortality, morbidity, and hospitalisations due to influenza lower respiratory tract infections, 2017: An analysis for the global burden of disease study 2017. *The Lancet. Respiratory medicine* **2019**, *7*, 69-89.
114. Aliberti, S.; Kaye, K.S. The changing microbiologic epidemiology of community-acquired pneumonia. *Postgraduate medicine* **2013**, *125*, 31-42.

115. Cunningham, M.W. Pathogenesis of group a streptococcal infections. *Clinical microbiology reviews* **2000**, *13*, 470-511.
116. McCullers, J.A. The co-pathogenesis of influenza viruses with bacteria in the lung. *Nature reviews. Microbiology* **2014**, *12*, 252-262.
117. Shirey, K.A.; Perkins, D.J.; Lai, W.D.; Zhang, W.; Fernando, L.R.; Gusovsky, F.; Blanco, J.C.G.; Vogel, S.N. Influenza "trains" the host for enhanced susceptibility to secondary bacterial infection. *Mbio* **2019**, *10*.
118. Dawson, H.D.; Loveland, J.E.; Pascal, G.; Gilbert, J.G.; Uenishi, H.; Mann, K.M.; Sang, Y.; Zhang, J.; Carvalho-Silva, D.; Hunt, T.*, et al.* Structural and functional annotation of the porcine immunome. *BMC genomics* **2013**, *14*, 332.
119. Tao, L.; Reese, T.A. Making mouse models that reflect human immune responses. *Trends in immunology* **2017**, *38*, 181-193.
120. Henritzi, D.; Petric, P.P.; Lewis, N.S.; Graaf, A.; Pessia, A.; Starick, E.; Breithaupt, A.; Strebelow, G.; Luttermann, C.; Parker, L.M.K.*, et al.* Surveillance of european domestic pig populations identifies an emerging reservoir of potentially zoonotic swine influenza a viruses. *Cell host & microbe* **2020**, *28*, 614-627 e616.
121. Mohiuddin, M.M.; Reichart, B.; Byrne, G.W.; McGregor, C.G.A. Current status of pig heart xenotransplantation. *International journal of surgery* **2015**, *23*, 234-239.
122. Niemann, H.; Petersen, B. The production of multi-transgenic pigs: Update and perspectives for xenotransplantation. *Transgenic research* **2016**, *25*, 361-374.
123. Meurens, F.; Summerfield, A.; Nauwynck, H.; Saif, L.; Gerdts, V. The pig: A model for human infectious diseases. *Trends in microbiology* **2012**, *20*, 50-57.
124. Summerfield, A. Special issue on porcine immunology: An introduction from the guest editor. *Developmental and comparative immunology* **2009**, *33*, 265-266.
125. Summerfield, A.; McCullough, K.C. The porcine dendritic cell family. *Developmental and comparative immunology* **2009**, *33*, 299-309.
126. Chiang, N.; Fredman, G.; Backhed, F.; Oh, S.F.; Vickery, T.; Schmidt, B.A.; Serhan, C.N. Infection regulates pro-resolving mediators that lower antibiotic requirements. *Nature* **2012**, *484*, 524-528.
127. Blaho, V.A.; Buczynski, M.W.; Brown, C.R.; Dennis, E.A. Lipidomic analysis of dynamic eicosanoid responses during the induction and resolution of lyme arthritis. *The Journal of biological chemistry* **2009**, *284*, 21599-21612.
128. Morita, E.; Schroder, J.M.; Christophers, E. Identification of a novel and highly potent eosinophil chemotactic lipid in human eosinophils treated with arachidonic-acid. *Journal of immunology* **1990**, *144*, 1893-1900.
129. Salina, A.C.; Souza, T.P.; Serezani, C.H.; Medeiros, A.I. Efferocytosis-induced prostaglandin E2 production impairs alveolar macrophage effector functions during streptococcus pneumoniae infection. *Innate immunity* **2017**, *23*, 219-227.
130. Krause, J.; Geginat, G.; Tammer, I. Prostaglandin E2 from candida albicans stimulates the growth of staphylococcus aureus in mixed biofilms. *Plos One* **2015**, *10*, e0135404.
131. Sheppe, A.E.F.; Kummari, E.; Walker, A.; Richards, A.; Hui, W.W.; Lee, J.H.; Mangum, L.; Borazjani, A.; Ross, M.K.; Edelmann, M.J. PGE2 augments inflammasome activation and M1 polarization in macrophages infected with salmonella typhimurium and yersinia enterocolitica. *Front Microbiol* **2018**, *9*, 2447.
132. Ikeh, M.A.C.; Fidel, P.L., Jr.; Noverr, M.C. Identification of specific components of the eicosanoid biosynthetic and signaling pathway involved in pathological inflammation during intra-abdominal infection with candida albicans and staphylococcus aureus. *Infection and immunity* **2018**, *86*.

133. Schwaiger, T.; Sehl, J.; Karte, C.; Schafer, A.; Huhr, J.; Mettenleiter, T.C.; Schroder, C.; Kollner, B.; Ulrich, R.; Blohm, U. Experimental h1n1pdm09 infection in pigs mimics human seasonal influenza infections. *Plos One* **2019**, *14*, e0222943.
134. O'Flaherty, J.T.; Thomas, M.J.; Lees, C.J.; McCall, C.E. Neutrophil-aggregating activity of monohydroxyeicosatetraenoic acids. *The American journal of pathology* **1981**, *104*, 55-62.
135. Luo, M.; Lee, S.; Brock, T.G. Leukotriene synthesis by epithelial cells. *Histology and histopathology* **2003**, *18*, 587-595.
136. Neels, J.G. A role for 5-lipoxygenase products in obesity-associated inflammation and insulin resistance. *Adipocyte* **2013**, *2*, 262-265.
137. Joshi, Y.B.; Pratico, D. The 5-lipoxygenase pathway: Oxidative and inflammatory contributions to the alzheimer's disease phenotype. *Front Cell Neurosci* **2015**, *8*.
138. Khan, R.; Spagnoli, V.; Tardif, J.C.; L'Allier, P.L. Novel anti-inflammatory therapies for the treatment of atherosclerosis. *Atherosclerosis* **2015**, *240*, 497-509.
139. Solleti, S.K.; Simon, D.M.; Srisuma, S.; Arikan, M.C.; Bhattacharya, S.; Rangasamy, T.; Bijli, K.M.; Rahman, A.; Crossno, J.T., Jr.; Shapiro, S.D*., et al.* Airway epithelial cell ppargamma modulates cigarette smoke-induced chemokine expression and emphysema susceptibility in mice. *American journal of physiology. Lung cellular and molecular physiology* **2015**, *309*, L293-304.
140. Brand, D.D.; Latham, K.A.; Rosloniec, E.F. Collagen-induced arthritis. *Nature protocols* **2007**, *2*, 1269-1275.
141. Rooney, M.; Condell, D.; Quinlan, W.; Daly, L.; Whelan, A.; Feighery, C.; Bresnihan, B. Analysis of the histologic variation of synovitis in rheumatoid arthritis. *Arthritis and rheumatism* **1988**, *31*, 956-963.
142. Oh, B.R.; Suh, D.H.; Bae, D.; Ha, N.; Choi, Y.I.; Yoo, H.J.; Park, J.K.; Lee, E.Y.; Lee, E.B.; Song, Y.W. Therapeutic effect of a novel histone deacetylase 6 inhibitor, ckd-l, on collagen-induced arthritis in vivo and regulatory t cells in rheumatoid arthritis in vitro. *Arthritis research & therapy* **2017**, *19*, 154.
143. Coras, R.; Kavanaugh, A.; Boyd, T.; Huynh, Q.; Pedersen, B.; Armando, A.M.; Dahlberg-Wright, S.; Marsal, S.; Jain, M.; Paravar, T*., et al.* Pro- and anti-inflammatory eicosanoids in psoriatic arthritis. *Metabolomics : Official journal of the Metabolomic Society* **2019**, *15*, 65.
144. Hamaguchi, M.; Wu, H.N.; Tanaka, M.; Tsuda, N.; Tantengco, O.A.G.; Matsushima, T.; Nakao, T.; Ishibe, T.; Sakata, I.; Yanagihara, I. A case series of the dynamics of lipid mediators in patients with sepsis. *Acute medicine & surgery* **2019**, *6*, 413-418.
145. Anania, V.G.; Randolph, A.G.; Yang, X.; Nguyen, A.; Newhams, M.M.; Mathews, W.R.; Rosenberger, C.M.; McBride, J.M. Early amplified respiratory bioactive lipid response is associated with worse outcomes in pediatric influenza-related respiratory failure. *Open Forum Infect Dis* **2020**, *7*, ofaa122.
146. Wang, J.; Kano, K.; Saigusa, D.; Aoki, J. Measurement of the spatial distribution of S1P in small quantities of tissues: Development and application of a highly sensitive LC-MS/MS method combined with laser microdissection. *Mass spectrometry* **2019**, *8*, A0072.
147. Vijayan, M.; Hahm, B. Influenza viral manipulation of sphingolipid metabolism and signaling to modulate host defense system. *Scientifica* **2014**, *2014*, 793815.
148. Baeyens, A.; Fang, V.; Chen, C.; Schwab, S.R. Exit strategies: S1P signaling and T cell migration. *Trends in immunology* **2015**, *36*, 778-787.

Eigenständigkeitserklärung

Hiermit erkläre ich, dass diese Arbeit bisher von mir weder an der Mathematisch-Naturwissenschaftlichen Fakultät der Universität Greifswald noch einer anderen wissenschaftlichen Einrichtung zum Zwecke der Promotion eingereicht wurde.

Ferner erkläre ich, dass ich diese Arbeit selbstständig verfasst und keine anderen als die darin angegebenen Hilfsmittel und Hilfen benutzt und keine Textabschnitte eines Dritten ohne Kennzeichnung übernommen habe.

Unterschrift des Promovenden

List of publications

Article I:

Schultz, D.; Methling, K.; KoInfekt Study, G.; Rothe, M.; Lalk, M. Eicosanoid Profile of Influenza A Virus Infected Pigs. Metabolites 2019, 9.

Article II:

Schultz, D.; Surabhi, S.; Stelling, N.; Rothe, M.; Group, K.S.; Methling, K.; Hammerschmidt, S.; Siemens, N.; Lalk, M. 16HBE Cell Lipid Mediator Responses to Mono and Co-infections with Respiratory Pathogens. Metabolites 2020, 10.

Article III:

Volzke, J.; **Schultz, D.**; Kordt, M.; Muller, M.; Bergmann, W.; Methling, K.; Kreikemeyer, B.; Muller-Hilke, B.; KoInfekt Study, G. Inflammatory Joint Disease Is a Risk Factor for Streptococcal Sepsis and Septic Arthritis in Mice. Front Immunol 2020, 11, 579475.

Article IV:

Schultz, D.; Cuypers, F.; Skorka, S.; Salazar, M.; Krieger, J.; Albrecht, D.; Lalk, M.; Siemens, N.; Methling, K. Bioactive Lipid Screening of Mice During Respiratory Tract Infections with Bacterial and Viral Pathogens. In preparation

Further publications:

Schultz, D.; Schluter, R.; Gerth, U.; Lalk, M. Metabolic Perturbations in a Bacillus subtilis clpP Mutant during Glucose Starvation. Metabolites 2017, 7.

Jarick, M.; Bertsche, U.; Stahl, M.; **Schultz, D.**; Methling, K.; Lalk, M.; Stigloher, C.; Steger, M.; Schlosser, A.; Ohlsen, K. The serine/threonine kinase Stk and the phosphatase Stp regulate cell wall synthesis in Staphylococcus aureus. Scientific reports 2018, 8, 13693.

Seinen, J.; Dieperink, W.; Mekonnen, S.A.; Lisotto, P.; Harmsen, H.J.M.; Hiemstra, B.; Ott, A.; **Schultz, D.**; Lalk, M.; Oswald, S., et al. Heterogeneous antimicrobial activity in broncho-alveolar aspirates from mechanically ventilated intensive care unit patients. Virulence 2019, 10, 879-891.

Siemens, N.; Oehmcke-Hecht, S.; Hossmann, J.; Skorka, S.B.; Nijhuis, R.H.T.; Ruppen, C.; Skrede, S.; Rohde, M.; **Schultz, D.**; Lalk, M., et al. Prothrombotic and Proinflammatory Activities of the Beta-Hemolytic Group B Streptococcal Pigment. Journal of innate immunity 2020, 12, 291-303.

Gierse, L.C.; Meene, A.; **Schultz, D**.; Schwaiger, T.; Karte, C.; Schroder, C.; Wang, H.; Wunsche, C.; Methling, K.; Kreikemeyer, B., et al. A multi-omics protocol for swine feces to elucidate longitudinal dynamics in microbiome structure and function. Microorganisms 2020, 8.

Danksagung

Herrn Prof. Dr. Michael Lalk danke ich für die Möglichkeit, diese Arbeit bei ihm durchführen zu können und für die großartige finanzielle Unterstützung, die für die Realisierung der verschiedenen analytischen Techniken notwendig sind. Vielen Dank für dein entgegengebrachtes Vertrauen und die Möglichkeit selbstständig an den vielen analytischen Geräten zu arbeiten.

Mein ganz besonderer Dank gilt Dr. Karen Methling für die Betreuung meiner Arbeit. Danke für all deine Hilfe, dein Mitdenken und Mitkämpfen bei allen Problemen. Ich habe von dir unglaublich viel über Analytik und gutes wissenschaftliches Arbeiten gelernt. Vielen Dank für dein großartiges Engagement!

Michael Rothe danke ich für die Unterstützung bei allen Fragen zur Eicosanoid-Analytik und die Übernahme der Betreuung. Danke, dass du dein Wissen um diese spannende und herausfordernde Stoffklasse mit mir geteilt hast. Das hat es mir ermöglicht, die Analytik im Labor zu etablieren.

An dieser Stelle bedanke ich mich bei allen, die mir durch das zur Verfügung stellen der Probenmaterialien diese Arbeit ermöglicht haben. Ein ganz großes Dankeschön an Dr. Nikolai Siemens und seinen Doktoranden Fabian, Nikolas, Sebastian und Surabhi für die vielen Zellkultur- und Mausproben. Die Zusammenarbeit war sehr schön für mich. Ich danke außerdem dem Team um Dr. Theresa Schwaiger vom FLI Riems für die Proben aus den Schweine-Infektionsexperimenten. Außerdem Prof. Müller-Hilke und Johann Volzke für die Arbeit an den Arthritis-Mäusen. Es war mir eine Freude und ich empfinde das interdisziplinäre Arbeiten als sehr bereichernd!

Mein Dank gilt außerdem Prof. Katharina Riedel für die Betreuung und die Möglichkeit an dem Solarix eigenständig MS-Imaging-Messungen durchzuführen. An dieser Stelle danke ich Dr. Dirk Albrecht für die Unterstützung, ich werde unser gemeinsames Schwimmtraining sehr vermissen! Danke auch an Manuela Gesell Salazar für die Proteomdaten aus den Mäuseversuchen.

Ebenfalls bedanke ich mich herzlich bei Heidi Land, Elvira Lutjanov und Dr. Jakob Krieger für die Unterstützung beim Arbeiten rund ums Imaging und Histologie. Meinem Arbeitskreis danke ich für die geleistete Hilfe und die freundliche und angenehme Arbeitsatmosphäre.

Meinen Eltern und meinen Großeltern danke ich für die wundervolle und liebe Unterstützung während des Studium und der Promotion! Ihr habt mir das Studium ermöglicht und ich danke euch von Herzen. Meiner Frau Doreen danke ich für alle Hilfe und Verständnis während der Zeit. Du bist so wunderbar. Seit Samuels Geburt sind wir beide bei unseren Promotionen noch mehr gefordert und ich bin glücklich, dass wir gemeinsam alles hinbekommen. Zuletzt danke ich all meinen Freunden, die größtenteils mit mir studiert haben für die gemeinsame, wunderbare Zeit.